

Understanding Ordered Silica

Linking Topology and Energetics

Martinus Antonius Zwijnenburg

Cover: Fragment of the FAU framework represented as a space-filling packing of polyhedral tiles (see chapters six and seven). Picture generated by Dr. O. Delgado-Friedrichs using the 3DTiler package.

Understanding Ordered Silica

Linking Topology and Energetics

Proefschrift

ter verkrijging van de graad van doctor
aan de Technische Universiteit Delft,
op gezag van de Rector Magnificus prof. dr. ir. J.T. Fokkema,
voorzitter van het College voor Promoties,
in het openbaar te verdedigen
op dinsdag 12 oktober 2004 om 10.30 uur

door

Martinus Antonius ZWIJNENBURG

scheikundig ingenieur
geboren te Den Haag

Dit proefschrift is goedgekeurd door de promotoren:

Prof. dr. J.C. Jansen

Prof. dr. G.J. Witkamp

Samenstelling promotiecomissie:

Rector Magnificus	voorzitter
Prof. dr. G.J. Witkamp	Technische Universiteit Delft, promotor
Prof. dr. J.C. Jansen	Universiteit van Stellenbosch, Zuid-Afrika, promotor
Prof. dr. ir. H. van Bekkum	Technische Universiteit Delft
Prof. dr. C.R.A. Catlow FRS	University College London, Verenigd Koninkrijk
Prof. dr. H. Gies	Ruhr-Universität Bochum, Duitsland
Prof. dr. F. Illas Riera	Universitat de Barcelona, Spanje
Dr. S.T. Bromley	Technische Universiteit Delft, adviseur

Dr. S.T. Bromley heeft als begeleider in belangrijke mate aan de totstandkoming van het proefschrift bijgedragen.

ISBN 90-9018459-7

Giles: Yes, let's not jump to any conclusions.

Buffy: I didn't jump. I took a tiny step, and there conclusions were.

Buffy the Vampire Slayer, season 2 episode 15 Phases

Voor mijn ouders.

Contents

1. Introduction.	1
2. The nature of the Si-O bond.	15
3. Fully coordinated silica nanoclusters: $(\text{SiO}_2)_n$ molecular rings and beyond	43
4. Two-ring vibrational modes on silica surfaces investigated via fully coordinated nanoclusters.	57
5. Prospects for a synthetic route towards well-defined stoichiometric silica nanoclusters: from Siloxane to Silica.	69
6. Towards understanding the energetics of (extra-large pore) zeolites; a polyhedral approach.	81
7. Understanding the thermodynamic viability of zeolite frameworks using a simple topological model.	103
8. Computational insights into the role of Ge in stabilizing double-four ring containing zeolites.	131
Summary.	141
Samenvatting.	145
Dankwoord.	149
Publications and oral presentations.	153
Curriculum vitae.	157

1

Introduction

1.1 Silica

Silica is enormously versatile, exhibiting a large and diverse spectrum of natural and synthetic polymorphs only to be equalled by isostructural solids such as aluminosilicates and aluminophosphates. Together with the related silicate minerals, silica is the most abundant material on earth, comprising more than 90% by weight and volume of the earth's mantle and crust^{1,2}. Furthermore, silica-based materials have found widespread application in the chemical industry (adsorbent, catalyst support), the rubber and plastic industry (filler) and in optical and microelectronic devices. The structural basis for the vast majority of silica structures is a three-dimensional network of silicon-centred corner-sharing SiO_4 tetrahedra, linked by Si-O-Si bonds. Silica tetrahedra can also participate in edge sharing, giving rise to rings containing two silicon and two oxygen atoms. The latter type of unit, however, is rare and has only been identified with certainty in one all-silica material (silica-W³) and several organic terminated siloxanes^{4,5,6}. Figure 1.1 depicts corner- and edge-sharing SiO_4 tetrahedra.

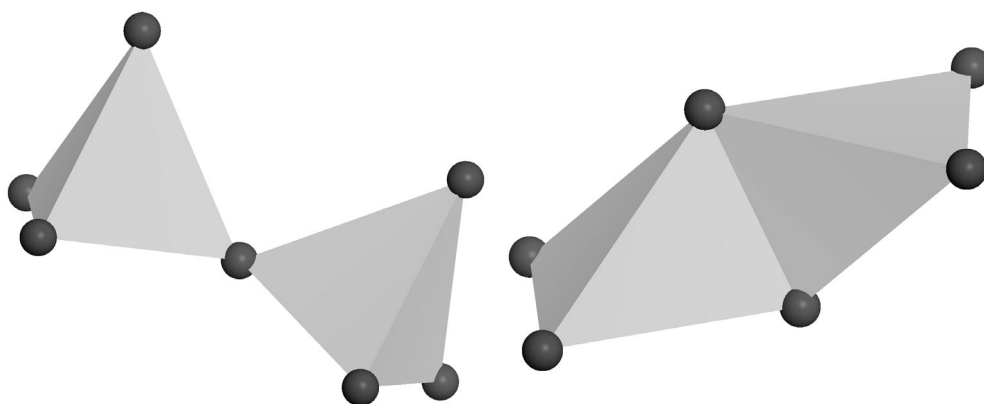


Figure 1.1. Corner- and edge-sharing SiO_4 tetrahedra.

Bonding in all-silica materials is traditionally thought of as largely covalent⁷; quartz, for example, often being treated as a super-molecular structure. However, this view contrasts somewhat with the successes of modelling such systems *via* the use of interatomic potentials; these models are, with few exceptions, charge-localised ionic methods.

1.1.1 Zeolites

Zeolites are networks of TO_4 tetrahedra, in which the tetrahedra are spatially arranged in such a way that structures with cavities and channels of molecular dimension arise. More than 40 naturally occurring zeolite frameworks are known⁸ (with mainly Si and Al as T-atoms), while currently more than 90 zeolite frameworks⁹ are available through synthesis (with, as T-atoms, mainly Si, Al, Ge, B and Be). Furthermore, more than 60 frameworks⁹ (of which more than 30 exclusively) can be synthesized as tetrahedral networks of alternating TO_4 and PO_4 tetrahedra, the so-named metallophosphates with predominantly Al, Ga, Mg and Co as T-atoms.

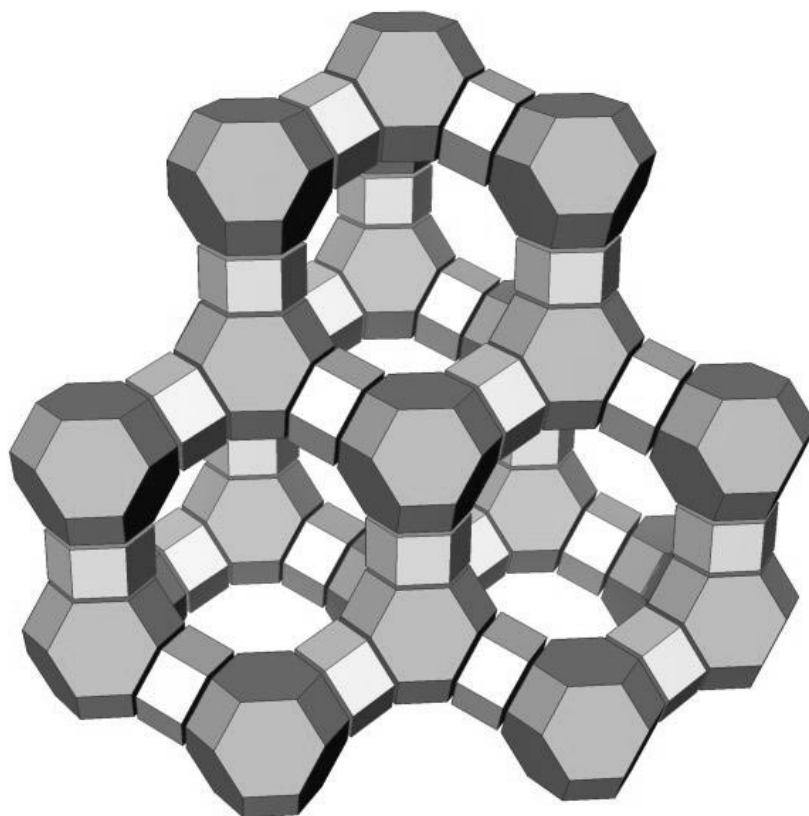


Figure 1.2. Part of the Faujasite (FAU) framework, clearly showing the cavities present in the structure (oxygen atoms omitted for clarity).

Molecules can be adsorbed into the cavities and channels of these framework structures and are subsequently free to diffuse through the material (see figure 1.3). This property has led to applications of zeolites in separation technologies that operate at the

molecular scale, e.g. in the separation of specific molecules from process-streams by means of adsorption-beds and membranes (e.g. the separation of normal and iso-fractions during alkane isomerisation¹⁰). The mechanism of separation differs with the type of molecules and framework under consideration, but is often related to size and shape differences between molecules analogous to macroscopic separation by means of a sieve. The latter fact has resulted in the term molecular sieve to become synonymous with zeolite. Besides for separation, zeolite can also be employed as catalyst to speed up chemical reactions. Cations that compensate charge for negatively charged TO_4 tetrahedra (like AlO_4^- and BeO_4^{2-}) present in non-all-silica zeolites can be exchanged for protons, resulting in an acid catalyst. Catalytic activity can also be induced by substitution of catalytically active metal-atoms (e.g. Ti for epoxidation¹¹) for framework atoms, or by using the zeolite's internal surface as a support for highly dispersed metal clusters (e.g. noble metal clusters for hydrogenation¹²). Furthermore, the specific size and shape of the zeolite's channels and cavities can be exploited to obtain catalysts with shape-selectivity towards certain products (i.e. other potential products are not formed as they, or the transition state towards them, do not fit inside the channels), that is not attainable in meso- and macroporous heterogeneous catalysts.

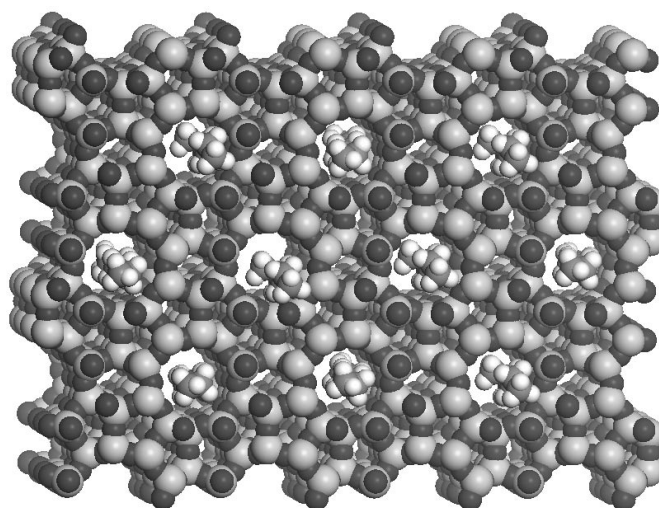


Figure 1.3. Linear and branched heptane molecules diffusing through the pores of the zeolite Silicalite-1 (MFI framework).

Zeolites are synthesized by a hydro- or solvothermal synthesis starting from a T-atom source (often an oxide), a mineraliser (OH^- or F^-) and a template. Depending on

the synthesis the latter can be an inorganic cation (e.g. Na^+ for zeolite-A), an organic cation (e.g. the tetrapropyl ammonium cation for ZSM-5) or a neutral water-soluble organic molecule (e.g. diethylamine for Dodecasils 1H¹³). The exact workings of zeolite synthesis and the role of the template are still under intensive debate, partly because much is still unknown. It is now, however, established by experimental calorimetry¹⁴ that the interaction enthalpy between template and framework is small and spans only a narrow range of values, consistent with the template/framework interaction being mainly due to weak dispersive forces. The latter suggests that a template cannot stabilise an otherwise thermodynamically unstable framework. Furthermore, Gies and Marler concluded, in their work on the role of organic templates in the synthesis of clathrasils, that the chemical character of templates with similar shape had no influence on their templating ability¹³. This result is also in accordance with Monte-Carlo docking calculations¹⁵⁻¹⁷ that have demonstrated that for an organic molecule to template a zeolite successfully, the template must effectively fill the void space of the framework. It, thus, appears that a template molecule imposes its effective inverse shape on the framework by maximizing its interactions with the silica, thereby selecting a certain cage-type, but that this selectivity is not influenced by the specific nature and strength of the interactions alone. The overall thermodynamics of zeolite synthesis are also still surrounded by uncertainties, especially due to the limited amount of data present for such complex systems. However, recent calorimetric data^{14,18,19} suggests that zeolites can be the thermodynamically preferred synthesis product in the presence of a template, even though the thermodynamic driving forces involved appear to be very small.

The diversity in zeolite frameworks allows one to select a structure which most ideally suits the desired application. Usage of a zeolite as membrane or shape-selective catalyst for instance requires a framework with channels/cage-windows of a certain size (expressed in the number of T-atoms circumscribing the channel), while adsorption applications call for frameworks with a high molecular adsorption volume. The latter is strongly related to the framework density of the zeolite (the number of T-atoms per 1000 cubic Å). Furthermore, optimisation of reaction selectivities or minimization of diffusion problems (e.g. channel blocking) might require a specific dimensionality of the channel system (i.e. one-, two- or three-dimensional). There appear however to be limits to zeolite structures, while 53 frameworks with an eight-ring as largest ring have been observed, 28 with a ten-ring and 41 with a twelve-ring, there are only six

frameworks synthesized with a fourteen-ring as largest ring and only two with an eighteen-ring⁹. Moreover, all these extra-large pore frameworks (i.e. which contain channels circumscribed by more than 12 T-atoms), with the exception of the thermally unstable OSO, have a one-dimensional channel-system⁹. Research into this class of materials, however, is still pursued extensively in both industry and academia²⁰⁻²⁷, because of the desire to perform shape-selective adsorption and catalysis on larger molecules than possible with the existing frameworks. The synthesis of the eighteen-ring framework ETR was for instance reported only very recently²⁷. Moreover, this research is additionally motivated by a great deal of recent work on the generation of hypothetical frameworks²⁸⁻³⁵ and the evaluation of their energetic and structural properties³⁶⁻³⁸, which demonstrated that the zeolite structural diversity is much richer than might be expected from a simple assessment of the already available frameworks.

1.1.2 Silica nanostructures

The fabrication and study of silica nanostructures has received considerable attention in recent years, largely due to their promise and potential in applications as diverse as photonics/optics, drug-delivery, microelectronics and catalysis. Silica can now be synthesized conveniently in many three-dimensional shapes with a characteristic size in the order of a nanometer, examples of which include nanotubes^{39,40}, nanospheres⁴¹, ultra-thin films⁴² and mesoporous silica⁴³⁻⁴⁵. Silica nanostructures are known to possess characteristic structural properties (two-membered Si_2O_4 rings as a result of edge sharing between two SiO_4 tetrahedra⁴⁶, non-bridging oxygen (NBO) defects⁴⁷) not commonly found in their bulk analogues, which is often reflected in their physical and chemical properties. Silica nanoparticles, nanowires and nanotubes, for instance, have been demonstrated to show photoluminescence, a property that has been directly linked to high defect concentrations resulting from their high surface area^{48,49}.

1.2 Computational modelling of silica materials

The modelling of silica materials can be performed at two fundamentally different levels of theory, atomistic modelling in which the atoms are treated as classical particles with the interactions described by an empirical force-field and quantum

chemical modelling in which the quantum nature of matter is explicitly taken into account. Below these approaches are discussed in more detail, as are their strength and weaknesses.

1.2.1 Atomistic modelling

In the case of atomistic modelling the atoms are treated as classical particles moving in a potential dependent on the spatial coordinates of all the particles in the system. This potential, often referred to as force field, describes the forces acting in a system by a set of selected interaction terms and corresponding parameters. Equation 1.1 gives an example of the form of such a potential (The FB nanosilica potential⁵⁰ employed in chapter five, and also the TTAM⁵¹ and BKS⁵² SiO₂ potentials) for two atoms a and b ($a, b \in [\text{Si}, \text{O}]$) at a distance r :

$$V_{ab} = \frac{\delta_a \delta_b}{4\pi\epsilon_0 r} + A_{ab} \exp\left(\frac{-r}{B_{ab}}\right) - \frac{C_{ab}}{r^6} \quad (1.1)$$

In which the terms represent the electrostatic and van der Waals type interactions (δ_a and δ_b are atomic charges, ϵ_0 is the permittivity of vacuum and A_{ab} , B_{ab} and C_{ab} are empirically determined interaction coefficients). Both the terms and the constants in the potentials are typically chosen to closely mirror the experimentally or *ab initio* determined properties of a specific system and are, thus, not routinely transferable to other systems. Furthermore, due to the classical nature of the description, potentials can only very approximately treat systems involving chemical reactions. In many systems these weaknesses are however compensated for by the computational efficiency of potentials compared to quantum chemistry methods, allowing one to at present to model systems of up to 10,000 atoms.

The potentials can be used to obtain the energy minimum for a given structure by relaxing the system, using a suitably chosen minimizer, until a state of minimum energy is reached. This type of calculations is typically used to get equilibrium geometries and relative energetics of structures. For crystals (like quartz and zeolites) periodic boundary conditions are employed and the energy can be minimized under the constraint of constant volume or constant external pressure.

In Molecular Dynamics (MD) calculations the time dependent behaviour of a system can be studied so as to investigate its kinetic (diffusion, kinetic stability) and dynamic (framework dynamics) properties. The system is allowed to evolve in time by iteratively solving Newton's equations of motion in one of three thermodynamic ensembles: NVE (constant number of atoms, volume and energy), NVT (constant temperature) or NPT (constant pressure). After a period of initialisation, equilibrium is reached in which the system properties no longer change with time, and the subsequent trajectory can be (statistically) analysed to obtain information about the system's steady-state properties.

1.2.2 Quantum chemical modelling

In the case of quantum chemical modelling, the quantum nature of matter is explicitly taken into account by using quantum mechanics instead of classical mechanics to describe the system and its interactions. The Schrödinger (or more formally Dirac's) equation describes, in principle, the behaviour of material in quantum mechanics, although it can only be exactly solved for small numbers of particles (max. 2). To apply quantum modelling to chemical problems, approximate methods have to be employed. The first approximation is to ignore the quantum nature of the nuclei (treat them as classical particles), and assume that they move slowly compared to electrons, as their mass is three to four orders of magnitude larger. Thus, the movement of nuclei and electron can be treated separately. This approximation, due to Born and Oppenheimer, allows us to optimise the electronic structure of a material while considering the nuclei to be stationary, and to only solve the electronic Schrödinger equation:

$$H_e \psi_e = E_e \psi_e \quad (1.2)$$

In which H_e is the electronic Hamiltonian (describing all electron-electron and electron-nuclei interactions), ψ_e the electron wavefunction and E_e the electronic energy. There are two main approaches to approximately solve this equation: the Hartree-Fock approach and Density Functional Theory.

In the Hartree-Fock^{53,54,55,56} (HF, or more formally Hartree-Fock-Roothaan⁵⁷) approach the unknown electron wavefunction is written as a function of N

single-electron wavefunctions. To ensure that the wavefunction will be antisymmetric under exchange of any two electrons, as required by the Pauli principle, the single-electron wavefunctions are combined, not as a product, but as a Slater determinant. The single-electron wavefunctions are subsequently expanded as a linear combination of basis functions (e.g. Gaussian functions, plane-waves) and the expansion constants are updated iteratively so as to minimise the energy of the wavefunction. The wavefunction obtained is the ground state HF wavefunction and its energy the ground state HF energy. The HF method, however, has two weaknesses. Firstly, electron-electron interactions are only treated in a mean-field manner, neglecting electron correlation, and secondly, the HF wavefunction depends on $3N$ spatial and N spin coordinates, which make the calculations involved rather complex for all but the simplest molecules. For instance, the HF wavefunction of the silicic acid monomer ($\text{Si}(\text{OH})_4$) depends on not less than 150 spatial and 50 spin coordinates. The neglect of electron correlation can (partially) be resolved by more advanced wavefunction based methods like Configuration Interaction or Møller-Plesset perturbation theory, but such calculations are even significantly more computationally intensive.

Density Functional (DF) theory is an alternative for the HF method, based around the electron density instead of the wavefunction. Hohenberg and Kohn proved that all the ground state properties of a material can in principle be calculated from only the electron density⁵⁸. This considerably reduces the computational effort involved, as the electron density only depends on 3 spatial coordinates instead of $4N$ (spatial and spin) coordinates. Kohn and Sham developed a formalism to obtain the DF ground state energy based around iteratively solving a HF-like equation for a fictitious system of non-interacting particles with the same density and energy as the real system⁵⁹. The coupling between both systems is an external potential in the fictitious system, which depends on the kinetic energy of the electrons, the electron-nuclei interaction, the classical Coulomb interaction and the exchange-correlation interaction in the real system. While the first three contributions can be conveniently expressed as functionals of the electron density, there is no exact formula known for the latter term, describing all non-classical electron-electron interactions. It turns out, however, that approximate forms of the exchange-correlation (XC) functional often still yield accurate estimates of the DF ground state energy, including a large part of the electron correlation energy.

Several approximate XC-functionals exist, differing in level of complexity. Simple functionals depend only on the value of the density (local functionals), while more elaborate functionals additionally depend on the gradient of the electron density (non-local functionals). While all these functionals include parameters fitted to *ab initio* or experimentally obtained exact exchange and correlation energies for specific systems, they are nevertheless transferable to other systems. Throughout this thesis we will use the B3LYP XC-functional⁶⁰, which has been widely and successfully used for the modelling of silica materials⁶¹⁻⁷⁵.

Besides energetics and equilibrium geometries, HF and DFT methods can also be used to calculate the infrared spectra of materials. The infrared frequencies can be obtained by calculating and subsequently diagonalising the Hessian, while the intensities of the modes can be calculated from the change in dipole moment with respect to a geometry displacement along the modes. Calculated spectra are often scaled to improve the match between theoretical and experimental results. For HF calculations for instance a scaling factor of 10% is usually applied to the computed frequencies to correct for the neglect of electron correlation and anharmonicity⁷⁶. For DFT calculated frequencies, scaling factors are less often recommended and/or applied, and are significantly smaller than those for HF calculations.

1.3 Overview of this thesis

The research described in this thesis focuses on expanding our (fundamental) knowledge of siliceous zeolites and nanostructures through computational modelling. The research was especially aimed at understanding the link between structure and energetics, and at using this link to predict which structures can be expected to be formed synthetically. For zeolites this should provide insight into the relationship between structural properties (e.g. pore-size, framework density) and the viability of their occurrence, aiming to explain for instance the relatively small number of synthesized extra-large-pore frameworks. While for silica nanostructures, the research was intended to shed light on the possibilities of synthesizing fully-coordinated silica nanoclusters and their stability when formed.

In chapter two, the chemical nature of the Si-O bond is investigated using different charge analysis schemes. Special attention is paid to the link between geometry (Si-O bond length) and the ionic nature of the bond.

Chapter three reports on fully-coordinated silica nanoclusters in the form of $(\text{SiO}_2)_N$ molecular rings. The energetic stability of rings compared to non-fully-coordinated silica chains is discussed in terms of ring strain, and compared with the bulk silica phases silica-W and α -quartz. Furthermore, the prospects and constraints for assembling the clusters into bulk-phases are reviewed.

Dehydrated silica surfaces show typical infrared-bands which have until now never been satisfactorily understood from a theoretical point of view. Chapter four employs the fully-coordinated silica nanoclusters from chapter three as model system to understand experimentally observed spectra in terms of Si_2O_4 two-rings.

In chapter five, the prospects for a new synthetic route towards well-defined stoichiometric silica nanoclusters is discussed, based on the calculated energetics of the reactants and expected products. Furthermore, the stability of the formed clusters at realistic reaction conditions is analysed through dedicated MD-calculations.

Chapter six is devoted to employing polyhedral tiles and their face-size distribution in understanding the link between framework topology and energetics in zeolites. A description of zeolite frameworks as space-filling packing of polyhedral tiles is introduced, and topological constraints to (extra-large-pore) frameworks are discussed.

In chapter seven the concepts introduced for isolated polyhedral tiles in chapter six are successfully employed to describe the energetics of extended zeolite frameworks. The influence of structural properties (e.g. pore-size, framework density) on the zeolite energetics is discussed, and used to explain the relatively small number of extra-large-pore and extra-low framework density frameworks.

Finally, in chapter eight the work of chapter six is extended to study substituted zeolite frameworks. Calculations on a range of Ge-substituted polyhedral tiles are performed to explain the experimentally observed effect of Ge in directing zeolite synthesis to double-four ring containing frameworks.

References

- ¹ Sosman R.B. The phases of Silica: Rutgers University Press: New Brunswick, U.S., 1965.
- ² Liebau F. Structural chemistry of Silicates – Structures, Bonding and Classification: Springer-Verlag: Berlin, Germany, 1985.
- ³ Weiss A. *Z. Anorg. Allg. Chem.* **1954**, 276, 95.
- ⁴ Millevolte A.J., Powell D.R., Johnson S.G., West R. *Organometallics* **1992**, 11, 1091.
- ⁵ Sohn H.L., Tan R.P., Powell D.R., West R. *Organometallics* **1994**, 13, 1390.
- ⁶ Willms S., Grybat A., Saak W., Weidenbruch M., Marsmann H. *Z. Anorg. Allg. Chem.* **2000**, 626, 1148.
- ⁷ Catlow C. R. A., Stoneham A. M. *J. Phys. C: Solid State Phys.* **1983**, 16, 4321.
- ⁸ Tschernich R.W. Zeolites of the World: Geoscience Press: Phoenix, U.S., 1992.
- ⁹ Baerlocher C., Meier W.M., Olson D.H. Atlas of Zeolite Framework Types: Elsevier, Amsterdam, The Netherlands, 2001 (updates on <http://www.iza-structure.org/>).
- ¹⁰ Sherman J.D. *Proc. Natl. Acad. Sci. USA* **1999**, 96, 3471.
- ¹¹ Bellussi G., Rigutto M.S. In Studies in Surface Science and Catalysis vol. 85; Jansen J.C., Stöcker M., Karge H.G., Weitkamp J.: Elsevier: Amsterdam, The Netherlands, 1994.
- ¹² Kawi S., Chang J.R., Gates B.C. *J. Am. Chem. Soc.* **1993**, 115, 4830.
- ¹³ Gies H., Marler B. *Zeolites* **1992**, 12, 42.
- ¹⁴ Piccione P.M., Yang S., Navrotsky A., Davis M.E. *J. Phys. Chem B.* **2002**, 106, 3629.
- ¹⁵ Lewis D.W., Freeman C.M., Catlow C.R.A. *J. Phys. Chem.* **1995**, 99, 11194.
- ¹⁶ Lewis D.W., Willcock D.J., Catlow C.R.A., Thomas J.M., Hutchings G.J. *Nature* **1996**, 382, 604.
- ¹⁷ Lewis D.W., Sankar G., Wyles J.K., Thomas J.M., Catlow C.R.A., Willcock D.J. *Angew. Chem. Int. Ed.* **1997**, 36, 2675.
- ¹⁸ Petrovic I., Navrotsky A. *Microporous. Mater.* **1997**, 9, 1.
- ¹⁹ Yang S., Navrotsky A. *Chem. Mater.* **2002**, 14, 2803.
- ²⁰ Davis M.E. *Chem. Eur. J.* **1997**, 3, 1745.
- ²¹ Davis M.E., Saldarriaga C., Garces J., Crowder C. *Nature* **1988**, 331, 698.
- ²² Estermann M., McCusker, L.B., Baerlocher C., Merrouche C.A., Kessler H. *Nature* **1991**, 352, 320.
- ²³ Jones R.H., Thomas J.M., Chen J., Xu R., Huo Q., Li S., Ma Z., Chippindale A.M. *J. Solid State Chem.* **1993**, 102, 204.
- ²⁴ Balkus, K.J., Gabrierlov A.G., Sandler N. *Mater. Res. Soc. Symp. Proc.* **1995**, 368, 369.
- ²⁵ Balkus K.J., Khanmamedova A., Gabrierlov A.G., Zones S.I. *Stud. Surf. Sci. Catal.* **1996**, 101, 1341.
- ²⁶ Lobo R.F., Tsapatsis M., Freyhardt C.C., Khodabandeh S., Wagner P., Chen C.Y., Balkus K.J., Zones S.I., Davis M.E. *J. Am. Chem. Soc.* **1997**, 119, 8474.
- ²⁷ Strohmaier K.G., Vaughan D.E.W. *J. Am. Chem. Soc.* **2003**, 125, 16035.
- ²⁸ Deem M.W., Newsam J.M. *J. Am. Chem. Soc.* **1992**, 114, 7189.
- ²⁹ Treacy M.M.J., Randall K.H., Rao S., Perry J.A., Chadi D.J. *Z. Kristallogr.* **1997**, 212, 768.
- ³⁰ Delgado Friedrichs O., Dress A.W.M., Huson D.H., Klinowski J., Mackay A.L. *Nature* **1999**, 400, 644.
- ³¹ Boisen M.B., Gibbs G.V., O’Keeffe M., Bartelmehs K.L. *Microporous Mesoporous. Mater.* **1999**, 29, 219.
- ³² Delgado Friedrichs O., Huson D.H. *Discrete. Comput. Geom.* **2000**, 24, 279.
- ³³ Mellot Draznieks C., Newsam J.M., Gorman A.M., Freeman C.V., Férey G. *Angew. Chem. Int. Ed.* **2000**, 39, 2270.
- ³⁴ Mellot Draznieks C., Girard S., Férey G. *J. Am. Chem. Soc.* **2002**, 124, 15326.
- ³⁵ Woodley S.M., Catlow C.R.A., Battle P.D., Gale J.D. *Chem. Commun.* **2004**, 22.
- ³⁶ Foster M.D., Delgado Friedrichs O., Bell R.G., Almeida Paz F.A., Klinowski J. *Angew. Chem. Int. Ed.* **2003**, 42, 3896.
- ³⁷ Simperler A., Foster M.D., Bell R.G., Klinowski J. *J. Phys. Chem. B* **2004**, 108, 869.
- ³⁸ Foster M.D., Simperler A., Bell R.G., Delgado Friedrichs O., Almeida Paz F.A., Klinowski J. *Nature Materials.* **2004**, 3, 234.
- ³⁹ Adachi M. *Colloid. Polym. Sci.* **2003**, 281, 370.
- ⁴⁰ Zhang M., Bando Y., Wada K. *J. Mater. Res.* **2000**, 15, 387.
- ⁴¹ Hentze H.P., Raghavan S.R., McKelvey C.A., Kaler E.W. *Langmuir* **2003**, 19, 1069.
- ⁴² Muller D.A., Sorsch T., Moccio S., Baumann F.H., Evans-Lutterodt K., Timp G. *Nature* **1999**, 399, 758.
- ⁴³ Beck J.S., Vartuli J.C., Roth W.J., Leonowicz M.E., Kresge C.T., Schmitt K.D., Chu C.T.W., Olson D.H., Sheppard E.W., McCullen S.B., Higgins J.B., Schlenker J.L. *J. Am. Chem. Soc.* **1992**, 114, 10834.
- ⁴⁴ Inagaki S., Fukushima Y., Kuroda K. *J. Chem. Soc. Chem. Commun.* **1993**, 680.

-
- ⁴⁵ Jansen J.C., Shan Z., Marchese L., Zhou W., van der Puil N., Maschmeyer T. *Chem. Commun.* **2001**, 713.
- ⁴⁶ Ferrari A.M., Garrone E., Spoto G., Ugliengo P., Zecchina A. *Surf. Sci.* **1995**, 323, 151.
- ⁴⁷ Zyubin A.S., Glinka Y.D., Mebel A.M., Lin S.H., Hwang L.P., Chen Y.T. *J. Chem. Phys.* **2002**, 116, 281.
- ⁴⁸ Yu D.P., Hang Q.L., Ding Y., Zhang H.Z., Bai Z.G., Wang J.J., Zhou Y.H., Qian W., Xiong G.C., Feng S.Q. *Appl. Phys. Lett.* **1998**, 73, 3076.
- ⁴⁹ Zhang M., Ciocan E., Bando Y., Wada K., Cheng L.L., Pirouz P. *Appl. Phys. Lett.* **2002**, 80, 491.
- ⁵⁰ Flikkema E., Bromley S.T. *Chem. Phys. Lett.* **2003**, 378, 622.
- ⁵¹ Tsuneyuki S., Tsukada M., Aoki H., Matsui Y. *Phys. Rev. Lett.* **1998**, 61, 869.
- ⁵² van Beest B.W.H., Kramer G.J., van Santen R.A. *Phys. Rev. Lett.* **1990**, 64, 1955.
- ⁵³ Hartree D.R. *Proc. Cambridge Phil. Soc.* **1927**, 24, 111.
- ⁵⁴ Hartree D.R. *Proc. Cambridge Phil. Soc.* **1928**, 24, 426.
- ⁵⁵ Hartree D.R. *Proc. Cambridge Phil. Soc.* **1929**, 25, 310.
- ⁵⁶ Fock V. *Z. Phys.* **1930**, 61, 126.
- ⁵⁷ Roothaan C.C.J. *Rev. Mod. Phys.* **1951**, 23, 69.
- ⁵⁸ Hohenberg P., Kohn W. *Phys. Rev. Lett.* **1964**, 136, B864.
- ⁵⁹ Kohn W., Sham L.J. *Phys. Rev. Lett.* **1965**, 140, A1133.
- ⁶⁰ Becke A.D. *J. Chem. Phys.* **1996**, 104, 1040.
- ⁶¹ Civalleri B., Garrone E., Ugliengo P. *J. Phys. Chem. B* **1998**, 102, 2373.
- ⁶² Civalleri B., Zicovich-Wilson C.M., Ugliengo P., Saunders V.R., Dovesi R. *Chem. Phys. Lett.* **1998**, 292, 394.
- ⁶³ Ugliengo P., Civalleri B., Dovesi R., Zicovich-Wilson C.M. *Phys. Chem. Chem. Phys.* **1999**, 1, 545.
- ⁶⁴ Vitiello M., Lopez N., Illas F., Pacchioni G. *J. Phys. Chem. A* **2000**, 104, 4674.
- ⁶⁵ Lopez N., Vitiello M., Illas F., Pacchioni G. *J. Non Cryst. Sol.* **2000**, 271, 56.
- ⁶⁶ Pacchioni G., Mazzeo C. *Phys. Rev. B* **2000**, 62, 5452.
- ⁶⁷ Civalleri B., Ugliengo P. *J. Phys. Chem. B* **2000**, 104, 9491.
- ⁶⁸ Walsh T.R., Wilson M., Sutton A.P. *J. Chem. Phys.* **2000**, 113, 9191.
- ⁶⁹ Chu T.S., Zhang R.Q., Cheug H.F. *J. Phys. Chem. B* **2001**, 105, 1705.
- ⁷⁰ Raghavachari K., Pacchioni G. *J. Chem. Phys.* **2001**, 114, 4657.
- ⁷¹ Zhang R.Q., Chu T.S., Cheung H.F., Wang N., Lee S.T. *Phys. Rev. B* **2001**, 64, 113304.
- ⁷² Pelmenchikov A., Leszczynski J., Petterson L.G.M. *J. Phys. Chem. A* **2001**, 105, 9528.
- ⁷³ Zyubin A.S., Glinka Y.D., Mebel A.M., Lin S.H., Hwang L.P., Chen Y.T. *J. Chem. Phys.* **2002**, 116, 281.
- ⁷⁴ Gnani E., Reggiani S., Rudan M. *Phys. Rev. B* **2002**, 66, 195205.
- ⁷⁵ Lopez-Gejo F., Busso M., Pisani C. *J. Phys. Chem. B* **2003**, 107, 2944.
- ⁷⁶ Scott A.P., Radom L. *J. Phys. Chem.* **1996**, 100, 16502.

The nature of the Si-O bond

Abstract

Atomic charge analysis is performed on the basis of electron densities obtained from systematic density functional cluster calculations on structural fragments from seven different all-siliceous zeolites and two all-silica minerals. Charges and ionicities for these fragments are calculated using three different charge analysis schemes: Mulliken, Hirshfeld and Bader methods. The dependency of the ionicity of the Si-O bond on geometric parameters of the clusters is investigated and it is demonstrated that a correlation exists between the Si-O bond length and its ionicity. Ionicities derived from Bader atomic charges were shown to have a trend opposite to that of ionicities derived from Mulliken and Hirshfeld charges. A simple model is proposed to account for these differences, demonstrating that these opposing trends may be reconciled. The results also suggest a possible link between Si-O bond ionicity and the energetic stability of the corresponding bulk silica polymorph.

The contents of this chapter have been published in:

Zwijnenburg M.A, Bromley S.T., Van Alsenoy C., Maschmeyer T. *J. Phys. Chem. A* **2002**, 106, 12376.

2.1 Introduction

Commonly, bonding in materials is described to be either ionic or covalent in nature. However, the bonding in many materials turns out to be neither completely ionic nor completely covalent, but rather some mixture of both. Understanding the degree of this ionic/covalent mixing, can help to rationalise observed (structural) trends, as both extremes in bonding yield materials with completely different properties. Typical ionicly bonded materials (e.g. alkali halides) for example have closed-packed structures with high coordination numbers (e.g. 8-12), while typical covalently bonded materials (e.g. diamond) show open structures with low coordination numbers (e.g. 4). Bonding in all-silica materials is traditionally thought of as largely covalent¹. However, this view contrasts somewhat with the successes of modelling such systems *via* the use of interatomic potentials; these models are, with few exceptions, charge-localised ionic methods. Furthermore, an estimate of the ionicity from the electronegativity of Si and O yields the intermediate value 52%². Silica thus appears to lie, in terms of bonding, somewhere in the middle. To further elucidate the ionicity of silica, this chapter reports density functional calculations on small silica clusters, which coupled with several charge-partitioning methods, yield novel insights into the nature of bonding in silica materials and its relation with the silica structure.

The degree of ionicity/covalency of a bond can be defined simply in terms of atomic charges alone³. However, such charges are, in fact, particularly difficult to obtain. More fundamentally, even in the case where an accurate model of the charge density is available, such as from high-level DF calculations, the derivation of the physical atomic charges is an ill-posed question with numerous possible answers. Atomic charges, like any other atom-in-molecule property, cannot be calculated directly from quantum mechanics⁴ since the Schrödinger equation for a molecule (or crystal) makes no reference to the constituent atoms. It is thus impossible to extract objective information about atomic charges from electronic structure calculations. Any method to obtain charges consists of partitioning a direct observable and requires an additional assumption about the partitioning method. As a result any method to obtain charges is non-unique and its merits can only be assessed in terms of its chemical sensibility and the way it predicts values of experimental observables such as the molecular dipole constant. Because of this lack of a unique definition, a multitude of methods for

calculating atomic charges have been developed. Wiberg and Rablen⁴ and Bachrach⁵ have given an overview of the different methods and their merits.

Previous electronic structure calculations on atomic charges of various all-silica zeolites employing the Mulliken charge partitioning scheme have given charges of between +1.32 |e| and +1.50 |e| on silicon and between -0.64 |e| and -0.78 |e| on oxygen using an Hartree-Fock (HF) approach with a STO-3G basis set^{6,7,8}. Using the same methodology, but with a higher-level basis set combination (6-21G for oxygen and 8-31G for silicon), atomic charges between +2.25 |e| and +2.41 |e| for silicon and between - 1.1 |e| and -1.25 |e| for oxygen were reported^{7,8}. Calculations using the higher-level DFT method (double numerical with polarisation basis set) using Hirshfeld partitioning, applied to various relaxed silica fragments, such as three- and four-membered silica rings, have yielded typical atomic charges of +0.47 |e| on silicon and -0.27 |e| on oxygen⁹, whereas similar periodic calculations on all-silica Mordenite give typical values of +0.57 |e| on silicon and -0.28 |e| on oxygen¹⁰. Atomic charges obtained experimentally by fitting the infrared spectra of α -Quartz to a rigid-ion model give ranges between 0.69|e| and 1.94|e| for the silicon and between -0.35|e| and -0.97|e| for the oxygen atoms^{11,12,13}. Furthermore, it has been also been speculated that the silicon and oxygen atomic charges are functions of the silica geometry¹⁴. The results from theory are thus far from conclusive and suggest that the measure of the ionicity/covalency in all-silica systems has, so far, not found a straightforward answer. The experimental (synthetic) chemistry and physics of SiO₂ materials also suggest that the binding in these system is not clear-cut, but has considerable covalent and ionic components¹. This viewpoint is further supported by tight-binding calculations¹⁵ that show that the properties of silica polymorphs can be understood in terms of a simple model containing, both, a covalent and a polar energy term. Because of the relative importance of both terms in all-silica materials, they are also perfect candidate materials to test the various theoretical methods for calculating atomic charges and to probe how they compare with the known properties of such materials.

2.2 Computational methodology

In this chapter we employ three commonly used charge-partitioning methods. Firstly, Mulliken analysis¹⁶ (probably the most widely-used method), which simply partitions the charge density derived from the overlap of atomically centred orbitals evenly between the two bonded atoms. Due to the dependence of this method on the atomic orbitals, the size of the basis set used in calculations of electronic bonding characteristics is known to often strongly influence the predicted atomic charges^{4,5}. Secondly, we employ the Hirshfeld¹⁷⁻¹⁹ (or Stockholder) method, which divides the electron density at every point in space between each of the constituent molecular atoms according to a partitioning function, depending on the electron density of the free atoms. Thirdly, Bader's approach is also employed which defines molecular atoms *via* a topological analysis of the electron density²⁰. The latter two methods have been shown to give atomic charges that are relatively basis-set-independent and, in contrast to many other schemes, accurately reproduce physical observables such as molecular dipole moments and electrostatic potentials for small organic and inorganic molecules^{4, 18}.

It is important to note, however, that although Hirshfeld and Bader analyses seem to perform equally well with respect to predicting properties largely dependent on the magnitude of the atomic charges, the magnitudes of the derived charges in each scheme are quite different. This difference can be understood from the fact that the physical observables predicted in each method are also dependent on higher order multipoles of the electron density, in particular on the atomic dipoles. It is found that for each method the relative magnitude, and thus importance, of the atomic charge term and the atomic dipole term differs considerably. Within Mulliken analysis, in contrast to Hirshfeld and Bader analyses, higher order moments (atomic dipole, atomic quadrupole, etc.) of the bonded atoms cannot be easily defined⁴. Within this investigation, we concentrate on how the various charge-partitioning methods differ regarding their ability to describe a bonded system *solely* in terms of an atomic charge interpretation. For a clear description of ionicity/covalency, concepts based on atomic charges, a method which models a system most appropriately and accurately at the single charge/monopole level is to be preferred over those methods requiring higher order moments. Such a description would, to the first order, give the most concise and

chemically intuitive assessment of the charge distribution, the ionicity/covalency and, thus, the chemistry of a system.

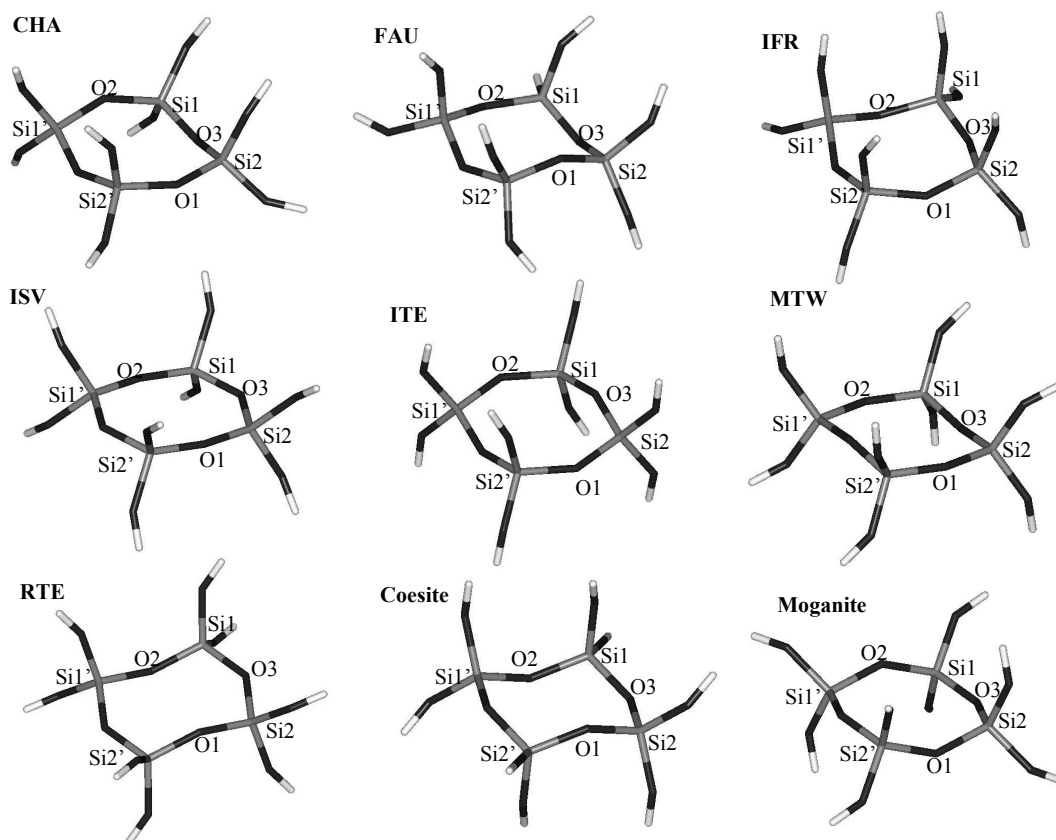


Figure 2.1. Four-ring fragment used in the calculations. The labels indicate the respective crystal structures from where the fragments were taken.

In this study, we employ a cluster approach to investigate a collection of known all-silica polymorphs (see Figure 2.1). For each extended structure a comparative fragment of 16 atoms (Si_4O_{12}), was used, in each case consisting of a ring of four oxygen atoms and four silicon atoms with two further oxygen atoms bonded to each silicon atom in the ring. Such four-rings are a good representative silica model being present in almost 90% of all zeolite frameworks, in various denser crystalline forms of silica and also within amorphous glassy silicas. To saturate the dangling oxygen bonds of each four-ring, eight hydrogen atoms were placed at an appropriate bond length of 0.98 \AA ²¹ in the direction of the missing O-Si bond from the respective periodic structure. This method of cluster termination has been widely and successfully used in

the modelling of extended silicas^{22,23,24} and owes much of its utility to the electronegativity of hydrogen lying between that of silicon and oxygen. In such a treatment, however, it is essential that the terminating hydrogens are not permitted to relax in any subsequent calculation as this is very likely to result in surface reconstruction effects e.g. the formation of intramolecular hydrogen bonds, which will destroy the role of the hydrogen atom as an approximate bulk-silicon embedding-atom and thus also mask any meaningful results¹⁰. Although fixing the hydrogens, the relaxation of the remainder of the silica is optional and advocated by some authors²⁵. In our study however, we wish to compare experimentally determined structures and thus use the respective published coordinates for each material investigated. As a reference system for these structures, a free-space silica four-ring, optimised at a high level of DFT theory was used, see figure 2.2. Optimisation of a free-space silica four-ring using the Gaussian 98 code, was, as expected, found to always yield a hydrogen-bonded conformation⁹. A preferred reference system was taken to be the non-hydrogen-bonded silica four-ring recently described by Pereira *et al.*⁹, also obtained as a valid minimum structure *via* high-level DFT optimisation. This silica four-ring, displayed in Figure 2.1, is preferred over the slightly lower energy hydrogen-bonded four-ring, as it more accurately mimics the fully connected silica rings found in all-silica structures, having no internal hydrogen bonds.

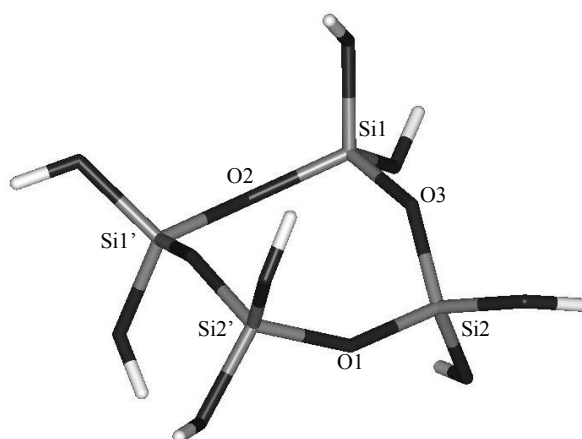


Figure 2.2. Reference four-ring silica fragment used in calculations obtained from free-space DFT optimisation.

The cluster approach was preferred over periodic calculations due to practical and methodological reasons. Firstly, the cluster approach allowed us to study a relatively large number of materials at a high DFT level of theory. To conduct such high level calculations periodically for every one of our structures would have been computationally prohibitively expensive at present. As a bulk comparison of our methodology it is possible to perform fully periodic DFT calculations of some small unit cell structures such as CHA²⁶, though often with assumptions of high symmetry to reduce the experimentally determined unit cell size. Such calculations are only of use if the same level of theory can be employed in the periodic case as in the cluster calculations. In practice periodic DFT codes traditionally use plane wave basis sets, which are difficult to compare with our Gaussian basis sets employed. With some codes however such a calculation may be possible although here it is found that basis sets including polarisation functions suitable for accurate silica cluster calculations are often not readily transferable to the corresponding periodic calculation. In addition to the problems of comparison of the calculation details, the three methods of charge analysis open to us i.e. Mulliken, Hirshfeld, and Bader, for molecular systems, are not, to our knowledge, all currently simply available in a single periodic DFT code. Furthermore, it has been shown in numerous previous studies^{22-24,27} that silica clusters with suitably fixed terminating hydrogens are very good models of extended all-silica solids.

To correct for the absence of long-range interactions in silica cluster calculations without using periodic methods, hybrid Quantum Mechanical/Molecular Mechanical (QM/MM) schemes are commonly applied. Such schemes often only treat the steric interactions of the immediate crystalline environment of the silica cluster²⁸, which, since we are taking fixed experimental geometries would, by definition be of no benefit in our study. Other schemes are able to further incorporate the long-range electrostatic field²⁹, and in some cases also polarisation effects of the bulk crystal³⁰. These latter embedding schemes, however, need values for the point charges around the cluster fitted to reproduce the long range Madelung field of the bulk material. In order to efficiently estimate the Madelung field a periodic calculation is required beforehand, usually at a lower level of theory than that used for the embedded cluster e.g. suitable interatomic potentials³⁰, or Hartee-Fock calculations²⁹. According to this prescription of forming the point charge embedding shell the charge values are by necessity fitted to a less accurate, or at best different, description of the electrostatic bulk environment than that of the

local environment of the embedded cluster itself. In the case of using charges from interatomic potentials, in particular, for calculating the embedding environment, we would in fact presuppose the very thing we are trying to ascertain in this study i.e. the atomic charges of the silicon and oxygen atoms. Although we are conscious of the need for a better description of the electrostatic environment for more accurate calculations, we feel that the main contribution of such long-range effects is on the total energy rather than on local properties such as the bonding and thus the charge distribution, which are rather more influenced by geometric and electronic factors. To demonstrate how the partitioned charges change with a fuller account of the bulk environment we have also performed calculations on significantly larger clusters taking into account of the order of 60 further atoms of the silica bulk material atoms around the respective 16 atom four-ring cluster. As we show later the corresponding partitioned charges from our 16 atom clusters shift by a small consistent percentage when going to the larger embedded clusters leaving our conclusions, based on ionicity trends, unchanged. Furthermore, as judged by published periodic calculations¹⁰, the atomic charges in our larger clusters seem to have already saturated at typical bulk values.

	Si1- O2	Si1- O3	Si1- OU	Si1- OD	Si2- O1	Si2- O3	Si2- OU	Si2- OD	Si1- O2- Si1'	Si1- O3- Si2	Si2- O1- Si2'
Ref	1.610	1.603	1.599	1.599	1.599	1.603	1.611	1.599	147.5	145.8	150.7
CHA	1.597	1.607	1.604	1.614	1.604	1.607	1.597	1.614	149.4	138.4	145.8
FAU	1.616	1.594	1.570	1.557	1.622	1.619	1.572	1.619	143.5	145.1	149.3
IFR	1.563	1.559	1.661	1.661	1.563	1.559	1.661	1.661	166.1	134.8	166.1
ISV	1.625	1.625	1.622	1.625	1.625	1.624	1.624	1.623	148.1	154.7	148.1
ITE	1.546	1.587	1.584	1.555	1.591	1.660	1.543	1.593	156.2	158.6	156.2
MTW	1.612	1.629	1.613	1.624	1.615	1.630	1.620	1.610	156.9	139.2	156.9
RTE	1.642	1.650	1.649	1.650	1.642	1.654	1.645	1.652	148.6	142.8	148.6
Coesite	1.607	1.631	1.598	1.598	1.619	1.617	1.608	1.625	145.0	136.1	145.0
Moganite	1.610	1.614	1.610	1.614	1.612	1.605	1.591	1.612	145.0	145.8	145.0

Table 2.1 Geometry of silica four-rings (all distances in Å, all angles in degrees), OU = terminating oxygen above the plane of the ring, OD = terminating oxygen below the plane of the ring.

All clusters, with exception of the reference four-ring, were obtained from crystal structure refinements of all-silica materials (indicated for zeolites by the reference code of their framework types: CHA³¹, FAU³², IFR³³, ISV³⁴, ITE³⁵, MTW³⁶

(see footnote A), RTE³⁷, Coesite³⁸, Moganite³⁹). Geometric details of the different silica four-rings can be found in Table 2.1. The DFT calculations were performed using the three-parameter B3LYP hybrid functional^{40,41}, as implemented in the program Gaussian 98⁴². Various basis sets, 3-21G⁴³⁻⁴⁷; 6-31G^{43,44}, 6-31G*^{43,44} and 6-31G**^{43,44} were employed to study the effect of the basis set on the result of the calculations. Mulliken charges were obtained from the Gaussian 98 code, Hirshfeld atomic charges were calculated using the Stock program¹⁸, and Bader (AIM) charges were calculated *via* the AIM2000 program⁴⁸.

2.3 Results

The charges calculated for all independent atoms in each four-membered silica ring are shown in Table 2.2 and were used in the calculation of ionicities in all reported graphs unless stated otherwise. All results presented are obtained *via* single point DFT calculations. The ionicity measure employed between two bonded atoms A and B is derived from the respective calculated Mulliken, Hirshfeld or Bader atomic charges via the equation

$$\mathcal{K}_{A-B} = \frac{1}{2} \left| \left(\frac{Q_A}{v_A} \right) - \left(\frac{Q_B}{v_B} \right) \right| \quad (2.1)$$

given in³. Q_A is the atomic charge of atom A and v_A is the valence of atom A. It should be noted that this measure of ionicity is dependent only on the magnitudes of the atomic charges, in line with chemical intuition of this concept. This definition of ionicity, as opposed to other possible ionicity measures²⁰, allows us to directly compare various atomic charge-partitioning schemes on an equal footing. The variation in ionicity for a range of all-silica clusters of different geometries and sizes, employing different basis sets and charge partitioning methods is reported below. In each case only the central ring silicon and oxygen atoms of each cluster were used to calculate the ionicities (i.e. oxygen atoms with a directly bonded hydrogen were not included). This choice of

^A The powder diffraction derived crystallographic data for the all-silica form of MTW has relatively large R-factors and a large range of Si-O bond lengths, making the structural parameters less reliable. The respective MTW data is, thus, highlighted in each plot by open data-points.

atoms better reflects the environment of the atoms in the O-Si-O and Si-O-Si embedded atoms found in the corresponding extended all-silica zeolites.

	Si1			Si2		
	Q _M	Q _H	Q _B	Q _M	Q _H	Q _B
Ref	1.117	0.513	3.262	1.110	0.512	3.265
CHA	1.070	0.501	3.326	1.081	0.509	3.326
FAU	1.105	0.511	3.320	1.078	0.503	3.321
IFR	1.056	0.489	3.341	1.094	0.506	3.322
ISV	1.020	0.519	3.308	1.020	0.519	3.308
ITE	1.119	0.509	3.310	1.120	0.514	3.308
MTW	0.971	0.484	3.355	1.047	0.512	3.332
RTE	1.106	0.511	3.311	1.114	0.512	3.314
Coesite	1.133	0.500	3.325	1.095	0.503	3.315
Moganite	1.077	0.502	3.313	1.099	0.509	3.314

	O1			O2			O3		
	Q _M	Q _H	Q _B	Q _M	Q _H	Q _B	Q _M	Q _H	Q _B
Ref	-0.619	-0.296	-1.647	-0.619	-0.296	-1.647	-0.634	-0.314	-1.662
CHA	-0.535	-0.281	-1.658	-0.575	-0.307	-1.671	-0.562	-0.300	-1.670
FAU	-0.578	-0.305	-1.675	-0.541	-0.287	-1.661	-0.575	-0.296	-1.661
IFR	-0.596	-0.320	-1.668	-0.590	-0.319	-1.672	-0.562	-0.300	-1.663
ISV	-0.476	-0.262	-1.689	-0.476	-0.262	-1.689	-0.440	-0.257	-1.649
ITE	-0.583	-0.304	-1.661	-0.583	-0.304	-1.661	-0.593	-0.313	-1.670
MTW	-0.488	-0.288	-1.677	-0.488	-0.288	-1.677	-0.585	-0.322	-1.671
RTE	-0.567	-0.276	-1.660	-0.567	-0.276	-1.660	-0.599	-0.314	-1.655
Coesite	-0.590	-0.300	-1.669	-0.590	-0.300	-1.669	-0.600	-0.316	-1.655
Moganite	-0.584	-0.295	-1.657	-0.584	-0.295	-1.658	-0.565	-0.296	-1.663

Table 2.2 Atomic charges for each of the four-ring fragments (Q_m is the Mulliken atomic charge, Q_H the Hirshfeld atomic charge, and Q_B the Bader atomic charge (6-31G* basis-set)).

2.3.1 Basis-Set Dependency

Mulliken, Hirshfeld and Bader atomic charges calculated over the central silicon and oxygen atoms of an ITE four-membered ring are given in Table 2.3. The charges were calculated using the electron density obtained from the DFT calculations for a series of four different basis sets (3-21G, 6-31G, 6-31G*, 6-31G**). The trends observed for the ITE silica ring were found to be representative of all silica clusters calculated.

		Si1	Si2	O2	O3
3-21G	Q _M	1.665	1.660	-0.900	-0.925
	Q _H	0.588	0.591	-0.346	-0.358
	Q _B	3.387	3.379	-1.719	-1.738
6-31G	Q _M	1.715	1.703	-0.917	-0.949
	Q _H	0.584	0.588	-0.312	-0.354
	Q _B	3.228	3.218	-1.632	-1.653
6-31G*	Q _M	1.119	1.120	-0.583	-0.593
	Q _H	0.509	0.514	-0.304	-0.313
	Q _B	3.310	3.308	-1.661	-1.670
6-31G**	Q _M	1.115	1.118	-0.581	-0.591
	Q _H	0.512	0.517	-0.304	-0.312
	Q _B	3.311	3.308	-1.663	-1.672

Table 2.3 Basis-set dependency for the ITE four-ring.

The first point to note is the marked difference between the three different charge-partitioning methods in the magnitude of the predicted charges of the silicon and oxygen atoms. All methods give the same sign of the charge for the corresponding atom type, but the Mulliken charges are between two to three times larger than the Hirshfeld atomic charges, and the Bader charges, in turn, over twice as big as the Mulliken charges depending on the basis set used.

The Mulliken charges are, as expected from literature^{4,5}, strongly dependent on the basis set used in the calculations, decreasing on average by 0.55 |e| (-33%) and 0.33 |e| (-36%) for the silicon and oxygen charges from the smallest to the largest basis set description. From the silicon/oxygen charge balance, it may be expected that this change in absolute magnitude of the atomic charges should be equal in both cases, thereby, maintaining charge neutrality. However, there is a moderate difference since the terminal hydroxyl groups are not included in this charge balance.

The Hirshfeld and Bader charges are much less sensitive to the choice of basis sets, inclusion of polarisation functions on the silicon and oxygen atoms having a small, yet still marked effect. The silicon and oxygen charges decrease each by a similarly modest amount 0.07 |e| (-13%) and 0.04 |e| (-12%) for Hirshfeld, and 0.07 |e| (-2%) and 0.06 |e| (-4%) for Bader respectively, when going from the smallest to the largest basis set. For all schemes, the largest component in this overall change arises when going from a non-polarisation basis set description (3-21G/6-31G) to basis sets where d polarisation functions are included on all the silicon and oxygen atoms (6-31G*). The effect of also adding an extra p function to the terminating hydrogen atoms has

relatively little influence on the predicted central ring atomic charges. The effect of polarisation functions on calculated atomic charges has been described previously^{4,18} and is caused by the extra spatial degrees of freedom for the electron density introduced by the d-functions, giving a better description of the Si-O bond. This is especially true for the relatively larger, more polarisable, oxygen-centred electron density. The treatment of oxygen as a polarisable species has also been found to be beneficial in classical models of siliceous materials *via* the use of shell models⁴⁹. The Si-O ionicity, $\kappa_{\text{Si-O}}$, which can be calculated easily from the charges derived from the three different partitioning methods is also found to simply follow the same basis-set-dependent trends observed for the actual charges. Considering the above, the 6-31G* basis set was used in all subsequent calculations.

2.3.2 Finite-Size effects

Ideally one should use the electron density from fully periodic DFT calculations on the respective zeolite crystals to obtain the atomic charges. However, since calculations on such systems are still rather demanding computationally, hydroxyl-terminated clusters were used. To estimate the error generated by taking clusters instead of the fully periodic lattice, five larger silica fragments based around a four-ring core were also studied. These clusters differ from the original silica four-membered rings in that every silicon atom in the original ring is now linked to at least one further silicon atom before terminating in a hydroxyl group, giving a second embedding “coordination sphere” around the original rings and increases the number of atoms in the cluster by approximately five times. An example of a larger cluster used, for ITE, can be seen in Fig. 2.2.

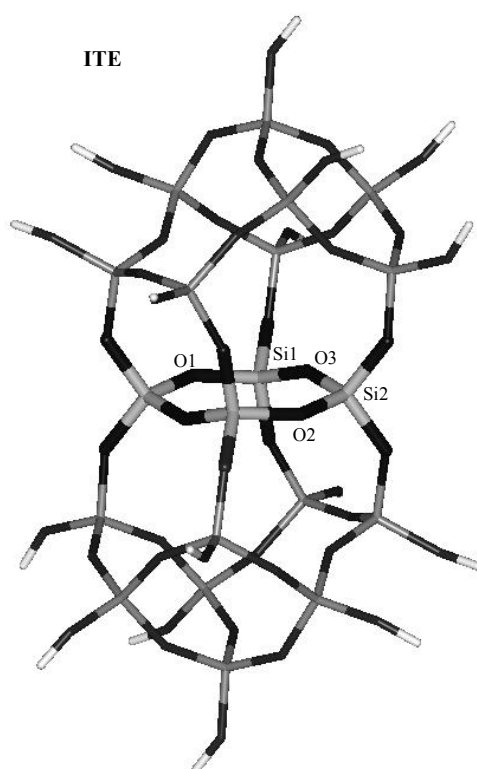


Figure 2.2 Example of a larger structural fragment (from the ITE framework) used in the finite-size calculations. The smaller “embedded” ITE four-ring is highlighted with thicker bonds.

Table 2.4 shows the change in the calculated atomic charges for, both, the original atoms in the four-ring and the relevant atoms in the larger embedded fragment for the both Mulliken and Hirshfeld charge-partitioning methods. The effects of cluster size on the magnitude of the Bader charges is not reported due to the very significant computational expense of the calculations, but is assumed to be similar to the reported small shifts for both Mulliken and Hirshfeld charges. From the tabulated data it can be seen that the calculated atomic charges in the ring, upon increasing the cluster size, are consistently shifted for each partitioning method. This shift however, is found to be rather small being on average -0.027 $|e|$ for the oxygen atoms and 0.065 $|e|$ for the silicon atoms using Mulliken partitioning and 0.052 $|e|$ and 0.012 $|e|$ respectively when using Hirshfeld partitioning. The change in the ionicities calculated from these shifted charges can be examined *via* the crossed data-points on each graph lying vertically above the data points of the smaller clusters. Importantly, there is little change in going to larger silica clusters in the trends observed for the smaller silica four-rings, showing

that the effects of cluster size play little part in determining reliable values of the atomic charges and ionicities, thus, further justifying the chosen cluster approach. This conclusion is further strongly confirmed by comparison with fully periodic DFT calculations on the all-silica form of Mordenite¹⁰ which give Hirshfeld atom charges of 0.57 |e| on silicon and -0.28 |e| on oxygen in excellent agreement with our average large cluster Hirshfeld values of 0.56 |e| and -0.28 |e| respectively, showing that the charges, and thus the derived ionicities, are close to their saturated periodic values for the clusters employed.

		Si1	ΔQ	Si2	ΔQ	O1	ΔQ	O2	ΔQ	O3	ΔQ
Mulliken	CHA	1.121	0.051	1.127	0.046	-0.540	-0.005	-0.606	-0.031	-0.582	-0.020
	FAU	1.158	0.053	1.148	0.070	-0.613	-0.036	-0.549	-0.008	-0.588	-0.013
	ITE	1.150	0.031	1.202	0.082	-	-	-0.609	-0.133	-0.631	-0.037
	MTW	1.071	0.100	1.124	0.077	-0.507	-0.019	-0.507	0.076	-0.628	-0.043
	RTE	1.174	0.068	1.186	0.072	-0.568	-0.002	-0.568	-0.081	-0.631	-0.031
Hirshfeld	CHA	0.562	0.061	0.560	0.051	-0.280	0.001	-0.288	0.019	-0.284	0.015
	FAU	0.558	0.048	0.560	0.057	-0.285	0.020	-0.278	0.009	-0.286	0.009
	ITE	0.558	0.049	0.561	0.047	-	-	-0.289	0.016	-0.291	0.021
	MTW	0.534	0.049	0.562	0.050	-0.279	0.009	-0.279	0.009	-0.300	0.022
	RTE	0.561	0.050	0.565	0.054	-0.278	-0.001	-0.278	-0.001	-0.290	0.025

Table 2.4 Partitioned atomic charges for large fragments and charge difference (ΔQ) between large and small fragments (6-31G* basis set).

2.3.3 Geometric Effect on Ionicity

Previous research has hinted on strong correlations between atomic charges and geometrical parameters of the zeolite¹⁴. Since atomic charges and ionicities are strongly connected with each other, we will explore the influence of geometry on the ionicity of bonds. The most important local geometric parameters in determining the long-range structure of all-silica materials are generally believed to be strongly linked to the Si-O bond lengths and the Si-O-Si angles. The O-Si-O angles, however, are often assumed to be relatively constant within silicon-centred rigid tetrahedra, a model which has found much success in describing the topologies and physical properties of numerous silica polymorphs^{50,51}. Following this proven philosophy, we have derived ionicities of all independent bonds within all the four-membered silica rings (shown in fig. 2.1 and 2.2, employing equation 2.1, using atomic charges calculated from the Mulliken, Hirshfeld and Bader partitioning methods) and calculated the values as a function of, both, Si-O bond length and Si-O-Si angle.

Fig. 2.4a-c shows how the calculated ionicity varies with Si-O bond length for each of the charge partitioning methods. In each case there is evidence of a strong correlation between Si-O bond length and ionicity of the respective bond. As for the calculated atomic charges (see table 2.2), for each charge-partitioning scheme the derived ionicities differ considerably in magnitude. It is to be noted that both Hirshfeld and Bader schemes, the best performing partitioning methods with respect to reproducing physical observables, give almost opposite predictions for the ionicity of the Si-O bonds (Bader : ~ -0.83 , Hirshfeld ~ -0.14). Mulliken analysis gives Si-O ionicities, according to equation 1, of a magnitude between these extremes (~ 0.28). Both, Hirshfeld and Mulliken methods show an increasing trend in ionicity with increasing Si-O bond length with the ionicities increasing by ~ 0.06 and ~ 0.035 respectively over the same range of Si-O bond lengths ($1.546 \text{ \AA} - 1.660 \text{ \AA}$). Over this bond length range, ionicities derived from Bader-partitioned atomic charges show a small decreasing trend of 0.019 in ionicity. It is noted that the trends observed for the silicon charges follow those of the respective ionicity trends.

Unlike the bond length plots, the change in ionicity with respect to the O-Si-O angle showed no discernible strong trends for any of the charge partitioning methods.

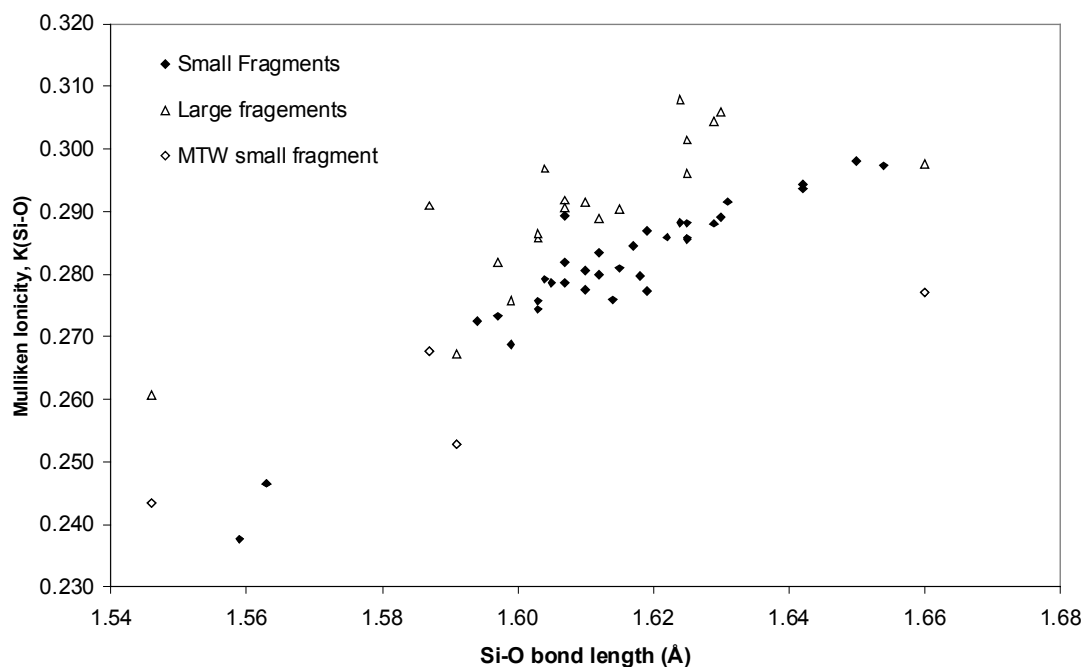


Figure 2.4 a. Calculated Mulliken ionicities versus Si-O bond length for the four-ring fragments. The open triangles indicate the finite size shift in ionicity, each lies vertically above its respective smaller fragment ionicity data point.

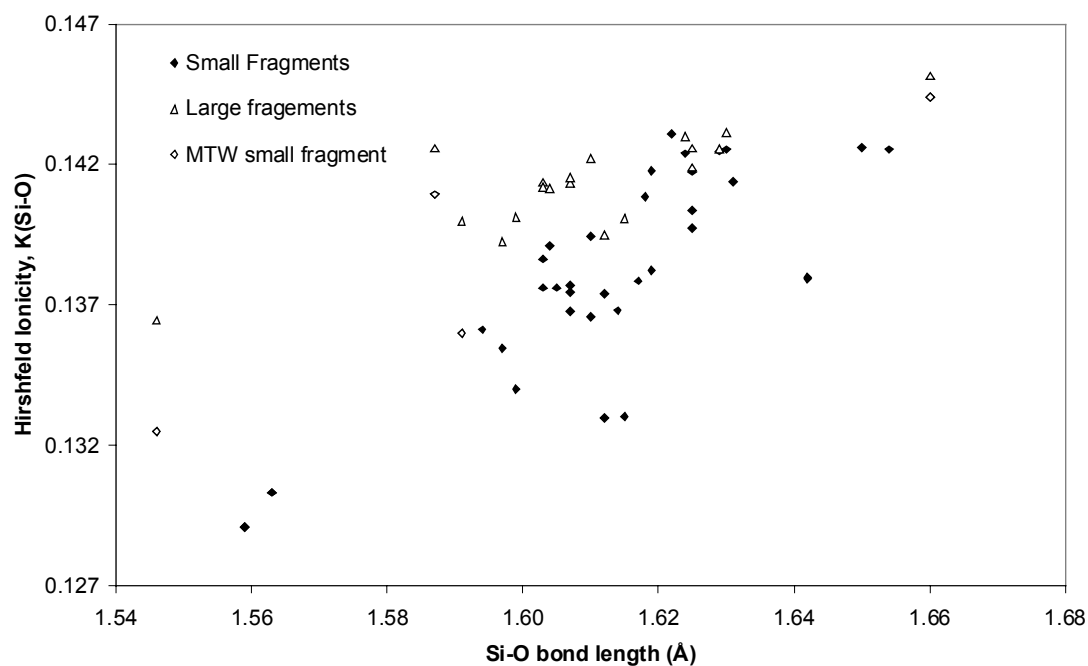


Figure 2.4 b. Calculated Hirshfeld ionicities versus Si-O bond length for the four-ring fragments. The open triangles indicate the finite size shift in ionicity, each lies vertically above its respective smaller fragment ionicity data point.

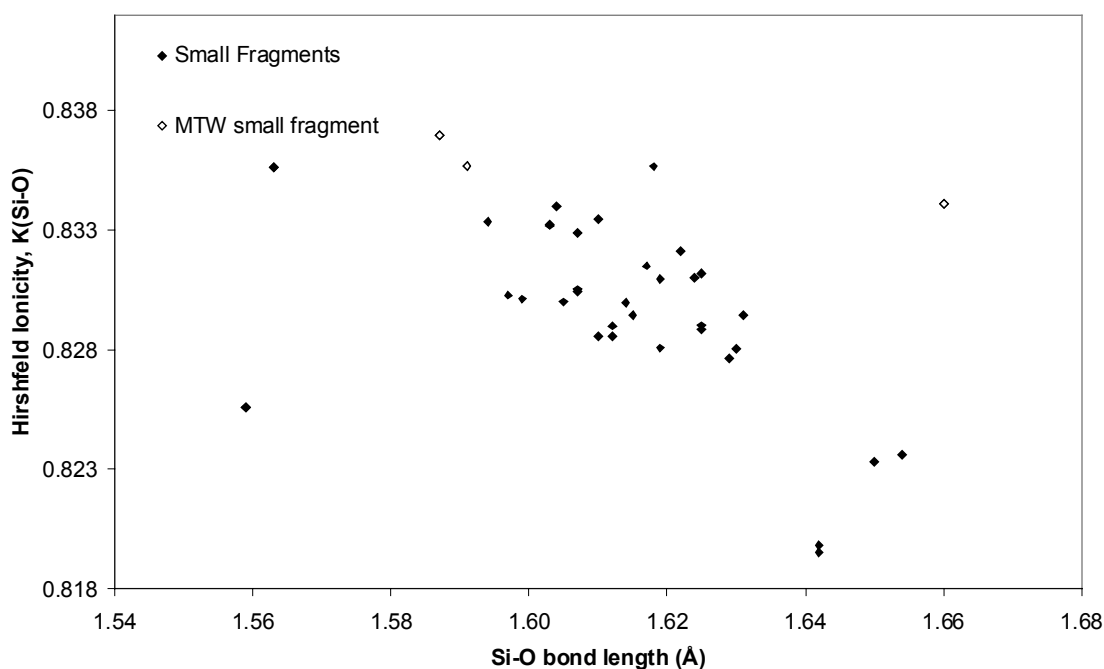


Figure 2.4 c. Calculated Bader ionicities versus Si-O bond length for the four-ring fragments.

2.3.4 Energy and Ionicity.

In Table 2.5, the total calculated energy of each of the four-membered silica ring fragments and the average ionicity of the respective Si-O bonds within each ring is shown. However, due to the small sample of representative Si-O bonds in each fragment, the reported relative energies do not necessarily reflect the energetic stability of each corresponding bulk silica polymorph. On the other hand, as each finite fragment represents the same structural unit in each polymorph, each four-ring cluster, via its geometry, gives an approximate comparative measure of the global, crystal-morphology-induced distortion away from its fully relaxed state. In this way we can imagine that for example fragments with relatively shorter Si-O bond-length are representations of relatively more compressed global topologies of the host silica material and fragments with longer Si-O bonds are representing more relaxed bulk structures. While a one to one correlation between ionicity and bulk energy is, thus, not to be expected, it is nevertheless interesting to note that for Mulliken and Hirshfeld analyses a tendency is observed for the energy of the fragment to increase with decreasing average ionicity along with the corresponding inverse tendency for Bader derived ionicities (see Table 2.5). We also compare published experimental heat of

formation data⁵² to ionicity and see similar, albeit less pronounced, tendencies. The corresponding data for Mulliken and Bader analysis is shown more clearly in Figures 2.5a, 2.5b.

	Total Energy (Ha)	Relative Energy (kcal/mol)	Average ionicity, $\kappa_{\text{Si-O}}$			$\Delta H_{\text{trans}}^{298}$ (kcal/mol)
			Mulliken	Hirshfeld	Bader	
4-RING	-2066.23428	0.00	0.296	0.140	0.822	-
Moganite	-2066.17144	39.40	0.280	0.137	0.829	0.81
ITE	-2066.15765	48.05	0.287	0.141	0.830	2.41
FAU	-2066.15711	48.39	0.278	0.137	0.831	3.25
RTE	-2066.15481	49.83	0.285	0.138	0.829	-
CHA	-2066.14410	56.55	0.274	0.137	0.832	2.72
Coesite	-2066.13648	61.33	0.288	0.140	0.830	0.70
IFR	-2066.12894	66.06	0.279	0.140	0.833	2.39
MTW	-2066.12738	67.04	0.260	0.138	0.836	2.08
ISV	-2066.06126	108.50	0.242	0.130	0.831	3.44

Table 2.5 Total energy of the cluster and experimental relative framework enthalpy⁵² versus average cluster ionicity (6-31G* basis set).

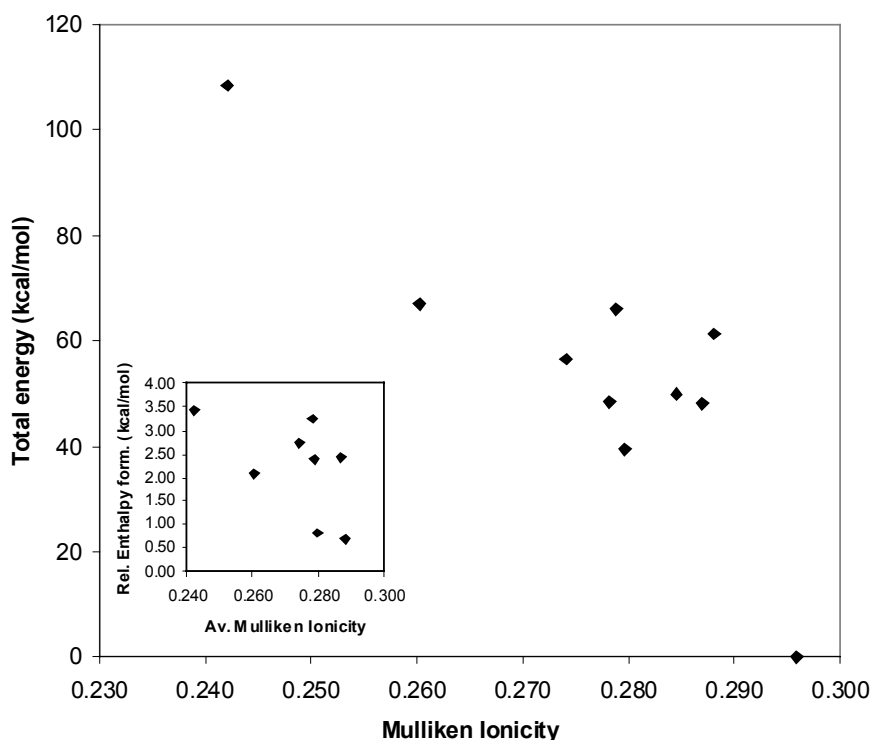


Figure 2.5 a. Average Mulliken ionicities versus total calculated energy of the fragments (inset shows average Mulliken ionicity versus experimental heat of formation data⁵² for all-silica crystals).

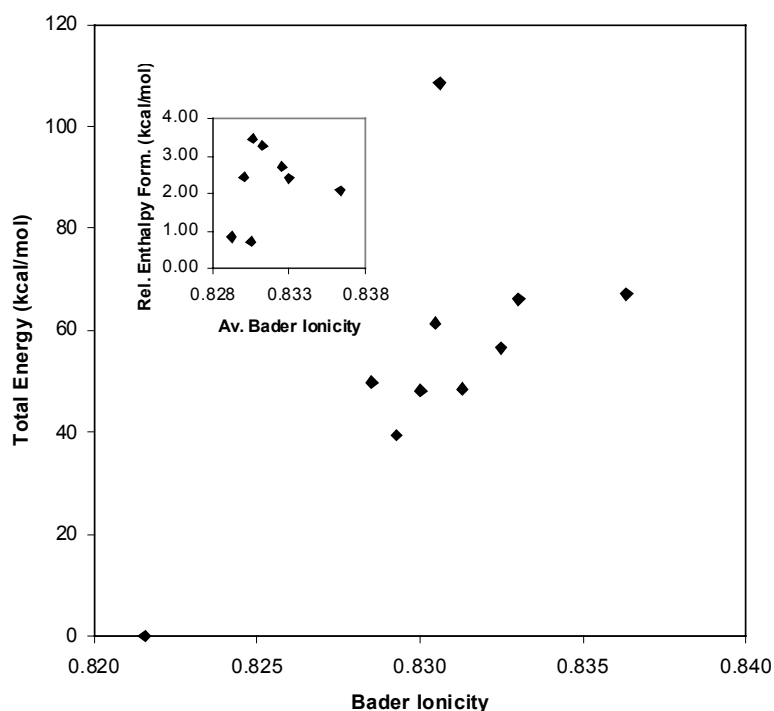


Figure 2.5 b. Average Bader ionicities versus total calculated energy of the fragment (insert shows average Bader ionicity versus experimental heat of formation data⁵² for all-silica crystals).

The lowest energy reference structure is the relaxed ring with the majority of the rest of the ring fragments lying between 39.4 and 67 kcal/mol higher in energy. The ISV fragment is found to be, by far, the highest energy structure lying 108.5 kcal/mol above the relaxed four-ring energy. This high energy is probably due to its rather distorted structure (see Table 2.1), which in turn is probably due to it being part of a unique double-four-ring strained configuration within the zeolite crystalline ISV structure. The MTW structure is also found to be relatively high in energy with respect to the relaxed 4-ring, which may again be indicative of some inaccuracies in the powder diffraction crystal structure.

2.3.5 Laplacian at the Bond Critical Point

An alternative measure of ionicity is the Laplacian of the electron density at the bond critical point ($\nabla^2\rho_{(rc)}$) as defined by Bader²⁰ and commonly used in the understanding of bonding in minerals^{53,54}. Negatively valued Laplacians are indicative of covalent interactions while positive Laplacians are characteristic of closed-shell

(ionic, van der Waals) or “intermediate” type of interactions. Fig. 6 shows the variation of $\nabla^2\rho_{(rc)}$ with Si-O bond length. Normally this type of information is obtained from densities calculated with computationally relatively uneconomical basis sets (6-311++G**). Our test calculations have show that the errors in $\nabla^2\rho_{(rc)}$, when going from a 6-311++G** to a 6-31G* basis set, are smaller than 10% for our system and, thus, the smaller basis sets is used throughout. The insert to figure 2.6 shows that there is a correlation between $\nabla^2\rho_{(rc)}$ and the calculated Hirshfeld ionicity. That such a correlation is shown to exist indicates that both yardsticks describe the same phenomena.

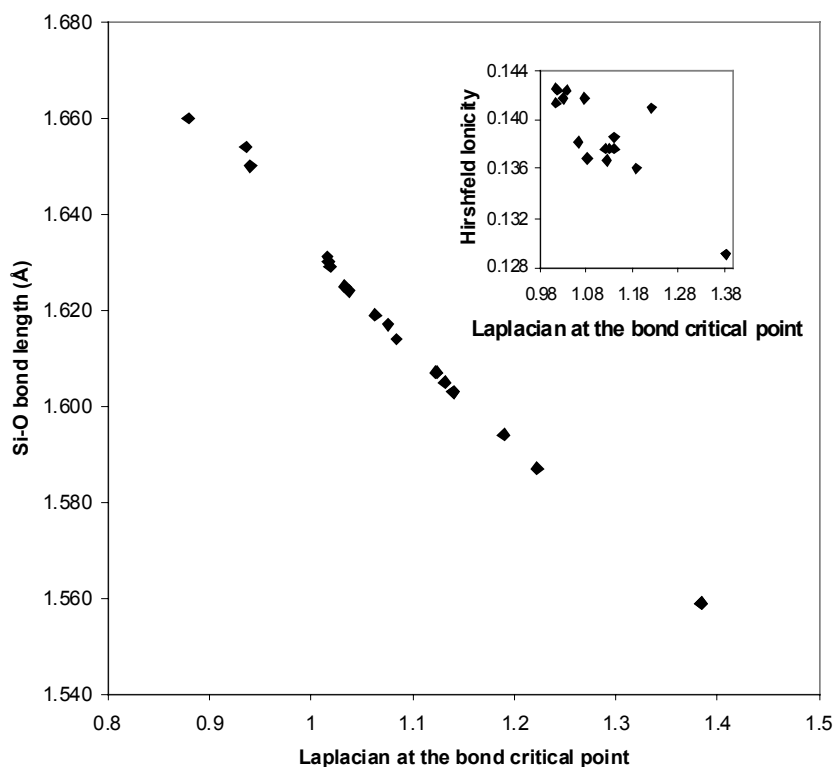


Figure 2.6 Laplacian at the bond critical point ($\nabla^2\rho_{(rc)}$) vs. Si-O bond length (insert shows $\nabla^2\rho_{(rc)}$ vs. Hirshfeld ionicity).

2.4 Discussion

As reviewed in the introduction, the degree of ionicity/covalency of silica materials has been subject to much discussion and speculation due to its fundamental role in the understanding, modelling and practical application of such materials. One of the prime reasons for the lack of clarity in this debate, is due to the fact that different

analysis methods give often conflicting results. From the result of our DFT calculations, Mulliken and Hirshfeld analysis give small atomic charges and equally moderate ionicities, reminiscent of a mainly covalent material with a minor ionic component in the bonding. Bader's atom-in-molecule analysis on the other hand predicts nearly fully charged silicon and oxygen ions and ionicities exceeding 80%, being characteristic of a "classical" ionic solid. Along with these striking differences in the calculated magnitudes of the atomic charges and ionicities for each of the partitioning methods, it is also found that the range of the predicted values for each measure differs considerably.

When comparing our calculated ionicities for each partitioning scheme against variations in the Si-O bond length, correlations were found. For both Mulliken and Hirshfeld analysis we see a tendency for the ionicity to increase with increasing Si-O bond length. Bader analysis on the other hand shows a decrease of ionicity with increasing Si-O bond length. In a previous study by Larin *et al*⁷, using Mulliken analysis with a periodic HF approach on a set of all-silica zeolite structures, a decrease in the silicon charge with an increase in average Si-O bond distance was observed. This would imply that the calculated ionicity would decrease with increase in Si-O bond length in contrast to our Mulliken-based ionicity trend. This difference could be due to a number of factors, but is likely to be due to the contrasting calculation methods and the zeolite structures employed. The DFT methodology employing in this work, although generally of a higher quality than the HF calculation approach *vide supra* should not give significantly different electronic densities and has been independently tested by us *via* a series of cluster HF calculations. The effect of using a cluster rather than a periodic structure has also been validated, with our finite size cluster calculations showing that our larger charge-saturated clusters give the same trends in the ionicities, and only consistent small shifts in atomic charge magnitudes, with respect to our smaller clusters. One rather large and important difference, though, is the size of the basis set employed in each respective set of calculations. It is well known that for oxygen, especially in anisotropic environments typical for siliceous materials, polarisation of the charge density on the oxygen atoms should be allowed for in the basis set⁵⁵. The inclusion of polarisation functions in the basis set, describing the oxygen atoms in silica materials is, thus, essential and has been found by us (see Table 2.3) and others to give a more saturated and accurate description of the oxygen charge

distribution. Larin *et al*^{7,8} did not use such polarisation functions, giving rise to doubt over the accuracy of the calculated charges. It should also be noted that, as opposed to our use of experimental crystallographic data for all atoms in the majority of our calculated silica structural fragments, Larin *et al*^{7,8} used only structures for which the oxygen atom positions were obtained, not from experiment, but from an approximate distance-least-squares procedure.

In an attempt to understand the trends predicted by our calculations, we may imagine the idealised case of an isolated silicon and oxygen atom. Bringing these atoms together will ultimately create a bond between the atoms, but what is less clear in this picture is the relative charge contributions of each atom to the bond. One extreme would be the complete charge transfer from one atom to the other, resulting in an ionic type of interaction, while in the other extreme no charge transfer between the atoms occurs but rather, there is a build up of electron density between the atomic nuclei. The comparative measure of ionicity we employ is a simple technique with which to describe the relative degree of atomic charge transfer throughout the range of possible bond types. The simple fact that there is a variation of ionicity with Si-O bond length, for all partitioning methods, indicates that partial atomic charge transfer occurs, showing that the interaction between the atoms is more than purely electrostatic.

The bond lengths of each crystalline silica material included in our study are all slightly shorter than those found in the relaxed-four-ring reference structure, due to them being in a state of natural bulk-induced compression. The range of Si-O bonds to be described is, thus, one of contracted lengths (with respect to the equilibrium distance). Simple electrostatic considerations suggest that shortening the inter-nuclear distance will lead to a progressive deepening of the potential well between the two atoms, increasing the chance of the electron to be found between the atoms rather than close to only one. This crude model for the electron distribution, comparable to the H_2^+ ion, leads to the prediction that ionicity will decrease with decreasing bond lengths as found for both Mulliken and Hirshfeld analyses.

While our simple model of the electron distribution in a heteronuclear bond explains the trends found for both Mulliken and Hirshfeld analyses, it can not explain the reverse trend as found in Bader analysis. The key to this problem rests in the fundamental differences between the partitioning schemes. Mulliken analysis disregards the details of the topology of the electron density between the two atoms and simply

divides it equally between the two atoms. Hirshfeld charges are also relatively insensitive to the details of electron density distribution between the atoms as the method biases its weighted charge density partitioning to the density closest to the respective atomic nuclei. Bader's method on the other hand is very sensitive to the density variations between the atoms, because the partitioning is based upon finding the minima in the electron density ($\nabla\rho=0$) along the inter-nuclear axis. The effects of polarisation of the density between the atoms are, thus, included in the Bader charges, while being neglected in Mulliken and, to a lesser degree, in Hirshfeld charges. This inclusion of polarisation though gives, as noted above, rather large integrated atomic charges in the Bader-scheme. If these charges were interpreted as classical coulombic atomic-centred charges, silica would be expected to have physical properties characteristic of strongly ionic compounds e.g. dense closed-packed structures, high atomic-coordination numbers, and a low number of polymorphs which are not observed in siliceous materials^{56,57}. This relationship between coordination number and ionicity has been made explicit in both experimental and theoretical studies^{1,58} of other materials using as a reference point an ionicity measure, due to Phillips⁵⁹ based on a dielectric model of the chemical bond. The Phillips ionicity of α -quartz (0.572⁵⁶) lies between that obtained from Bader and Mulliken charges and is one of the lowest for oxides^{1,58}. This relatively low ionicity for silica together with its low coordination is also consistent with the division between high and low coordination compounds based on the Phillips scale^{58,59}. While the Phillips ionicity values can't be used to discriminate between our results based on the different charge analysis schemes, they seem to support the fact that silica has a moderate ionicity, thus indicating further that the obtained Bader ionicities are too high. From a more practical point of view Mulliken and Hirshfeld methods predict charges which are much more inline with the observed structural properties and are, thus, more suitable than Bader charges for applications in which the electrostatic interactions are modelled as pure point charges, as for instance in the development of force fields.

For silica we have demonstrated that the absolute magnitude of Mulliken-derived atomic charges shows a strong basis set dependency, whilst Hirshfeld charges are more stable. Furthermore Hirshfeld partitioned atomic charges are known, especially in the multipole expansion, to well reproduce physical observables (molecular dipole moments, electrostatic potential). We, therefore, expect that Hirshfeld charges give a

more accurate atomic-charge-based interpretation of the Si-O system. In this respect, it is interesting to note that the Hirshfeld charges, of all the partitioning schemes tested, gives the most covalent description of the Si-O bond.

Our simple model of the heteronuclear bond can now be improved by assuming that the potential well between the atoms is also asymmetric and deeper on the side of the more electronegative element (oxygen). When the inter-nuclear distance is now decreased, the chance of finding an electron between the two atoms rather than close to only one atom is again increased. Furthermore, there is an increased probability of finding an electron in the bond close to the more electronegative element. The model can now explain, both, the trends for Mulliken and Hirshfeld as well as for Bader analyses. When the bond length is decreased, electron density flows from the oxygen atom into the bond, thereby lowering the Mulliken and Hirshfeld ionicities and increasing Bader ionicity due to the polarisation of the bond.

Our model is further supported by the observation that the Laplacian at the bond-critical point is strongly positive ($\nabla^2\rho_{(rc)} > 0.9$) and increases with bond length. The strongly positive Laplacian is indicative of the intermediate interaction type (between ionic and covalent) of bonds²⁰ as can be also found in molecules like formaldehyde and carbon dioxide. The fact that the Laplacian increases with decreasing bond length is, as with our calculated Bader ionicities, a sign of increasing polarisation of the electron density between the atomic nuclei. Furthermore, we find the Hirshfeld ionicity and the Laplacian at the bond critical point to be correlated (see figure 2.6) and to be describing the same phenomena as suggested in our model.

In a similar way that individual Si-O bond lengths correlate with the degree of Si-O bond ionicity, there also appears to be an intriguing consistent tendency for the energetic stability of each fragment, and potentially its respective host crystal, to correlate with the *average* Si-O ionicity. Although with our small representative sample of Si-O bonds a strong statistical correlation is not to be expected, the results are suggestive of a tantalising link between global energetic stability of siliceous material frameworks and a fundamental property of the constituent Si-O bonds. Such a link may help to explain the correlations between the measured enthalpy of formation and framework density as observed by Piccione *et al*⁵² for all-siliceous materials.

2.5 Conclusions

Our investigation has shown that the cluster approach, using high level DFT calculations and a comparative atomic-charge-based ionicity measure, can give useful insight into the fundamental properties of all-silica materials. In particular, we have shown that the complex procedure of assigning the appropriate description of the Si-O bonds in these materials is largely dependent on the method of charge partitioning analysis employed. The reasons for these differences are discussed, with the degree of polarisability of the oxygen-centred charge density being shown to be particularly important. Irrespective of the diversity in predicted ionicities and charges, we have shown how the trends from each method may be reconciled within a simple model. For a chemically intuitive atomic charge-based interpretation of the ionicity of siliceous materials Hirshfeld charges are shown to be preferred over Bader and Mulliken charges. Correlations between the individual Si-O bond lengths and individual bond ionicity are observed for all atomic charge partitioning schemes. Our results also suggest that average Si-O ionicity may be linked to the energetic stability of all-siliceous frameworks.

References

- 1 Catlow C. R. A., Stoneham A. M. *J. Phys. C: Solid State Phys.* **1983**, 16, 4321.
- 2 Pauling L. *Am. Miner.* **1980**, 65, 321.
- 3 Chulviken N.D., Zhidomirov V.B. *Kinet. Katal.* **1977**, 18, 903.
- 4 Wiberg K.B., Rablen P.R. *J. Comp. Chem.* **1993**, 14, 1504.
- 5 Bachrach S.M. In *Reviews in Computational Chemistry* vol. 5; Lipkowitz K.B., Boyd D.B., VCH: New York, U.S., 1994.
- 6 White J.C., Hess A.C. *J. Phys. Chem.* **1993**, 97, 8703.
- 7 Larin A.V., Vercauteren D.P. *Int. J. Inorg. Mater.* **1999**, 1, 201.
- 8 Larin A.V., Leherste L., Vercauteren D.P. *Chem. Phys. Lett.* **1998**, 287, 169.
- 9 Pereira J.C.G., Catlow C.R.A., Price G.D. *J. Phys. Chem.* **1999**, 103, 3252
- 10 Kessi A., Delley B. *Int. J. Quantum Chem.* **1998**, 68, 135.
- 11 Elcombe M.M. *Proc. Phys. Soc.* **1967**, 91, 946.
- 12 Barron T.H.K., Huang C.C., Pasternak A. *J. Phys. C* **1976**, 9, 3925.
- 13 Striefler M.E., Barsch G.R. *Phys. Rev. B* **1975**, 12, 4553.
- 14 Smirnov K.S., van de Graaf B. *J. Chem. Soc. Faraday Trans.* **1996**, 92, 2475.
- 15 Pantelides S.T., Harrison W.A. *Phys. Rev. B* **1976**, 13, 2667.
- 16 Mulliken R.S. *J. Chem. Phys.* **1955**, 23, 1833.
- 17 Hirshfeld F.L. *Theor. Chim. Acta (Berl.)* **1977**, 44, 129.
- 18 Rousseau B., Peeters, A., Van Alsenoy C. *Chem. Phys. Lett.* **2000**, 324, 189.
- 19 Nalewajski R.F., Parr R.G. *Proc. Natl. Acad. Sci.* **2000**, 97, 8897.
- 20 Bader, R.F.W. *Atoms in Molecules - A Quantum theory*; Oxford University Press; Oxford, U.K., 1990.
- 21 Vitiello M., Lopez N., Illas F., Pacchioni G. *J. Phys. Chem. A* **2000**, 104, 4674.
- 22 Sauer J. *Chem. Rev.* **1989**, 89, 199.
- 23 Boronat M., Zicovich-Wilson C.M., Corma A., Viruela P. *Phys. Chem. Chem. Phys.* **1999**, 1, 537.
- 24 Lopez N., Pacchioni G., Maseras F., Illas F. *Chem. Phys. Lett.* **1998**, 294, 611.
- 25 Teunissen E. H., Roetti C., Pisani C., de Man A. J. M., Jansen A. P. J., Orlando R., van Santen R. A., Dovesi R. *Model. Simulation Mater. Sci. Eng.* **1994**, 2, 921.
- 26 Shah R., Gale J. D., Payne M. C. *J. Phys. Chem B* **1997**, 101, 4787.
- 27 Mihaleva V.V., van Santen R.A., Jansen A.P.J. *J. Phys. Chem. B* **2001**, 105, 6874.
- 28 Ricci D., Pacchioni G., Szymanski M. A., Shluger A. L., Stoneham A. M. *Phys. Rev. B* **2001**, 64, 224104.
- 29 Greatbanks S. P., Hillier I. H., Burton N. A., Sherwood P. *J. Chem. Phys.* **1996**, 105, 3770.
- 30 Sauer J., Sierka M. *J. Comp. Chem.* **2000**, 21, 1470.
- 31 Diaz-Cabañas M.J., Barrett P.A., Cambor M.A. *Chem. Commun.* **1998**, 1881.
- 32 Hriljac J.J., Eddy M.M., Cheetham A.K., Donohue J.A., Ray G.J. *J. Solid State Chem.* **1993**, 106, 66.
- 33 Barrett P.A., Cambor M.A., Corma A., Jones R.H., Villaescusa L.A. *Chem. Mater.* **1997**, 9, 1713.
- 34 Villaescusa L.A., Barret P.A., Cambor M.A. *Angew. Chem. Int. Ed.* **1999**, 38, 1997.
- 35 Cambor M.A., Corma A., Lightfoot P., Villaescusa L.A., Wright P.A. *Angew. Chem. Int. ed.* **1997**, 36, 2659.
- 36 Fyfe C.A., Gies H., Kokatailo G.T., Marler B., Cox D.E. *J. Phys. Chem.* **1990**, 94, 3718.
- 37 Marler B., Grünewald-Lüke A., Gies, H. *Microporous Mesoporous Mater.* **1998**, 26, 49.
- 38 Araki T., Zoltai T. *Z. Kristallogr.* **1969**, 129, 381.
- 39 Heaney P.J., Post J.E. *Am. Mineral.* **2001**, 86, 1358.
- 40 Becke A.D. *J. Chem. Phys.* **1993**, 98, 5648.
- 41 Lee C., Yang W., Parr R.G. *Phys. Rev. B* **1988**, 37, 785.
- 42 Frisch M.J. *Gaussian 98*, Revision A.9, Gaussian, Inc.: Pittsburgh PA, 1998.
- 43 Binkley J.S., Pople J.A., Hehre W.J. *J. Am. Chem. Soc.* **1980**, 102, 939.
- 44 Gordon M.S., Binkley J.S., Pople, J.A., Pietro W.J., Hehre W.J. *J. Amer. Chem. Soc.* **1982**, 104, 2797.
- 45 Dobbs K.D., Hehre W.J. *J. Comp. Chem.* **1986**, 7, 359.
- 46 Dobbs K.D., Hehre W.J. *J. Comp. Chem.* **1987**, 8, 861.
- 47 Dobbs K.D., Hehre W.J. *J. Comp. Chem.* **1987**, 8, 880.
- 48 AIM2000, version 1.0, University of Applied Sciences: Bielfeld, 1998.
- 49 Catlow C.R.A., Freeman C.M., Islam M.S., Jackson R.A., Leslie M., Tomlinson S.H. *Philosophical Magazine A*, **1988**, 58, 123.
- 50 Hammonds K.D., Heine V., Dove M.T. *J. Phys. Chem. B* **1998**, 102, 1759.
- 51 Hobbs W., Jeresum C.E., Pulim V., Berger B. *Philosophical Magazine A*, **1998**, 78, 679.

- ⁵² Piccione P.M., Laberty C., Yang S., Cambor M.A., Navrotsky A., Davis M.E. *J. Phys. Chem. B* **2000**, 104, 10001.
- ⁵³ Silvi B., Savin A., Wagner R.F. In *Modelling of Minerals and Silicated Materials*; Silvi B., D'Arco P., Kluwer Academic Publishers: Dordrecht, The Netherlands, 1997.
- ⁵⁴ Gibbs G.V., Hill F.C., Boisen Jr. M.B. In *Modelling of Minerals and Silicated Materials*; Silvi B., D'Arco P. Kluwer Academic Publishers: Dordrecht, The Netherlands, 1997.
- ⁵⁵ Nedelec J.M., Hench L.L. *J. Non-Cryst. Solids* **2000**, 277, 106.
- ⁵⁶ Engel G.F., Defregger S. *Phys. Stat. Sol. B* **1991**, 163,389.
- ⁵⁷ Lucovsky G. *J. Non-Cryst. Solids* **2002**, 303, 40.
- ⁵⁸ Christensen N.E., Satpathy S., Pawlowska Z. *Phys. Rev. B* **1987**, 36, 1032
- ⁵⁹ Phillips J.C. *Rev. Mod. Phys.* **1970**, 42, 317

Fully coordinated silica nanoclusters: $(\text{SiO}_2)_N$ molecular rings and beyond

Abstract

A new form of finite silica with edge-sharing SiO_2 units connected in a ring is proposed. High-level density functional calculations for $(\text{SiO}_2)_N$ $N=4-14$ show the rings to be energetically more stable than the corresponding $(\text{SiO}_2)_N$ linear chains for $N>11$. The rings display frequency modes in remarkable agreement with infrared (IR) bands measured on dehydrated silica surfaces indicating their potential as models of strained extended silica systems. Silica rings may also be useful precursors for new bulk silica polymorphs with tubular or porous morphologies.

The contents of this chapter have been published in:

Bromley S.T., Zwijnenburg M.A., Maschmeyer T. Phys. Rev. Lett **2003**, 90, 035502.

Bromley S.T., Zwijnenburg M.A., Flikkema E., Maschmeyer T. Phys. Rev. Lett **2004**, 92, 039602.

3.1 Introduction

The discovery of well-defined fully-coordinated carbon nanoclusters^{1,2,3} and nanotubes^{4,5} (Fullerenes) and their fascinating novel properties has stimulated great interest in the synthesis of their inorganic analogues. The interest in the preparation of such materials resulted amongst other things in the synthesis of boron carbide⁶, boron nitride^{7,8,9}, tungsten sulfide¹⁰ and molybdenum sulfide¹¹ nanoclusters and -tubes. The work on nano-silica however has been limited to very small charged clusters¹²⁻¹⁵ and ill-defined amorphous nanoparticles¹⁶⁻¹⁸. In this chapter a computational investigation into fully-coordinated silica nanoclusters in the form of a two-ring based $(\text{SiO}_2)_N$ rings (see figure 3.1) is reported, focussing on the relationship between the finite-size, the thereby induced strain and the energetics and reactivity of the nanoclusters.

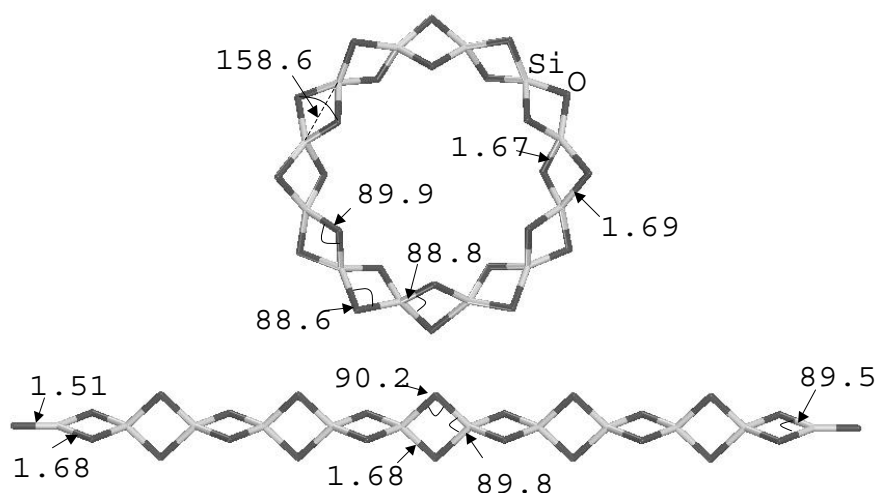


Figure 3.1. Structures of the $N = 12$ $(\text{SiO}_2)_N$ molecular ring and chain. Bond lengths are in Å, angles in degrees.

Recent experimental and theoretical studies have provided a wealth of evidence confirming that two-rings exist at the surface of amorphous and dense crystalline silica, as well as within silica thin films and bulk silica¹⁹⁻²⁵. Two-rings at silica surfaces form, at moderate temperatures (800 K), from the condensation of pairs of vicinal hydroxyl groups. These two-ring defects are known to be strained reactive species and are readily reversibly hydrolysed^{19,20}. At higher temperatures (1400-1700 K), in the absence of

water, thermodynamic rearrangement of the pure silica structure favours the formation of two-rings at the surface^{22,23}. The elevated temperatures of this process cause the surface to be more flexible and potentially allows for more stable two-rings to form within a relaxed environment. The formation of two-rings via this process is probably energetically favoured over forming reactive non-bridging oxygen (NBO) surface defect sites, and also entropically, due to the restrictive two-dimensional surface layer, making large surface-rings unlikely. As with the thermally driven formation of two-rings on the two-dimensional surface of silica, high temperatures can also be used to synthesise one-dimensional silica structures with edge-sharing units. Combining more than one SiO_2 unit as to only have edge-sharing gives rise to chains of two-rings, as shown in figure 3.1. Such chains are predicted to be the most thermodynamically stable form of silica for $(\text{SiO}_2)_N$ ($N=1-6$), being energetically favoured over all other such stoichiometric silica clusters^{26,27}. For larger N , two-ring chains of arbitrary length may be formed in the high temperature synthesis of silica-w²⁸. These examples of two-ring-containing structures show that the energetic disadvantage of strain within two-rings can be outweighed by the energy of their formation and may suggest that edge-sharing may be thermodynamically favoured in environments of reduced dimensions.

3.2 Computational methodology

To investigate the effects of environmental strain on the energetic stability of multi-two-ring silica systems in low-dimensions, high-level DF calculations on $(\text{SiO}_2)_N$ edge-sharing chains and rings were performed. The chains are formed by edge-sharing two-rings terminated at either end by an NBO group. Our proposed molecular rings can be thought of as structures resulting from joining the NBO end-groups of a chain, forming a new two-ring in the process. Unlike the chains, the rings have the novel property of being a fully-coordinated cluster: each oxygen to two silicon atoms and each silicon to four oxygen atoms. Whereas the strain in a linear chain is not expected to vary significantly with N , the interconnectivity of the rings allows us to systematically vary the structural strain by changing the number of SiO_2 units.

For all DF calculations the Becke-type three-parameter hybrid exchange-correlation functional, B3LYP²⁹ was employed. DF calculations have accurately reproduced the properties of silica clusters obtained from both experimental

studies and other high-level MP2 calculations^{26,27}. The B3LYP functional in particular has been successfully employed to elucidate the role of silica clusters in forming Si nanostructures³⁰. Cluster geometries were optimised at the AM1 semi-empirical level and then further at the B3LYP/6-31G*³¹⁻³³ level, imposing no symmetry constraints. For the final optimisations we used a large basis set, including both polarisation and diffuse functions, 6-311+G**³⁴⁻³⁷, to account for oxygen polarisation effects and for an accurate description of strained bonding environments. Each optimised cluster structure was verified to be an energy minimum, having all positive Hessian eigenvalues. Binding energies (BE) were calculated from the difference between the total energy of a cluster, $E_{N\text{-clus}}$, and the energy of the corresponding isolated triplet-state O and Si atoms at the B3LYP/6-311+G(d,p) level. Gaussian 98³⁸ was used throughout.

3.3 Results and discussion

The silica chains were all found to consist of planar two-rings, with each two-ring having a ninety degree orientation relative to its neighbouring rings (each with a very similar geometry regardless of the chain length) see figure 3.1. This alternating structure enables the silicon atoms to be as close as possible to the energetically favoured SiO_4 tetrahedral coordination. At the ends of the chains the terminating NBOs cause small distortions to the peripheral two-rings, with a decreasing effect towards the centre of the chain. For the molecular rings structural distortion is caused by the enhanced internal strain needed to form a fully-coordinated system. We define this "cyclic strain", E_{cyc} , to be distinguished from the intrinsic strain possessed by the constituent two-rings, as the difference between the energy, $E_{\text{ring-formation}}$, consumed or released in deforming a chain to form a single molecular ring, and the energy, $E_{\text{chain-formation}}$, released in forming a chain from two smaller similarly-sized sub-chains (see equations 3.1-3.3).

$$E_{\text{ring-formation}} = E_{N\text{-ring}} - E_{N\text{-chain}} \quad (3.1)$$

$$E_{\text{chain-formation}} = E_{N\text{-chain}} - 2E_{N/2\text{-chain}} \quad (3.2)$$

$$E_{\text{cyc}} = E_{\text{ring-formation}} - E_{\text{chain-formation}} \quad (3.3)$$

The underlying assumption in this Born-Haber cycle estimate is that the energy released in forming a localised two-ring when combining two small chains, E_2 , is similar to that in the corresponding process in joining a suitably bent N-chain. This is supported by examining the main structural consequence of imposing the molecular ring topology i.e. the cyclic strain, which is found, not in the individual two-rings, which stay relatively intact, but in the bending of the links between them. This results in the outer (furthest from molecular ring centre) oxygen atoms being spaced farther from each other relative to the chain oxygens, and the inner (nearest to molecular ring centre) oxygens being relatively closer together, see table 3.1.

	Si-O Outer	Si-O Inner	O-O Outer	O-O Inner	Si-Si	$\angle_{\text{Si-O-Si}}$ Outer	$\angle_{\text{Si-O-Si}}$ Inner	$\angle_{\text{O-Si-O}}$	$\angle_{\text{O-Si-Si-O}}$ Fold
4-R	1.78	1.70	3.56	3.03	2.35	82.4	87.5	82.2	126.0
6-R	1.73	1.67	3.39	2.80	2.35	85.6	89.0	86.2	141.6
8-R	1.70	1.67	3.26	2.78	2.35	87.0	89.2	87.8	149.6
10-R	1.69	1.67	3.18	2.79	2.35	87.9	89.6	88.4	154.9
12-R	1.69	1.67	3.13	2.80	2.36	88.6	89.9	88.7	158.6
14-R	1.69	1.67	3.10	2.81	2.36	89.0	90.1	88.9	161.3
14-C	1.70	1.67	2.90	2.90	2.38	90.5	90.5	89.4	180.0

Table 3.1 N-even (SiO₂)_N ring geometric parameters. Two-ring parameters of the 14-chain are given for comparison. Distances are in Å and (interior) angles in degrees. 'Outer' and 'Inner' refer to the distance from the molecular ring centre.

The cyclic strain in molecular rings also leads to some folding of the two-rings along their Si-Si axes with the two oxygen atoms moving away from the molecular ring centre. The folded two-rings slowly open as the molecular ring size increases, being only 20 degrees from planarity for the 14-ring. The cyclic strain of the molecular rings also manifests itself to a lesser extent in a mismatch between the inner and outer Si-O-Si internal two-ring angles and Si-O bond lengths. The inner Si-O-Si internal two-ring angles are slightly larger than the outer internal two-ring Si-O-Si angles and the inner Si-O bond lengths are slightly smaller than their outer counterparts. The inner and outer Si-O lengths and Si-O-Si angles of the two-rings quickly converge to constant equal values, equivalent to those in the silica chains, as N increases. The (SiO₂)_N molecular rings naturally divide into an N-even set, and an N-odd set. The N-even set all consist of linked structurally-equivalent folded two-rings with a regular alternating orientation pattern giving each N-even ring high rotational symmetry ($D_{N/2d}$), about an axis through

its radial centre, perpendicular to the ring plane. The N-odd set, however, has only C_2 symmetry about an axis within the ring plane through the radial centre, with half of the two-rings being structurally non-equivalent. This division comes about through the ability of the rings to mimic the favoured alternating structure found in the chains. For N-even this is achieved with the opposite orientations of the two-rings at the ends of an N-even chain. For N-odd there is no such match and the ring attempts to distribute this extra cyclic strain throughout the ring. The separation of the two sets of rings due to this mismatch strain can be seen in the E_{cyc} values in table 3.2, the BEs in figure 3.2, and in the energy gap in figure 3.3, where an oscillation between the lower N-even and higher N-odd ring energy scales is observed with varying N.

	4-R	6-R	8-R	10-R	11-R	12-R	13-R	14-R
ΔBE	2.310	0.712	0.229	0.056	0.059	-0.024	-0.015	-0.066
E_{cyc}	3.453	1.474	0.801	0.514	0.473	0.354	0.334	0.260
E_{cyc}/BE	0.274	0.101	0.053	0.033	0.030	0.023	0.021	0.016
$E_{\text{Q} \rightarrow \text{R}}$	4.073	2.094	1.421	1.134	1.093	0.974	0.953	0.880

Table 3.1 Molecular ring energetics (eV/SiO₂). $\Delta\text{BE} = \text{BE}_{\text{N-chain}} - \text{BE}_{\text{N-ring}}$, E_{cyc} = cyclic strain energy, E_{cyc}/BE = ratio of cyclic strain to binding energy, and $E_{\text{Q} \rightarrow \text{R}}$ = formation energy difference between α -quartz and an N-ring.

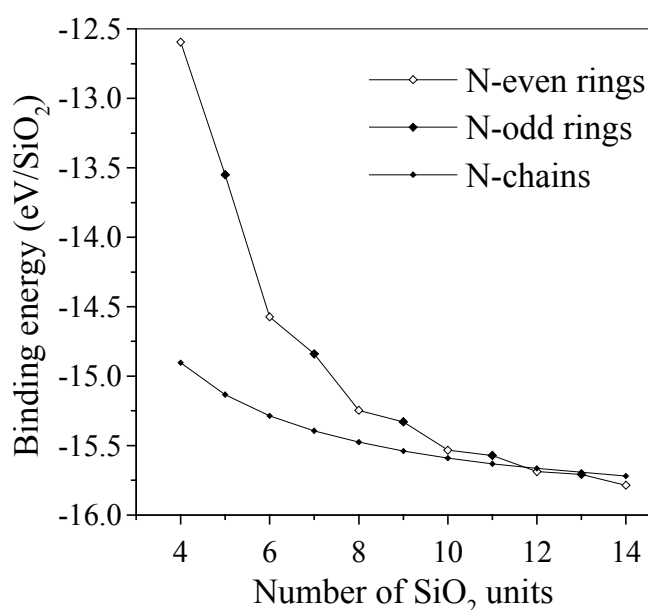


Figure 3.2 Variation of the binding energy of the $(\text{SiO}_2)_N$ molecular rings and chains with N.

Spectroscopically, molecular rings possess IR bands characteristic of their connectedness distinct from those of the chains. Calculated 12-chain harmonic frequencies give prominent modes (866, 915, 838 cm⁻¹), and the 12-ring, three main modes (902, 886, 933 cm⁻¹). The 12-ring modes are in remarkable agreement with experimental IR measurements on dehydrated silica surfaces (908, 888, 932 cm⁻¹)^{19,39,40} strongly indicating their potential use as practical models for strained extended silica systems in an analogous way to modelling silica defects with terminated silica clusters¹³ (see chapter four). The surface-like signature of the rings contrasts with the chains, which also display NBO modes at 1321 cm⁻¹.

For (SiO₂)₃ rings we found that E_{cyc} was too great and that the cluster would spontaneously break into the corresponding chain. For $N > 3$ fully-coordinated molecular rings could always be stabilised, due to the greater stabilisation from the bonding of two terminal NBO-groups relative to the cyclic strain induced in the ring. Moving through $N = 4-14$, we observe a monotonic increase in energetic stability of the molecular rings and chains, see figure 3.2, with a corresponding decrease in the cyclic strain in the rings, see table 3.2. For $N = 4$ the rings are much higher in energy than the chains, with E_{cyc} being over a quarter of the BE per SiO₂ unit. With increasing N , however, the stabilisation rate is greater for the rings than the chains, and, eventually for $N = 12$ the energetic stability of the rings exceeds that of the chains by 0.024 eV/SiO₂, with E_{cyc} being only 1.6 percent of the BE per SiO₂ unit. For additional increases in N , E_{cyc} continues to drop, along with the BE of the rings dropping further below that of the corresponding chains, with both energy scales stabilising at steadily decreasing rates.

By definition, E_{cyc} does not include the intrinsic internal strain of the constituent individual two-rings. The strain energy of a relaxed two-ring has been estimated by numerous high-level calculations in the literature, all giving similar values. Cluster DF calculations using hydrogen-terminated two-rings yield relatively high estimates (0.72 eV/SiO₂⁴¹) but neglect the known stabilising effect of an extended silica bonding environment⁴². Periodic DF calculations on two-rings in a relaxed amorphous silica surface give a value of 0.69 eV/SiO₂²⁴ whilst similar calculations comparing the energy of silica-w to that of the most stable silica polymorph, α -quartz, yield 0.62 eV/SiO₂⁴³. Using the latter value, and adding it to the cyclic strain in our molecular rings, gives an estimate of the formation energy of our rings with respect to α -quartz per SiO₂ unit,

$E_{Q \rightarrow R}$, see table 3.2. E_{cyc} for the smaller molecular rings is found to be much larger than the intrinsic strain of a two-ring giving relatively large $E_{Q \rightarrow R}$ values (for $N < 8$ $E_{Q \rightarrow R} > 1.5$ eV/SiO₂). For $N > 11$ though, where the molecular ring BE is lower than that of the chains, E_{cyc} falls to approximately half the intrinsic two-ring strain yielding, for the 12-ring, $E_{Q \rightarrow R} = 0.97$ eV/SiO₂.

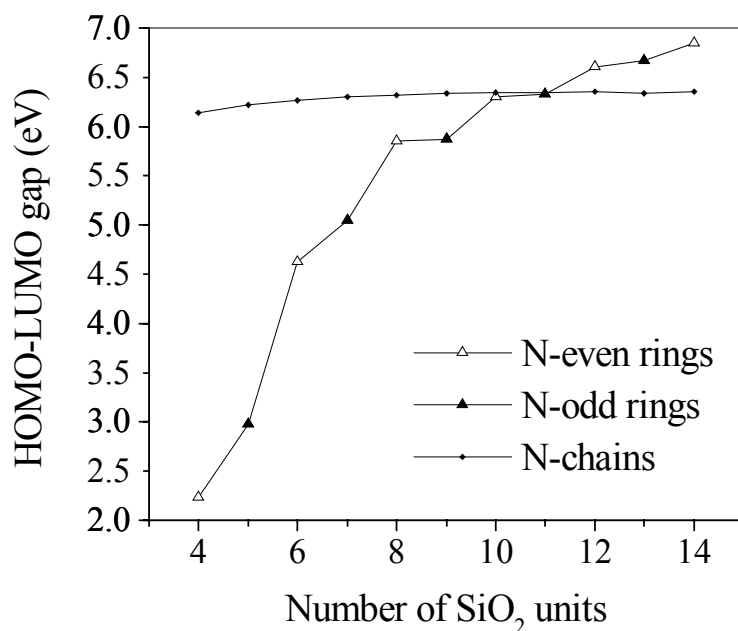


Figure 3.3 Variation of the HOMO-LUMO gap of the (SiO₂)_N rings and chains with N.

Although important in assessing the likely formation of a system and the energy released once broken, the strain tells little about the stability of a ring, as once formed it is the energy required to break the connected (SiO₂)_N structure (e.g. by external force, or reaction), which is more important. In addition to the energetic stability of $N > 11$ rings, having lower total energies and BEs over the $N > 11$ chains, due to the similarity of each bonded SiO₂ unit throughout a ring or chain, the lower BE (eV/SiO₂) also indicates a corresponding excess structural stability. The reactive stability of an SiO₂ cluster can also be assessed by the size of the energy gap between the highest occupied molecular orbital (HOMO) and the lowest unoccupied molecular orbital (LUMO)⁴⁴. For increasing (SiO₂)_N chain lengths this gap remains almost constant. For the rings, the HOMO-LUMO gap is initially smaller than that of the chains, but increases rapidly with increasing N, exceeding that of the chains by 0.25 eV for $N = 12$, see figure 2.3. The spatial distribution of the occupied and virtual molecular orbitals influences the location

of likely reactive attack. We find that the frontier orbitals on the rings and chains have different characters: the chains have both HOMO and LUMO highly localised on the NBO end-groups, while the rings have both orbitals distributed regularly over all atomic centres. The spatial extent of the electron-accepting LUMO of the rings is radially asymmetric with significant magnitude only around the outer periphery of the ring, but an almost total absence towards the centre of the ring (see figure 3.4). This radial orbital asymmetry is linked to the corresponding structural asymmetry in the inner and outer oxygen spacing described above and is also observed in the sign of the electrostatic potential around the rings. Our calculations show the outer environment of the rings has a mostly positive potential, whereas towards the centre of the rings the potential is negative, indicating, along with the spatial extent of the LUMO, that the ring interiors would be much less reactive than the exteriors. The ends of the chains have a dipolar character, which, together with the tendency of the frontier orbitals to be located over the NBOs, make these regions likely reactive centres.

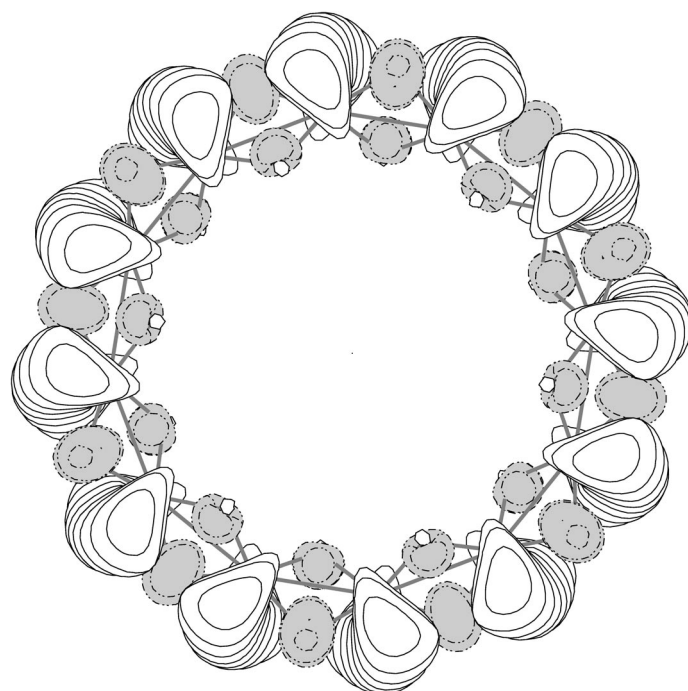


Figure 3.4 Spatial extent of the electron-accepting LUMO of the $(\text{SiO}_2)_{12}$ ring.

Recent DF/B3LYP calculations of the reaction of isolated hydrogen-terminated two rings with water give a barrier of 0.71 eV, but which increases to 1.11 eV when including a more realistic extended silica bonding environment⁴². Other studies found it

necessary to include two-rings in extended surface models of annealed silica to reproduce its known hydrolysis stability²³. In our silica rings each two-ring is, as on an extended surface, fully coordinated in a constrained environment, helping to increase its hydrolysis barrier over isolated two-rings, or terminated two-ring clusters. Experimentally, extended two-ring containing fibres of silica-w are structurally stable but susceptible to hydrolysis, although with only isolated bonds being attacked leaving intact two-ring $(\text{SiO}_2)_N$ chains estimated to have $12.5 < N < 100$ units²⁸. A more recent report additionally shows that extraction with water followed by drying is a successful method for isolating silica-w⁴⁵ from other amorphous synthesis products, suggesting that this hydrolysis is, at least, partially reversible.

3.4 Outlook

In the literature very recently NBO-containing $(\text{SiO}_2)_{12}$ clusters were proposed with a lower BE's than our $(\text{SiO}_2)_{12}$ rings⁴⁶, suggesting that for this cluster size the bonding strain in the ring still adversely increases the energy to above that of cluster containing some NBO's. However, with increasing cluster-size the bonding strain becomes progressively smaller, leading to cage-like cluster like the one shown in figure 3.5 for $(\text{SiO}_2)_{24}$. This cluster, more extensively discussed in chapter five, is the lowest energy $(\text{SiO}_2)_{24}$ cluster currently known in literature and can be calculated to lie only 0.07 eV/ SiO_2 above α -quartz. While the latter value should be treated as a ballpark figure (due to the approximations used in calculating the cyclic strain), it shows these larger silica clusters to have energies comparable to or only slightly higher than extended all-silica zeolites and considerable lower than silica-w (0.55 eV/ SiO_2). Increasing the cluster size appears thus to be the way to make even more stable fully-coordinated silica nanoclusters.

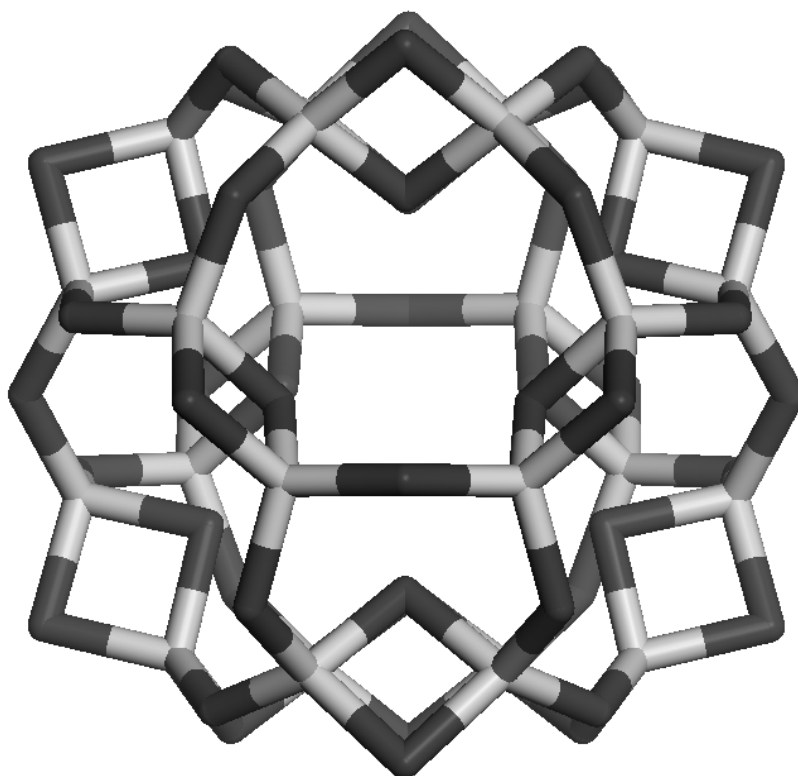


Figure 3.5 Fully-coordinated cage-like (SiO₂)₂₄ cluster with $E_{Q \rightarrow R}$ of only 0.07 eV/SiO₂.

To form a rigid and stable multi-two-ring silica material we envisage, instead of long flexible chains (as in silica-w), fully connected small clusters, such as our molecular rings, as material building blocks (as discussed in⁴⁷). If our proposed silica nanoclusters could be successfully synthesised, then via their mutual interaction, the possibility arises for new extended silica polymorphs, which may show bulk features reminiscent of its building blocks such as tubular or porous morphologies. The interiors of such tubes or pores, due to the properties of the rings described above, are also likely to be relatively stable to hydrolysis, and the size of such pores even tailored by the size of the molecular ring employed. Compared to lower-energy NBO-containing silica nanoclusters proposed in literature⁴⁶, the fully coordinated clusters (like (SiO₂)_N rings) are ideal for building such assembled phases as the enticing properties of such materials are inherently linked to the discrete nature of the material building blocks. The fully coordinated clusters are due to their high reactive stability relatively inert and are expected to stay discrete during assembling, while their NBO containing counterparts are inherently reactive and most likely will condense into “conventional” amorphous silica.

Although such ideas are highly speculative, we feel that if the synthetic challenge, inherent in this chapter, could be mastered successfully, fully-coordinated finite silica clusters and polymorphs based upon their combination, as proposed here, could provide a new route to the synthesis of novel materials and the further fundamental understanding of silica.

3.5 Conclusions

A new form of finite silica with edge-sharing SiO_2 units connected in the form of a ring is proposed, and compared to non-bridging oxygen terminated chains of a similar length. High-level density functional calculations for $(\text{SiO}_2)_N$ $N=4-14$ show the rings to be more energetically and reactively stable than the corresponding $(\text{SiO}_2)_N$ linear chains for $N>11$. The $(\text{SiO}_2)_N$ rings are shown to lie considerably higher in energy than α -quartz, with the difference in energy being the result of the intrinsic strain of the two-rings and the cyclic strain in the ring. The latter component, resulting from the curvature induced by the finite dimensions of the cluster, is demonstrated to become progressively smaller with increasing cluster-size. Moreover, it is speculated that further increases in cluster-size will allow cage-like clusters to form with destabilisations compared to α -quartz of only 0.1 eV/ SiO_2 . The rings are furthermore shown to display frequency modes in remarkable agreement with infrared (IR) bands measured on dehydrated silica surfaces indicating their potential as models of strained extended silica systems. Finally, it is suggested that silica rings or similar fully-coordinated silica nanoclusters may be utilised as precursors for new bulk silica cluster assembled materials.

References

- ¹ Kroto H.W., Heath J.R., O'Brien S.C., Curl R.F., Smalley R.E. *Nature* **1985**, 318, 162.
- ² Kroto H.W. *Nature* **1987**, 329, 529.
- ³ Kroto H.W. *Science* **1988**, 242, 1139.
- ⁴ Iijima S. *Nature* **1991**, 354, 56.
- ⁵ Iijima S., Ichuhashi T. *Nature* **1993**, 363, 603.
- ⁶ Miyamoto Y., Rubio A., Louie S.G., Cohen M.L. *Phys. Rev. B* **1994**, 50, 18360.
- ⁷ Chopra N.G., Luyken R.J., Cherrey K., Crespi, V.H., Cohen M.L., Louie S.G., Zettl A. *Science* **1995**, 269, 966.
- ⁸ Oku T., Hirano T., Kuno M., Kusenose T., Niihara K., Suganuma K. *Mater. Sci. Eng. B* **2000**, 74, 206.
- ⁹ Oku T., Nishiwaki A., Narita I. Gonda M., *Chem. Phys. Lett.* **2003**, 380, 620.
- ¹⁰ Tenne R., Margulis L., Genut M., Hodes G. *Nature* **1992**, 360, 444.
- ¹¹ Parilla P.A., Dillon A.C., Jones K.M., Riker G., Schulz D.L. Ginley D.S., Heben M.J. *Nature* **1999**, 397, 114.
- ¹² Lafargue P.E., Gaumet J.J., Muller J.F., Labrosse A. *J. Mass Spectrom.* **1996**, 31, 623.
- ¹³ Wang L-S, Nicholas J.B., Depuis M., Wu H., Colson S.D. *Phys. Rev. Lett.* **1997**, 78, 4450.
- ¹⁴ Wang L-S., Desai S.R., Wu H., Nicholas J.B. *Z. Phys. D* **1997**, 40, 36.
- ¹⁵ Xu C., Wang L., Qian S., Zhao L., Wang Z., Li Y. *Chem. Phys. Lett* **1997**, 281, 426.
- ¹⁶ Adachi M. *Colloid. Polym. Sci.* **2003**, 281, 370.
- ¹⁷ Zhang M., Bando Y., Wada K. *J. Mater. Res.* **2000**, 15, 387.
- ¹⁸ Hentze H-P., Raghavan S.R., McKelvey C.A., Kaler E.W. *Langmuir* **2003**, 19, 1069.
- ¹⁹ Ferrari A.M., Garrone E., Spoto G., Ugliengo P., Zecchina A. *Surf. Sci.* **1995**, 323, 151.
- ²⁰ Bunker B.C., Haaland D.M., Michalske T.A., Smith W.L. *Surf. Sci.* **1989**, 222, 95.
- ²¹ Chaing C.M., Zegarski B.R., Dubois L.H. *J. Phys. Chem.* **1993**, 97, 6978.
- ²² Roder A., Kob W., Binder K. *J. Chem. Phys.* **2001**, 114, 7602.
- ²³ Bakaev V.A., Steele W.A. *J. Chem. Phys.* **1999**, 111, 9803.
- ²⁴ Ceresoli D., Bernasconi M., Iarlori S., Parrinello M., Tosatti E. *Phys. Rev. Lett.* **2000**, 84, 3887.
- ²⁵ Benoit M., Ispas S., Tuckerman M.E. *Phys. Rev. B* **2001**, 64, 224205.
- ²⁶ Chu T.S., Zhang R.Q., Cheug H.F. *J. Phys. Chem. B* **2001**, 105, 1705.
- ²⁷ Nayak S.K., Rao B.K., Khanna S.N., Jena P. *J. Chem. Phys.* **1998**, 109, 1245.
- ²⁸ Weiss A. *Z. Anorg. Allg. Chem.* **1954**, 276, 95.
- ²⁹ Becke A.D. *J. Chem. Phys.* **1993**, 98, 5648.
- ³⁰ Zhang R.Q., Chu T.S., Cheung H.F., Wang N., Lee S.T. *Phys. Rev. B* **2001**, 64, 113304.
- ³¹ Hehre W.J., Ditchfield R., Pople J.A. *J. Chem. Phys.* **1972**, 56, 2257.
- ³² Franci M.M., Petro W.J., Hehre W.J., Binkley J.S., Gordon M.S., DeFrees D.J., Pople J.A. *J. Chem. Phys.* **1982**, 77, 3654.
- ³³ Hariharan P.C., Pople J.A., *Theor. Chimica Acta* **1973**, 28, 213.
- ³⁴ Krishnan R., Binkley J.S., Seeger R., Pople J.A. *J. Chem. Phys.* **1980**, 72, 650.
- ³⁵ McLean A.D., Chandler G.S. *J. Chem. Phys.* **1980**, 72, 5639.
- ³⁶ Krishnan R., Binkley J.S., Seeger R., Pople J.A. *J. Chem. Phys.* **1980**, 72, 650.
- ³⁷ Clark T., Chandrasekhar J., Schleyer P.V.R. *J. Comp. Chem.* **1983**, 4, 294.
- ³⁸ Frisch M.J. *Gaussian 98*, Revision A.9, Gaussian, Inc.: Pittsburgh PA, 1998.
- ³⁹ Morrow B.A., Cody I.A. *J. Phys. Chem.* **1978**, 80, 1998.
- ⁴⁰ Boccuzzi F., Coluccia S., Ghiotti G., Morterra C., Zecchina A. *J. Phys. Chem.* **1978**, 82, 1298.
- ⁴¹ Lopez N., Vitiello M., Illas F., Pacchioni G. *J. Non. Cryst. Solids.* **2000**, 271, 56.
- ⁴² Walsh T.R., Wilson M., Sutton A.P. *J. Chem. Phys.* **2000**, 113, 9191.
- ⁴³ Hamann D.R., *Phys. Rev. B* **1997**, 55, 14784.
- ⁴⁴ Yoshida S., Sakaki S., Kobayashi H. *Electronic Processes in Catalysis – A Quantum Chemical Approach to Catalysis*: VCH: Tokyo, Japan, 1994.
- ⁴⁵ Kajiwara M. *Jap. J. Appl. Phys.* **1988**, 27, 1373.
- ⁴⁶ Sun Q., Wang Q., Jena P. *Phys. Rev. Lett.* **2004**, 92, 039601.
- ⁴⁷ Khanna S.N., Jena P. *Phys. Rev. B* **1995**, 51, 13705.

4

Two-ring vibrational modes on silica surfaces investigated via fully coordinated nanoclusters

Abstract

Vibrational modes of rings containing two silicon atoms and two oxygen atoms, so-called two-rings, found on a variety of silica surfaces, are modelled with fully-connected $(\text{SiO}_2)_{12}$ clusters containing no terminating groups. Such clusters naturally reflect the embedding of surface two-rings in a silica matrix without the need for large calculations of silica surface layers. The chosen size of the clusters allows us not only to employ the recommended high levels of theory for vibrational calculations, but also to study a range of two-ring-containing conformations. The calculated spectra for the clusters display many peaks in the experimental window, with some in excellent frequency and intensity agreement with measured bands. The results are discussed with respect to the structural nature of the clusters and the possibility of collective two-ring surface modes.

The contents of this chapter have been published in:

Bromley S.T., Zwijnenburg M.A., Maschmeyer T. *Surf. Sci.* **2003**, 539, L544.

4.1 Introduction

Silica surfaces, in the absence of water are characterised (in the partial transparency window between 850-1000 cm^{-1}) by three specific infra-red (IR) bands: two strong peaks at 888 cm^{-1} and 908 cm^{-1} , and a weaker shoulder at 932 cm^{-1} . This particular spectroscopic signature is found for dehydroxylated surfaces of amorphous silica¹⁻⁴, and for annealed thin films of pure silica⁵, with a similar IR fingerprint also observed for surfaces of dehydroxylated crystalline silicalite,⁶ strongly indicating the presence of specific structural features common to silica surfaces. It is generally accepted that the responsible agents for these IR-peaks are silica two-rings. Supporting this assignment are numerous experimental studies^{4,5,7,8}, and electronic structure calculations on, both, small terminated two-ring-containing clusters^{4,7,9-11}, and on silica surfaces¹². Thus far, calculations have concentrated on assigning two-ring vibrational modes to the two main experimental peaks at 888 cm^{-1} and 908 cm^{-1} , ignoring the shoulder at 932 cm^{-1} . Semi-empirical PM3 modelling of small clusters has assigned the two main experimental bands to a localised two-ring mode and a mode mainly located on the cluster's terminating hydroxyl groups¹⁰. Higher level HF^{7,8} and DF¹² calculations give two modes for the bands, which, although also influenced by non-two-ring effects, are both characterised by motions of the two-ring atoms only, however, giving at best frequency differences of over 35 cm^{-1} when compared to experimental values.

In this study, rather than using terminated two-ring-containing clusters or periodic surfaces, we employ the fully-coordinated clusters (FCCs) from chapter three. Using FCCs, two-rings can be modelled in an environment where all silicon atoms are four-coordinated to oxygen atoms, and each oxygen atom is coordinated to two silicon atoms without termination, as in a bulk material. One immediate advantage over other cluster investigations is that modes, due to for example, terminating H or OH groups are naturally excluded. Furthermore, unlike in periodic DFT calculations of silica surface layers, it is possible to perform a number of calculations for less computational cost: for each changing the ratio of two-rings to single Si-O-Si bridges, and thus simply varying the type of two-ring sites present.

4.2 Computational details

The vibrational spectra of four different $(\text{SiO}_2)_{12}$ FCCs (the ring from chapter three and three other cage-like clusters) and one NBO terminated $(\text{SiO}_2)_{12}$ cluster (the chain from chapter three) were calculated, using high-level DFT calculations, after they were first optimised at the same level of theory. The DFT calculations were performed using the three parameter B3LYP functional¹³ and a 6-311+G** basis-set¹⁴⁻¹⁷, as implemented in the program Gaussian98¹⁸. To ensure that a good starting minimum-energy structure was achieved, the further options of an ultra-fine integration grid and tight SCF convergence were also employed.

The comparison between theoretical and experimental IR modes is often complicated by the application of scaling factors to the calculated frequencies. As, already mentioned in chapter one, for HF calculations a scaling factor of approximately 10 percent is usually applied to the computed frequencies to correct for the neglect of electron correlation effects and anharmonicity¹⁹. For DF calculated frequencies, scaling factors are less often recommended and/or applied, and are significantly smaller than those for HF calculations. For optimal DF-based vibrational calculations (regarding accurate reproduction of both intensities and frequencies from experiment and very high level *ab initio* calculations) the combination of the B3LYP functional with a large basis set, as applied in this chapter, is recommended¹⁹⁻²¹. For this level of theory the empirical frequency scaling factor of between 0.99-1.0, based on averaged deviations from experimental molecular IR bands²² for 205 molecules and 1729 associated vibrational modes²⁰, is particularly close to unity. In this chapter thus, as with other similar DF calculations^{23,24}, only un-scaled calculated frequencies are reported, whilst reminding the reader to bear in mind the likely very small systematic downshift correction to all the calculated frequencies (<1%) and the small chance of scatter by up to ~5% for some individual frequencies.

4.3 Results and discussion

The vibrational spectra of the four $(\text{SiO}_2)_{12}$ FCCs and the $(\text{SiO}_2)_{12}$ chain are presented in figures 4.1-5. In FCCs, the calculated frequencies generally correspond to collective whole-cluster modes. Thus, the schematic assignments accompanying the

reported spectra should be interpreted as localised two-ring decompositions of these complex cluster vibrations. The various clusters contain between six and twelve two-rings each, and all display a number of modes in the experimentally studied 850-1000 cm^{-1} window.

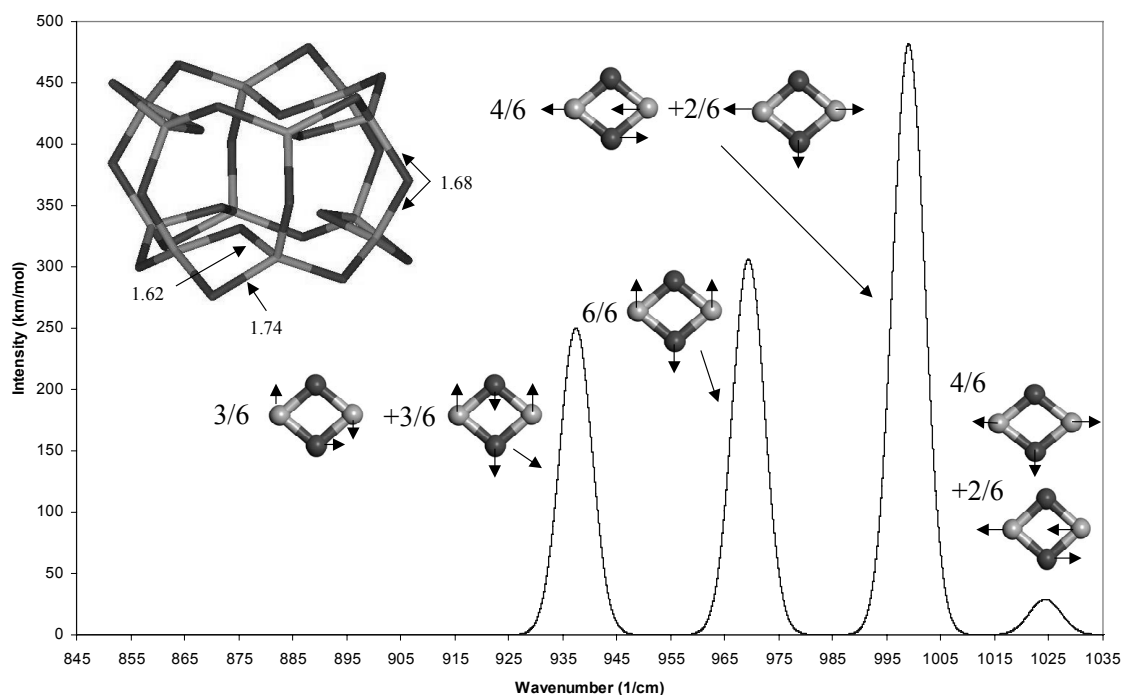


Figure 4.1. Calculated harmonic frequency spectrum for cluster A. Cluster two-ring modes only are shown, approximately decomposed into localised in-plane modes. The denominator of each fraction denotes the total number of two-rings in the cluster, with the respective numerator denoting the number of two-rings participating in the accompanying two-ring mode. Unassigned peaks have no significant two-ring contribution. Selected bond distances of the optimised cluster are shown in Ångstroms. Silicon atom positions are in light grey and oxygen positions in dark grey. All peaks are Gaussian broadened with a half-width of 7cm^{-1} .

Starting with the two FCCs containing the lowest number of two-rings (A and B), the main frequency modes are all above 900 cm^{-1} . As representations of a low density of two-rings embedded in a silica surface, it may be argued that these FCCs are

to be preferred due to their relatively high degree of two-ring isolation. FCCs A and B are the most compact of all the clusters investigated, and furthermore found to be lower in energy than FCCs C and D, but their small size introduces much structural strain on the Si-O-Si bridges between the two-rings. For FCCs A and B, and to a lesser extent C, modes arising from strained Si-O-Si bridges are also found to contribute to the calculated peaks, complicating the spectra. Although we may also consider such modes as those that could naturally arise from the strained Si-O-Si bonds of a silica surface, we concentrate solely on modes that can be assigned to two-rings.

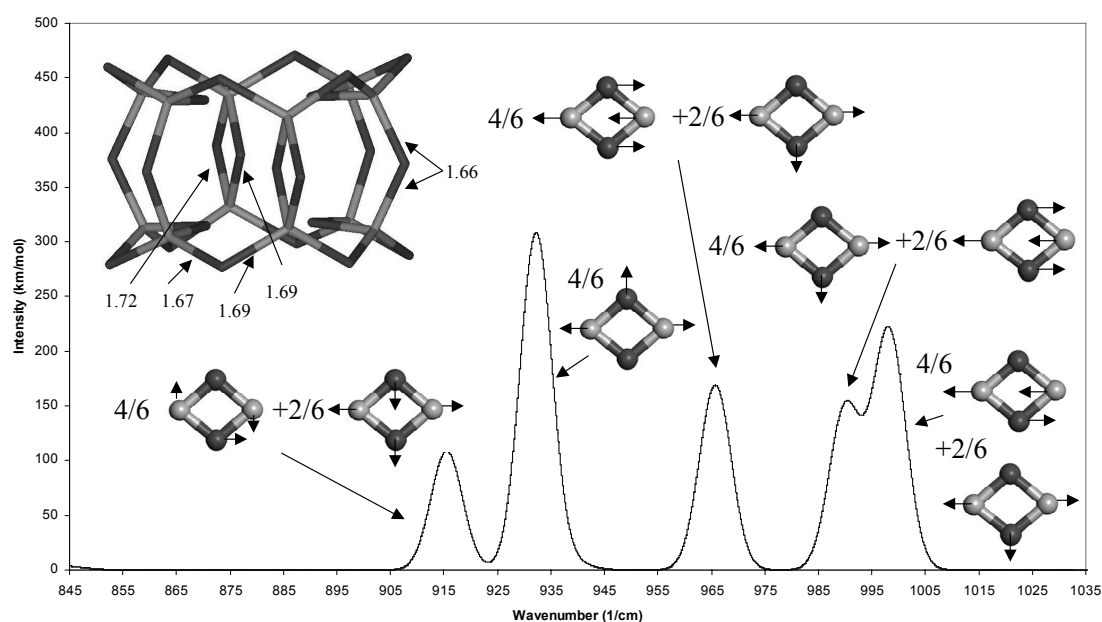


Figure 4.2 Calculated harmonic frequency spectrum for cluster B. See caption to figure 4.1 for details.

Both A and B contain six two-rings and possess structures with two planar rings containing six silicon atoms sitting face to face. In A all two-rings are in the planes of the six-rings, whereas in structure B two two-rings are between the six-rings. Examining the calculated spectra of A and B respectively, we find in both cases three corresponding peaks of strong intensity at (i) 932/937 cm^{-1} , (ii) 966/969 cm^{-1} and (iii) 998/999 cm^{-1} . Each peak is found to be linked to similar structural vibrational modes in both clusters: (i) single Si-O-Si bridge “rocking modes” and two-ring modes in the

planes of the six-rings, (ii) modes predominantly involving the Si-O-Si bridges (or in B the two-rings) between the two six-rings, (iii) modes mainly involving only the oxygen atoms of the two-rings towards the centre of the cluster. The additional mode for FCC A at 1024 cm^{-1} is an anti-phase version of mode (iii). The extra peaks at 915 cm^{-1} and 989 cm^{-1} for FCC B arise mainly from the two two-rings linking the silica six-rings, together with Si-O-Si modes. In both cases the spectra are a poor match to the experimental bands and even for the few calculated frequencies in the possible 5% error range for assignment (approx. $< 950\text{ cm}^{-1}$) the peaks are not solely due to two-ring modes.

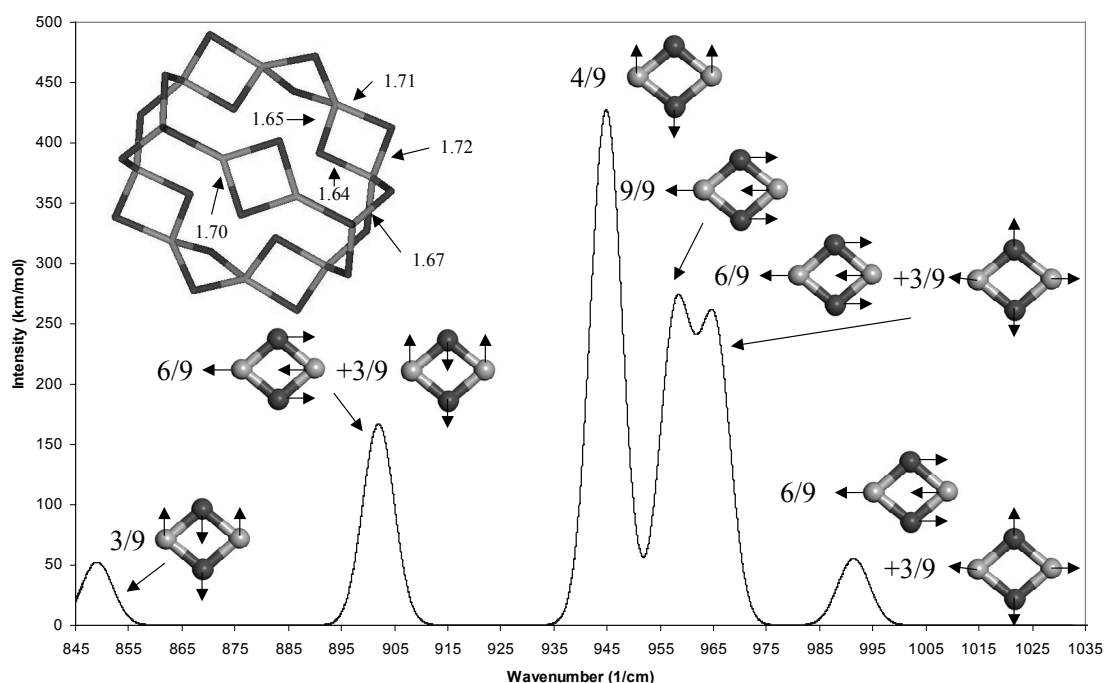


Figure 4.3 Calculated harmonic frequency spectrum for cluster C. See caption to figure 4.1 for details.

FCC C contains nine two-rings, in the form of three chains of three two-rings, all linked at either end by a silica ring containing three silicon atoms. The calculated spectrum is the most complicated of all the FCCs but can be simply divided into two sets: (i) peaks corresponding predominately only to two-ring modes at 849 , 902 and 958 cm^{-1} , and (ii) peaks mainly due to modes involving the silica three-rings at 945 , 965 , and 991 cm^{-1} . Considering the first set only, it can be seen that it is a reasonable match

to the experimental band positions (888, 908, 932 cm^{-1}). Although the calculated peaks at 849 cm^{-1} and 958 cm^{-1} are well-represented by the quoted single localised two-ring mode decomposition, the mode at 902 cm^{-1} , matching with the experimental IR peak at 908 cm^{-1} , is intrinsically a mixed two-ring mode consisting of a combination of two different localised modes (see figure 4.3). Comparing the intensity profile of the three calculated two-ring modes with the experimental IR intensities, there is a poor match with the calculated intensities showing the opposite trend to experiment.

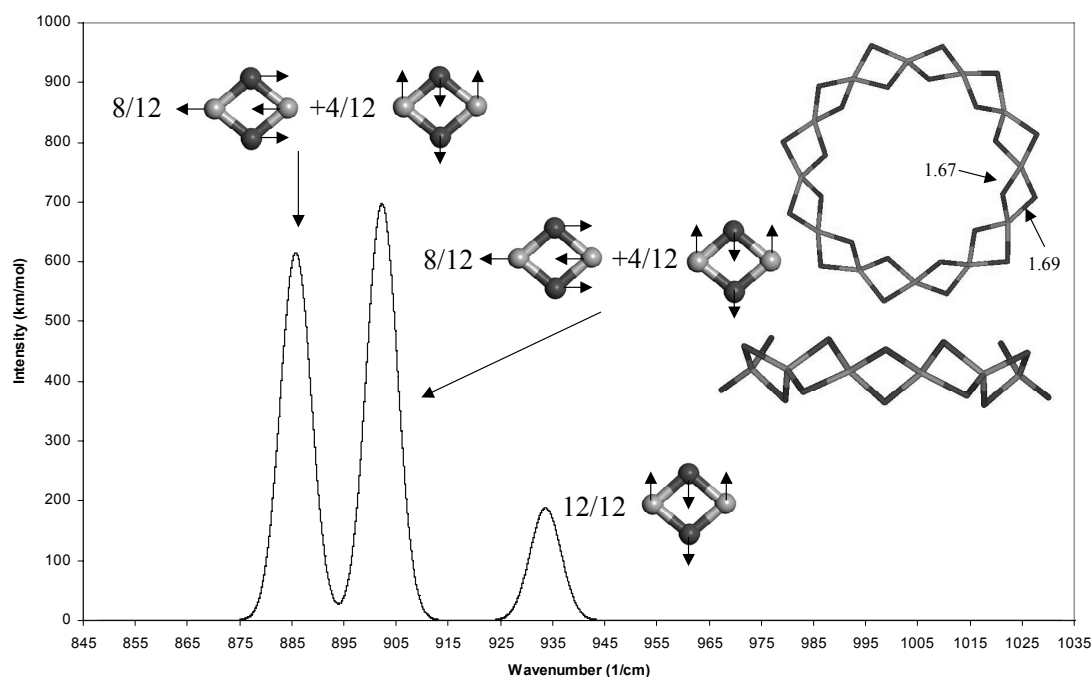


Figure 4.4 Calculated harmonic frequency spectrum for the ring (cluster D). See caption to figure 4.1 for details.

For the ring, D, the match of the calculated spectrum and the experimental IR spectra is remarkably good with both displaying only three modes with a very similar intensity profile, and with corresponding peaks within 6 cm^{-1} (<1%) of each other. Although such a good agreement seemingly makes for an attractively simple assignment of the experimental IR modes, for the two main calculated peaks (886 and 902 cm^{-1}) the associated two-ring modes are, like the 902 cm^{-1} mode for FCC C, intrinsically collective mixed two-ring modes. These modes cannot each be simply represented by a single

localised two-ring mode, and are thus difficult to reconcile with silica surfaces having only a sparse population of relatively isolated two-rings.

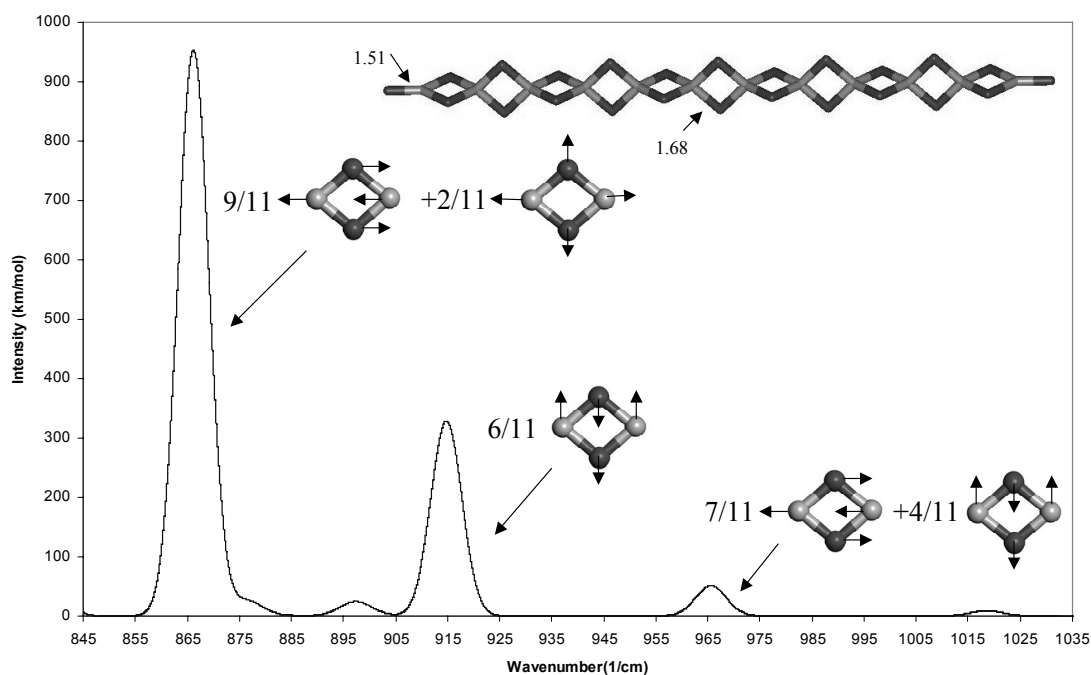


Figure 4.5 Calculated harmonic frequency spectrum for the chain (cluster E). See caption to figure 4.1 for details.

To try to understand the nature of these collective modes it is instructive to compare the spectra of the ring D, and the analogous decoupled chain structure, E, shown in figure 4.5. Ignoring the very small intensity peaks between 875-900 cm^{-1} for E, which are simply variants of the strong mode at 915 cm^{-1} , both E and D display three main modes in good agreement with the experimental IR spectra regarding both peak positions and relative intensities (902, 886, 934 cm^{-1} for D, and 866, 915, 966 cm^{-1} for E). For the chain, the strongest modes at 866 cm^{-1} and the 915 cm^{-1} match within 22 cm^{-1} ($\sim 2.5\%$) the main experimental modes at 888 and 908 cm^{-1} , respectively. These chain modes are well-described by a localised two-ring mode decomposition (see figure 4.5) and coincide with assignments from terminated cluster⁷, and periodic¹² electronic structure calculations. It is further tempting to assign the smaller peak at 966 cm^{-1} to the weak shoulder found in the experimental IR spectra at 932 cm^{-1} . This peak is, however,

a collective mixed two-ring mode not decomposable into localised modes. The 915 cm^{-1} peak for the chain, and the ring peak at 934 cm^{-1} , are both due to the same repeated localised two-ring mode. For the chain we assign the mode associated with this peak to the 908 cm^{-1} experimental IR peak. For the connected ring, however, this peak is shifted up in frequency to 934 cm^{-1} , possibly due to the relative increase in the ring's structural strain, and is also reduced in intensity. This ring peak is assigned to the nearby experimental IR shoulder at 932 cm^{-1} . For the large 866 cm^{-1} chain peak, with a corresponding repeated localised two-ring mode assigned to the 888 cm^{-1} experimental IR band, the ring gives two peaks of relatively lower intensity at 886 cm^{-1} and 902 cm^{-1} . These are collective two-ring modes displaying some of the character of the single repeated two-ring mode of the chain at 866 cm^{-1} . But, perhaps due the ring's fully-connectedness and size, they are not commensurate with the ring structure. A possible interpretation of these ring modes is, therefore, a split of the chain's 866 cm^{-1} peak. As with the $915\text{-}934\text{ cm}^{-1}$ peak up-shift, we can further imagine that the relative increased structural strain of the ring causes the two split peaks also to be shifted to higher frequencies. With this interpretation of the vibrational spectrum of the ring, as a split and up-shifted chain spectrum, the two intense peaks at 886 cm^{-1} and 902 cm^{-1} should both be associated with the single experimental peak at 888 cm^{-1} and the smaller peak at 934 cm^{-1} with the experimental IR peak at 908 cm^{-1} . This interpretation retains the mode assignments of previous studies^{7,12} for the two main IR peaks, but unfortunately takes away the one-to-one correspondence between the ring spectrum's peaks and all three experimental signals.

If, however, the correlated collective nature of the FCC two-ring modes were truly representative of the experimental vibrational response, it would indicate that there should be a similar correlation between the two-rings on silica surfaces. In view of the remarkable experimental agreement of the calculated spectrum of the ring, and that of the 908 cm^{-1} IR peak by a similar collective mode at 902 cm^{-1} for FCC C, it is interesting to speculate that the vibrational response of two-rings on silica surfaces may also be somehow coupled or correlated. Due, perhaps, to a tendency for surface two-rings to form in localised groups, or maybe due to a particular pattern of variation in surface two-ring orientation and associated strain, surface two-rings may be sufficiently correlated together such that their collective modes are analogous to those

of the ring FCC. As a physical realisation of the former idea, we may imagine that for silica surfaces possessing high concentrations of vicinal and geminal hydroxyl groups, under dehydroxylation conditions, clusters of two or more linked two-rings could be formed. Such small chains of two-rings, embedded in the silica surface, would be very likely to display the collective two-ring-based modes exhibited by our FCC models.

4.3 Conclusions

Overall, we have shown that FCCs can yield a complex variety of two-ring-based spectra in the experimentally known transparency window unpolluted by accompanying modes of terminating groups. The vibrational modes and corresponding spectra of the FCCs can be altered simply by the number of two-rings present in any one structure. Considering the likely small errors associated with our calculations, the ring and chain structures yield the best match with experimental silica surface IR spectra with respect to intensity and wavenumber. The ring FCC in particular gives a particularly good match to the three-peaked experimental spectrum and is discussed with respect to its FCC structure, and in relation to the possibility of correlated surface two-ring modes.

References

- ¹ Morrow B.A., Devi A. *Trans. Faraday Soc.* **1972**, 68, 403.
- ² Morrow B.A., Cody I.A. *J. Phys. Chem.* **1976**, 80, 1995.
- ³ Boccuzzi F., Coluccia S., Ghiotti G., Morterra C., and Zecchina A. *J. Phys. Chem.* **1978**, 82, 1298.
- ⁴ Ferrari A.M., Garrone E., Spoto G., Ugliengo P., Zecchina A. *Surf. Sci.* **1995**, 323, 151.
- ⁵ Chiang C.M., Zegarski B.R. Dubois L. *J. Phys. Chem.* **1993**, 97, 6948.
- ⁶ Bordiga S., Ugliengo P., Damin A., Lamberti C., Spoto G., Zecchina A., Spanò G., Buzzoni R., Dalloro L., Rivetti F. *Topics Catal.* **2001**, 15, 43.
- ⁷ Bunker B.C., Haaland D.M., Ward K.J., Michalske T.A., Smith W.L., Binkley J.S., Melius C.F., Balfe C.A. *Surf. Sci.* **1989**, 210, 406.
- ⁸ Bunker B.C., Haaland D.M., Michalske T.A., Smith W.L. *Surf. Sci.* **1989**, 222, 95.
- ⁹ Kudo T., Nagase S. *J. Am. Chem. Soc.* **1985**, 107, 2589.
- ¹⁰ Bendale R.D., Hench L.L. *Surf. Sci.* **1995**, 338, 322.
- ¹¹ Bromley S.T., Zwijnenburg M.A., Maschmeyer T. *Phys. Rev. Lett.* **2003**, 90, 035502.
- ¹² Ceresoli D., Bernasconi M., Iarori S., Parinello M., Tosatti E. *Phys. Rev. Lett.* **2000**, 84, 3887.
- ¹³ Becke A.D. *J. Chem. Phys.* **1993**, 98, 5648.
- ¹⁴ Krishnan R., Binkley J.S., Seeger R., Pople J.A. *J. Chem. Phys.* **1980**, 72, 650.
- ¹⁵ McLean A.D., Chandler G.S. *J. Chem. Phys.* **1980**, 72, 5639.
- ¹⁶ Krishnan R., Binkley J.S., Seeger R., Pople J.A. *J. Chem. Phys.* **1980**, 72, 650.
- ¹⁷ Clark T., Chandrasekhar J., Schleyer P.V.R. *J. Comp. Chem.* **1983**, 4, 294.
- ¹⁸ Frisch M.J. *Gaussian 98*, Revision A.9, Gaussian, Inc.: Pittsburgh PA, 1998.
- ¹⁹ Scott A.P., Radom L. *J. Phys. Chem.* **1996**, 100, 16502.
- ²⁰ Halls M.D., Schlegel H.B. *J. Chem. Phys.* **1998**, 109, 10587.
- ²¹ Yoshida H., Ehara A. Matsuura H. *Chem. Phys. Lett.* **2000**, 325, 477.
- ²² Shimanouchi T. *Tables of Molecular Vibrational Frequencies, Consolidated Vol. I: Natl. Stand. Ref. Data. Ser., Natl. Bur. Stand.: Gaithersburg, US, 1972.*
- ²³ Uzunova E.L., Nikolov G.S. *J. Phys. Chem. B* **2000**, 104, 7299.
- ²⁴ Ricchiardi G., Damin A., Bordiga S., Lamberti C., Spanò G., Rivetti F., Zecchina A. *J. Am. Chem. Soc.* **2001**, 123, 11409.

5

Prospects for a synthetic route towards well-defined stoichiometric silica nanoclusters: from Siloxane to Silica

Abstract

Based upon computational considerations, a novel synthetic route towards well-defined stoichiometric silica nanoclusters is proposed. DF calculations demonstrate the viability of a route based on siloxane cage thermolysis, while molecular dynamics calculations were performed to test the stability of the cages formed. We predict for small siloxane cages defect-rich structures to be the main product, and for larger siloxane cages fully-coordinated silica nanoclusters (iso-structural to their precursor) to be formed. Overall, thermolysis of siloxane cages is expected to present a viable route towards specific types of metastable yet, well-defined silica nanoclusters, not obtainable by less targeted cluster generation methods.

The contents of this chapter have been published in:

Zwijnenburg M.A., Bromley S.T., Flikkema E., Maschmeyer T. *Chem. Phys. Lett.* **2004**, 385, 389.

5.1 Introduction

Silica nanoclusters and nanoparticles (of the order of 0.5-50 nm) are typically synthesized *via* laser ablation¹⁻⁶, plasma discharge^{7,8}, secondary ion mass spectrometry^{9,10}, and flame oxidation⁷. However, these methods generally produce ionic $(\text{SiO}_2)_n\text{X}$ clusters where X is typically a hydrogen or OH species¹⁻¹⁰, derived from surface impurities in the target or from water formed as side-product. Furthermore, it is difficult to control the stoichiometry and the structure of the clusters generated, with often a mixture of sub- or super-oxides being formed, rather than nanoclusters with a well-defined Si:O atomic ratio^{1-3,6}. These clusters are reactive, non-reproducible and, hence, difficult to use in further applications involving ordered self-assembly. In chapter three it was demonstrated that well-defined fully-coordinated silica nanoclusters should be relatively reactively stable, and therefore ideal for being assembled into novel materials. In this chapter, based on computational considerations, we propose a new molecularly-based route to produce well-defined and stoichiometric silica nanoclusters. Furthermore, this route should make it possible to selectively produce only certain cluster sizes and structures.

It is well known that hydroxyls on the surface of amorphous and crystalline silica can be removed by degassing at temperatures above 700K under high-vacuum¹¹⁻¹⁵, resulting in silica surfaces containing Si_2O_2 rings (two-rings) formed *via* the condensation of adjacent hydroxyls; a fact recently also observed in *ab-initio* molecular dynamics of dehydrated silica surfaces¹⁶. We propose that the dehydroxylation procedure, if similarly applied to siloxane $(\text{Si}_n\text{O}_{1.5n}(\text{OH})_n)$ cages (examples of which are discussed in the literature¹⁷⁻¹⁹), may potentially yield stoichiometric silica clusters. Such a method could either be realised by flash vacuum thermolysis, or alternatively, by absorbing a siloxane cage (either synthesized directly or prepared by *in-situ* oxidation of a silsesquioxane²⁰ precursor) on a suitable support followed by thermolysis. This method is analogous to the rational chemical synthesis of C_{60} ²¹ and to procedures for synthesizing supported “naked” (bi)metallic clusters from anionic carbonyl clusters^{22,23}. We demonstrate in this chapter the viability of the method proposed by means of both Density Functional (DF) and classical Molecular Dynamics (MD) calculations on the double six-ring $(\text{Si}_{12}\text{O}_{18}(\text{OH})_{12})$ and the “sodalite cage” $(\text{Si}_{24}\text{O}_{36}(\text{OH})_{24})$ precursor molecules.

5.2 Computational Details

To investigate the viability of siloxane dehydroxylation as a route towards well-defined stoichiometric silica nanoclusters, high-level Density Functional geometry optimisations on five $\text{Si}_{12}\text{O}_{24}$ silica and two $\text{Si}_{24}\text{O}_{48}$ silica nanoclusters were performed. The initial $\text{Si}_{12}\text{O}_{24}$ cluster structures were based upon the skeleton of the “double six ring” $\text{Si}_{12}\text{O}_{18}(\text{OH})_{12}$ precursor, for which six of the Si-O-Si bonds are replaced by Si_2O_2 rings resulting in a number of different cluster structures from which we took the three relatively symmetrical clusters: 1A, 1B and 1C (see fig. 5.1). Two further silica clusters previously described by us: the $\text{Si}_{12}\text{O}_{24}$ ring and $\text{Si}_{12}\text{O}_{24}$ chain (see chapter three) have been included for comparison. The initial structure of the $\text{Si}_{24}\text{O}_{48}$ clusters is based upon the Sodalite cage, for which twelve of the original Si-O-Si bonds are replaced by two-rings, giving rise to a number of different cluster structures from which two symmetrical clusters, 2A and 2B (see fig. 5.2), were taken.

Cluster geometries were first optimised using the recently developed FB force-field²⁴ and then further at the B3LYP²⁵/6-31G*²⁶⁻²⁸ level, imposing no symmetry constraints. For the final optimisation, we employed a basis-set including both polarisation and diffuse functions, 6-311+G**²⁹⁻³², to accurately account for both oxygen polarisation and strained bonds ($\text{Si}_{24}\text{O}_{48}$ clusters, due to their size, were optimised at the 6-31G* level). The geometric parameters for all clusters were fully optimised using standard optimisation criteria (max force = 450×10^{-6} au, RMS force = 300×10^{-6} au, max displacement 1800×10^{-6} au, RMS displacement 1200×10^{-6} au) and a fine integration grid, using the code Gaussian 98³³. To ensure that true minima were found, the use of symmetry in the wavefunction and gradient evaluation was explicitly disabled for all clusters.

To study the thermal stability against isomerisation of the clusters under potential synthesis conditions (1000K and high-vacuum, extrapolated from reaction conditions for the dehydroxylation of bulk silica-surfaces), NVT molecular dynamic runs were performed. No effect of water was taken into account as under the high-vacuum condition needed to drive the dehydroxylation reaction to completion (typically 1×10^{-4} - 1×10^{-5} Pa¹¹⁻¹⁵), we expect that all water formed is immediately swept away. Although it would be preferable to perform *ab-initio* MD calculations, being ideally suited to describe electronic effects such as bond-breaking and -formation, due to their

computationally intensive nature these methods are restricted to simulation times of only a few pico-seconds. Since relatively short runs are too limited to assess adequately the trends in nanocluster stability, we decided to perform classical MD runs of two nano-seconds, employing the dedicated FB²⁴ force-field and the GULP code³⁴. As the FB force-field is fitted not only to the energy of DF-optimised (SiO₂)_n structures, but also to the energies and gradients of deformed (SiO₂)_n structures²⁴, we expect that the force-field should still approximately recover the barriers of bond-breaking and -formation and, thus, be a viable alternative to *ab-initio* MD for silica clusters.

5.3 Results and Discussion

A first test of the viability of the novel route towards silica nanoclusters is given by the amount of energetic cost involved, i.e. the heat of dehydroxylation. For all clusters, the heat of dehydroxylation was calculated from the difference in energy between the dehydroxylation products ($E_{\text{prod}} = E_{\text{silicacluster}} + 0.5N \cdot E_{\text{water}}$) and the siloxane precursor. Table 5.1 shows the dehydroxylation reaction to be strongly endothermic for all the clusters involved, with the heat of dehydroxylation ranging from 21.75 to 23.87 eV for the Si₁₂O₂₄ clusters (19.75 to 21.76 eV at the 6-31G* level of theory) and from 24.91 to 25.46 eV for the Si₂₄O₄₈ clusters.

	BE	ΔH_{dehyd}	E_{LB}
1A	-15.81 ; -16.18	21.75 ; 19.57	3.63 ; 3.26
1B	-15.73 ; -16.09	22.70 ; 20.57	3.78 ; 3.43
1C	-15.63 ; -15.99	23.87 ; 21.76	3.98 ; 3.63
ring	-15.69 ; -16.08	23.19 ; 20.78	3.87 ; 3.46
chain	-15.66 ; -16.04	23.48 ; 21.27	3.91 ; 3.54
2A	-16.96	25.46	2.12
2B	-16.98	24.91	2.08

Table 5.1 Binding energy, heat of dehydroxylation and ligand binding energies for the silica nanoclusters (code see fig. 5.1 and 5.2), all values in eV. Values in bold have been calculated using the 6-311+G** level of theory, all other values using the 6-31G* basis-set.

	S i - S i			S i - O
	2 - r i n g	e x c l. 2 - r i n g s	o v e r a l l	o v e r a l l
1 P		3 . 0 6	3 . 0 6	1 . 6 5
1 A	2 . 4 2	2 . 8 6	2 . 7 1	1 . 6 8
1 B	2 . 4 3	2 . 8 8	2 . 7 3	1 . 6 8
1 C	2 . 4 3	2 . 8 8	2 . 7 3	1 . 6 9
2 P		3 . 0 8	3 . 0 8	1 . 6 4
2 A	2 . 3 7	2 . 9 5	2 . 7 6	1 . 6 6
2 B	2 . 3 8	2 . 9 1	2 . 7 4	1 . 6 6

Table 5.2 Geometric parameters for the silica nanoclusters and their precursors (all values in Ångstrom, code see fig 5.1 and 5.2). Average Si-Si distance for two-rings, excluding two-rings and the overall structure and average Si-O bond-length.

To compare the heat of dehydroxylation with results from previous calculations on amorphous silica surfaces, it was divided over the number of water molecules formed, thereby obtaining the ligand (i.e. water) binding energy (E_{LB}). Table 5.1 shows that the water binding energies decrease in magnitude upon an increase in the cluster size, ranging from 3.63 to 3.98 eV for the $Si_{12}O_{24}$ clusters (3.26 to 3.63 eV at the 6-31G* level of theory) and 2.08 to 2.12 eV for the $Si_{24}O_{48}$ clusters. Comparing these ligand binding energies with those from the heat of formation of an isolated two-ring on an amorphous silica surface (1.7 eV, calculated via periodic slab DF calculations¹⁶), those of the nanoclusters are all found to be higher than that of the silica surface: $E_{LB}(Si_{12}O_{24}) > E_{LB}(Si_{24}O_{48}) > E_{LB}(SiO_2 \text{ surface})$. It, thus, appears that the ligand binding energy increases with the curvature and strain of a cluster. This strain can be directly related to the introduction of two-rings, as the Si-Si distances become considerably shorter in the dehydroxylated cluster (3.06 Å \rightarrow 2.71-2.73 Å, see table 5.2). Furthermore, the energy for forming the first two-ring on the surface of the $Si_{12}O_{18}(OH)_{12}$ precursor structure, resulting in $Si_{12}O_{19}(OH)_{10}$, is 1.72 eV, i.e. almost identical to that for the two-ring formation on the silica surface. Based on the above, we expect that the first two-rings on the cluster surface are formed at temperatures comparable to those needed for forming isolated two-rings on extended surfaces, and that for the full dehydroxylation of the clusters higher temperatures are needed. Furthermore, we expect that the temperature needed for full dehydroxylation decreases with increasing cluster-size to the temperature found for extended surfaces. Finally,

while of limited relevance to their synthesis, as the heat of hydroxylation (i.e. dissociative adsorption of water) is by definition the negative of the heat of dehydroxylation, we predict the energetics of silica nanocluster hydroxylation to become more exothermic with increasing curvature and strain in the clusters.

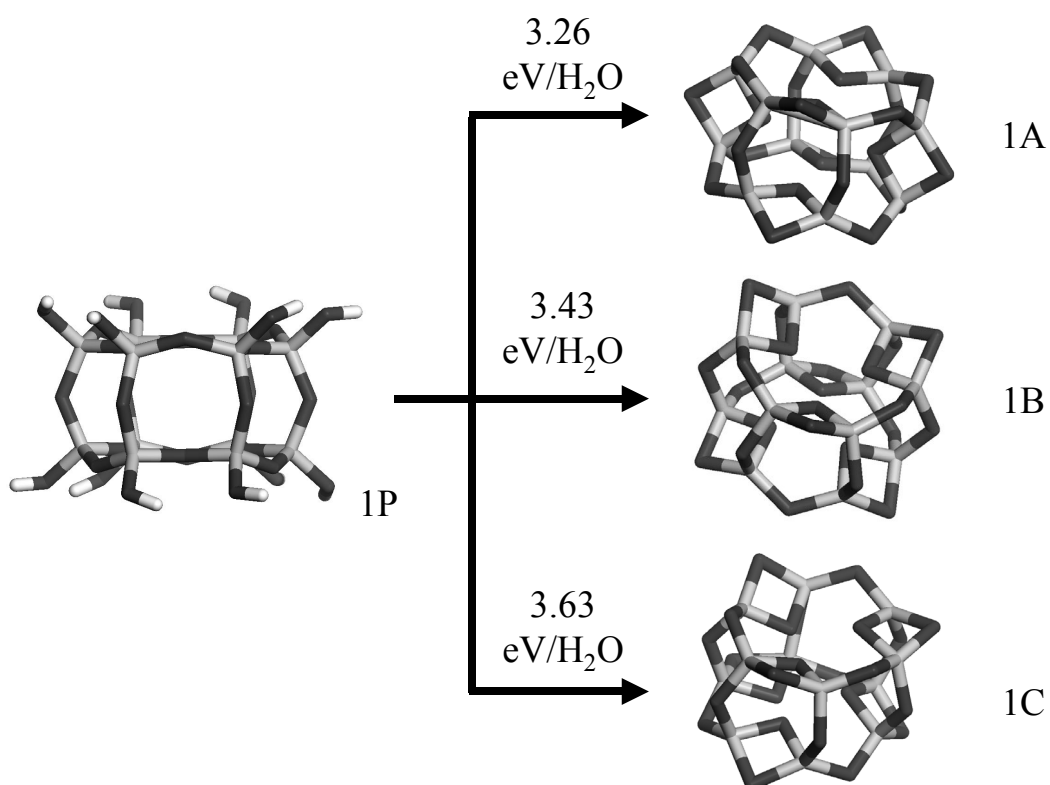


Figure 5.1 DFT optimised $\text{Si}_{12}\text{O}_{24}$ clusters (1A-1C) and their precursor, with corresponding ligand binding energies calculated at the 6-31G* level of theory. Dark grey centres represent oxygen atoms, light grey centres represent silicon atoms and the white terminating centres represent hydrogen atoms.

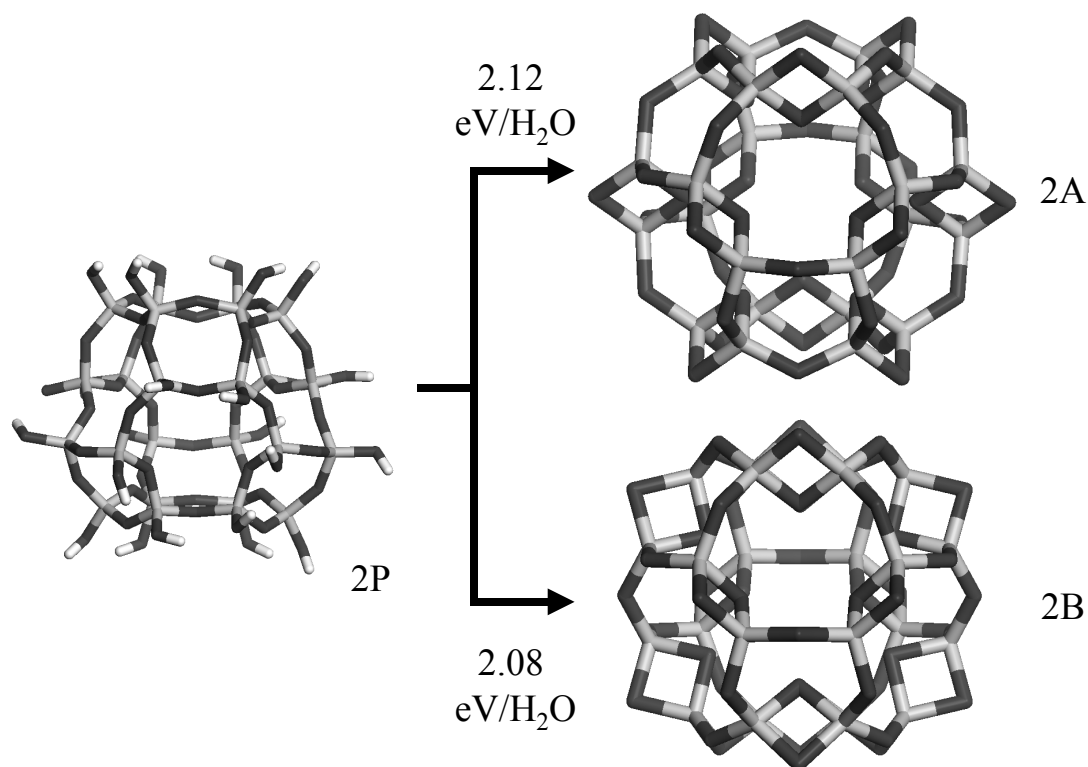


Figure 5.2 DFT optimised $\text{Si}_{24}\text{O}_{48}$ clusters (2A-2B) and their precursor, with corresponding ligand binding energies calculated at the 6-31G* level of theory.

To test the thermal stability against isomerisation of the dehydroxylated silica nanoclusters under the synthesis conditions envisaged (1000K), MD runs were performed on the $\text{Si}_{12}\text{O}_{24}$ cages, the $\text{Si}_{12}\text{O}_{24}$ ring and the $\text{Si}_{24}\text{O}_{48}$ cages. From these clusters the $\text{Si}_{12}\text{O}_{24}$ cages were found to collapse, while the $\text{Si}_{12}\text{O}_{24}$ ring and the $\text{Si}_{24}\text{O}_{48}$ cages stayed intact throughout the whole of each run. Interestingly, cage 2A undergoes an energy lowering transformation to cage 2B during the MD run, however, it remains fully coordinated, rather than break-up as observed for the $\text{Si}_{12}\text{O}_{24}$ cages. The stability of the 1A cage was also studied at the lower temperature of 298K by means of MD and it was found to collapse also, albeit into a less deformed structure. The three $\text{Si}_{12}\text{O}_{24}$ cages (1A-1C), based on the skeleton of the $\text{H}_{12}\text{Si}_{12}\text{O}_{30}$ precursor, convert into structures containing non-bridging oxygen defects and compensating three-coordinated oxygen centres, conserving much of the original skeleton. Since the $\text{Si}_{12}\text{O}_{24}$ cages collapse into defect-rich lower-energy structures, while the $\text{Si}_{24}\text{O}_{48}$ cages retain their full connectivity during heating, one might speculate that the thermal stability of silica

clusters is linked to their size. However, the $\text{Si}_{12}\text{O}_{24}$ ring, in line with its remarkable overall stability (see chapter three) and in contrast to its isomers, does not collapse. Thus, this indicates a more subtle link between structure and thermal stability. If one compares the average two-ring Si-Si distances in the clusters (see table 5.2) with the Si-Si distance in a free two-ring (2.407 Å for Si_2O_4 or 2.400 Å for two-ring on a silica surface¹⁶) then all cages which collapse have on average longer Si-Si distances than the free two-ring. The two-rings in the unstable clusters are, therefore, all stretched; while the two-rings in the stable clusters are all compressed with respect to the free two-ring. The thermal stability of silica nanoclusters, the structure of which is predominantly governed by two-rings, thus, appears to be linked to the fact that the (two-)rings present are all slightly compressed relative to a free two-ring. This observation is consistent with previous observations by us that four-rings in stable bulk SiO_2 phases are under slight bulk-induced compression (see chapter two). For silica cages obtained from siloxane precursors (1A-1C, 2A-2B) the two-rings change from being strained to being compressed upon increasing the size of the cage (see table 5.2), i.e. the thermal stability and chance of successful synthesis, indeed, increases with size. The geometries of the collapsed structures of the 1A cage (cages 3A-3C, see figure 5.3) were optimised by means of DFT, the resulting heats of dehydroxylation and ligand binding energies can be found in table 5.3. The collapsed structures are all found to be lower in energy than the fully-coordinated cages.

	BE	ΔH_{dehyd}	E_{LB}
3A	-15.87	21.07	3.51
3B	-15.88	20.86	3.48
3C	-15.96	19.93	3.32

Table 5.3 Binding energy, dehydroxylation heat and ligand binding heat for the broken $\text{Si}_{12}\text{O}_{24}$ silica nanoclusters, all values are calculated at the 6-311+G(d,p) level of theory and given in eV.

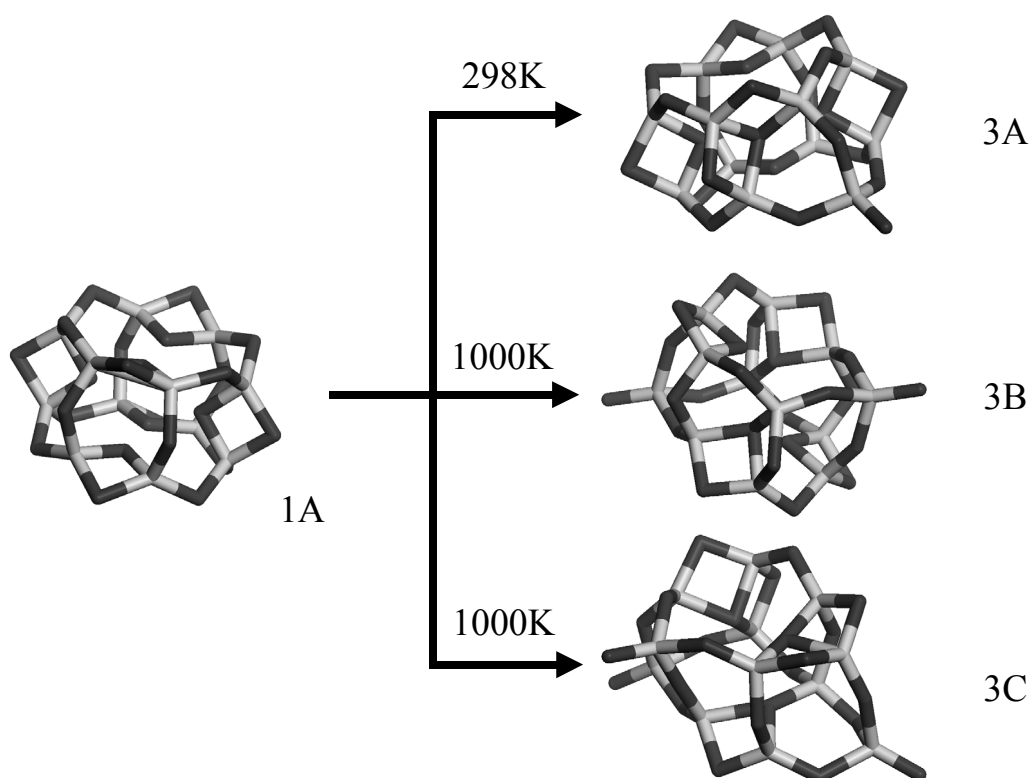


Figure 5.3 DFT optimised broken $\text{Si}_{12}\text{O}_{24}$ clusters (3A-3C).

Preliminary global optimisation calculations by us have shown that for both the $\text{Si}_{12}\text{O}_{24}$ and $\text{Si}_{24}\text{O}_{48}$ clusters the expected products, although thermally stable, are not the ground-state structures for their respective cluster size. Thermolysis of siloxane cages under high-vacuum is, thus, expected to selectively lead to nanocluster structures which are thermally accessible from the precursor structure. Therefore, it presents a viable route towards specific types of metastable yet, well-defined silica nanoclusters. The reaction conditions required for the siloxane cage thermolysis are predicted to be similar to those for the dehydroxylation of bulk silica, only with, depending on the cluster size, more elevated temperatures.

5.4 Conclusions

Dehydroxylation of siloxane molecules by means of thermolysis is shown, by means of high-level DFT and dedicated MD calculations, to be a viable route towards well-defined and stoichiometric silica nanoclusters. For small siloxane cages defect-rich structures are expected to be the main product, while, for larger siloxane cages fully-coordinated silica nanoclusters with the same skeleton as the precursor molecule are the expected product. In summary, our proposed synthesis method is a promising alternative to less-targeted cluster generation methods as laser ablation, plasma discharge and flame oxidation.

References

- ¹ Lafargue P.E., Gaumet J.J., Muller J.F., Labrosse A. *J. Mass Spectrom.* **1996**, 31, 623.
- ² Wang L.S., Nicholas J.B., Dupuis M., Wu H., Colson S.D. *Phys. Rev. Lett.* **1997**, 78, 4450.
- ³ Wang L.S., Desai S.R., Wu H., Nicholas J.B. *Z. Phys. D* **1997**, 40, 36.
- ⁴ Xu C., Wang L., Qian S., Zhao L., Wang Z., Li Y. *Chem. Phys. Lett* **1997**, 281, 42.
- ⁵ Xu C., Long Y., Zhang R., Zhao L., Qian S., Li Y. *Appl. Phys. A* **1998**, 66, 99.
- ⁶ Xu C., Wang W., Zhang W., Zhuang J., Liu L., Kong Q., Zhao L., Long Y., Fang K., Qian S., Li Y. *J. Phys. Chem. A* **2000**, 104, 9518.
- ⁷ Balabanova E. *Vacuum* **2000**, 58, 174.
- ⁸ Whyman D. *Phys. Chem. Chem. Phys.* **2001**, 3, 1348.
- ⁹ Schenkel T., Barnes A.V., Hamza A.V., Schneider D.H. *Eur. Phys. J. D* **1998**, 1, 297.
- ¹⁰ Schenkel T., Schlathöler T., Newman M.W., Machicoane G.A., McDonald J.W., Hamza A.V. *J. Chem. Phys.* **2000**, 113, 2419.
- ¹¹ Morrow B.A., Cody I.A. *J. Phys. Chem.* **1976**, 80, 1995.
- ¹² Boccuzzi F., Coluccia S., Ghiotti G., Morterra C., and Zecchina A. *J. Phys. Chem.* **1978**, 82, 1298.
- ¹³ Bunker B.C., Haaland D.M., Ward K.J., Michalske T.A., Smith W.L., Binkley J.S., Melius C.F., Balfe C.A. *Surf. Sci.* **1989**, 210, 406.
- ¹⁴ Bunker B.C., Haaland D.M., Michalske T.A., Smith W.L. *Surf. Sci.* **1989**, 222, 95.
- ¹⁵ Ferrari A.M., Garrone E., Spoto G., Ugliengo P., Zecchina A. *Surf. Sci.* **1995**, 323, 151.
- ¹⁶ Masini P., Bernasconi M. *J. Phys. : Condens. Mater.* **2002**, 14, 4133.
- ¹⁷ Hoebel D., Wieker W., Franke P., Otto A. *Z. Anorg. Allg. Chem.* **1975**, 418, 35.
- ¹⁸ Smolin Y.I., Shepelev Y.F., Ershov A.S., Hoebel D., Wieker W. *Sov. Phys. Crystallogr.* **1984**, 29, 421.
- ¹⁹ Wiebcke M., Emmer J., Felsche J. *Chem. Commun.* **1993**, 1604.
- ²⁰ Pescarmona P.P., Maschmeyer T. *Aust. J. Chem.* **2001**, 54, 583.
- ²¹ Scott L.T., Boorum M.B., McMahon B.J., Hagen S., Mack J., Blank J., Wegner H., de Meijere A. *Science* **2002**, 295, 1500.
- ²² Shephard D.S., Maschmeyer Th., Johnson B.F.G., Thomas J.M., Sankar G., Ozkaya D., Zhou W., Oldroyd R.D., Bell R.G. *Angew. Chem. Int. Ed. Engl.* **1997**, 36, 2242.
- ²³ Bromley S.T., Sankar G., Catlow C.R.A., Maschmeyer Th., Johnson B.F.G., Thomas J.M. *Chem. Phys. Lett.* **2001**, 340, 524.
- ²⁴ Flikkema E., Bromley S.T. *Chem. Phys. Lett.* **2003**, 378, 622.
- ²⁵ Becke A.D. *J. Chem. Phys.* **1993**, 98, 5648.
- ²⁶ Hehre W.J., Ditchfield R., Pople J.A. *J. Chem. Phys.* **1972**, 56, 2257.
- ²⁷ Franci M.M., Petro W.J., Hehre W.J., Binkley J.S., Gordon M.S., DeFrees D.J., Pople J.A. *J. Chem. Phys.* **1982**, 77, 3654.
- ²⁸ Hariharan P.C., Pople J.A., *Theoret. Chimica Acta* **1973**, 28, 213.
- ²⁹ Krishnan R., Binkley J.S., Seeger R., Pople J.A. *J. Chem. Phys.* **1980**, 72, 650.
- ³⁰ McLean A.D., Chandler G.S. *J. Chem. Phys.* **1980**, 72, 5639.
- ³¹ Krishnan R., Binkley J.S., Seeger R., Pople J.A. *J. Chem. Phys.* **1980**, 72, 650.
- ³² Clark T., Chandrasekhar J., Schleyer P.V.R. *J. Comp. Chem.* **1983**, 4, 294.
- ³³ Frisch M.J. *Gaussian 98*, Revision A.9, Gaussian, Inc.: Pittsburgh PA, 1998.
- ³⁴ Gale J.D. *J. Chem. Soc. Faraday Trans.* **1997**, 93, 629.

6

Towards understanding the energetics of (extra-large pore) zeolites; a polyhedral approach

Abstract

Presently the maximum pore size for zeolites stable enough to be of commercial use is approximately 8 Å. Extending the applicability of porous crystalline materials to encompass the control of molecules significantly larger than simple gases, and thus be of potential interest in the areas of fine-chemicals, pharmaceuticals and nanotechnology, requires stable materials with larger pores. Unfortunately, no systematic, rational method exists to guide the development of such materials. In this chapter, it is shown how for a large class of porous crystalline materials certain considerations of the topology and energetics of the constituent cages (using topological descriptors and quantum mechanical calculations), can lead to definite predictions regarding the stability of large pore/channel materials. The analysis formally demonstrates why smaller rings in such structures naturally compensate and help to stabilise large pores. These new insights allow us not only to predict the *relative* thermodynamic stability of a range of desirable (but as yet unmade) porous materials, but also to give practical advice to the experimentalist to guide their actual synthesis.

The contents of this chapter have been published in:

Zwijnenburg M.A., Bromley S.T., Jansen J.C., Maschmeyer T. *Chem. Mater.* **2004**, 16, 12.

6.1 Introduction

As reviewed in the introduction of this thesis, the desire to perform shape-selective adsorption and catalysis with molecules that are greater than 8Å in size has fuelled the demand for zeolites with extra-large pores (i.e. which contain rings circumscribed by more than 12 T-atoms), and research into these materials has been pursued extensively in both industry and academia¹⁻⁸. The search for such extra-large pore materials, however, is hindered by the lack of a theoretical framework connecting the energetic stability of zeolites and their structure. Recent solution calorimetry experiments^{9,10,11}, have demonstrated that zeolites can become the thermodynamically preferred reaction product under synthesis conditions, i.e. in the presence of a template. Furthermore, for the calcined zeolite frameworks the measured entropic contributions are found to be an order of magnitude smaller than those of the corresponding enthalpic terms^{12,13}. The entropic contribution also spans a considerably narrower range. Therefore, we believe that focussing on the framework energetics alone will still lead to useful results. In this chapter it is demonstrated that a better understanding of the link between zeolite structure and energetics can be obtained by decomposing zeolites into space-filling sets of face-sharing polyhedral units, leading to insights useful in the pursuit of extra-large pore zeolite syntheses.

Zeolites can be described formally and intuitively as a space-filling packing of face-sharing polyhedra¹⁴⁻¹⁶ and, thus, equivalently as tilings of Euclidian space with the polyhedra as tiles^{14,17,18}. The zeolite framework CHA for example can be seen as a 1:1 space-filling packing of chabazite ($4^{12}6^28^6$) and “double 6-ring” (4^66^2) polyhedral tiles, while, the zeolite framework FAU can be described as a 1:1:2 space-filling packing of faujasite ($4^{18}6^412^4$), sodalite (4^66^8) and “double 6-ring” (4^66^2) polyhedral tiles (see figure 6.1). The latter fact has been used, for instance, in combinatorial tiling theory to systematically enumerate novel zeolite frameworks¹⁷⁻²⁰. The faces of these polyhedra are, in contrast to e.g. rings, well-defined and their geometrical properties (e.g. number of faces, total surface area and average face size) will be demonstrated to be directly and uniquely related to the number of vertices through Euler’s formula (Eq. 6.3a-b)^A. In this study, rather than employing the concepts from polyhedral packing to classify and/or

^A Omitting T-atoms that are only two-connected after decomposition since they do not represent vertices of the polyhedron, but merely points at which an edge is bent.

enumerate zeolites, we analyse the properties of the sets of polyhedra resulting from the *space-filling decomposition* of zeolites in order to gain insights into fundamental questions of zeolitic stability. An additional benefit of focussing on the properties of polyhedra is that combinatorial tiling methods often already output such sets of space-filling polyhedra into which a structure can be decomposed¹⁷⁻²⁰, opening the possibility for high-speed analysis of structures obtained by enumeration. Furthermore, this “coarse-grained” description of zeolites opens the possibility of rationally designing new zeolites by combining different polyhedra into a space-filling packing.

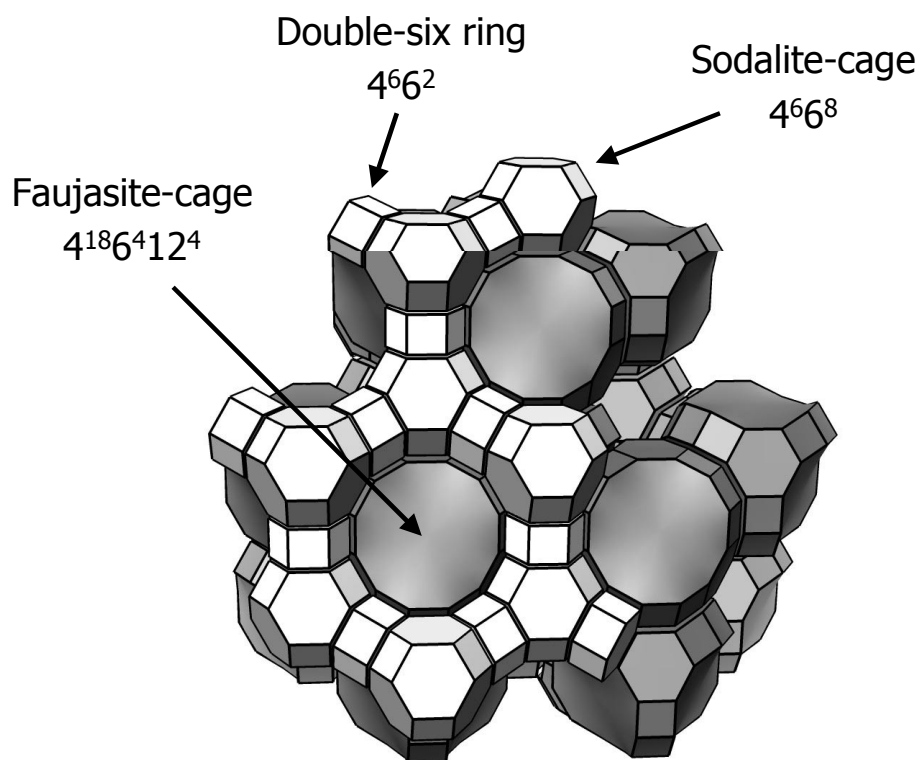


Figure 6.1. The FAU framework, clearly showing the constituting polyhedra.

Based on the above a new descriptor is proposed, which depends only on the underlying framework (i.e. using the polyhedra and their faces only), to relate the single values of energy for each zeolite to the more diffuse concept of structure. Our descriptor is given by two variables: the Average and the Variance of the face-size distribution of the polyhedra obtained from decomposing the zeolite, i.e. the first two cumulants.

Furthermore, it is demonstrated that these parameters are not only descriptive, but also predict which combinations of faces are needed to create the desired extra-large pores.

This chapter will concentrate on the correlation between energetics (binding energies) of such polyhedra and their face-size distribution (see chapter seven, for work on extended zeolite frameworks). The rationale to first explore clusters rather than extended structures follows from the ease with which it is possible to generate such polyhedra and, thus, to extensively sample the various face-size distributions and their associated cumelants. We mainly focus on polyhedra in which all the vertices are three-connected. For the purpose of calculations they are treated as silsesquioxanes ($H_nSi_nO_{1.5n}$). A significant percentage of all known zeolites can be decomposed in solely such polyhedra including among others SOD, LTA, FAU, RHO, KFI, DOH, AST and CHA, the so-called simple tilings. To describe polyhedra in which some of the vertices are only two-connected (as appearing in frameworks as MFI, VFI, GIS and MOR and dense polymorphs such as Quartz, Cristobolite and Tridymite), a more extended version of theory is required which will be only touched upon presently and treated more elaborately in future work. In this chapter, the energetics of bare silica cages is studied, even though; zeolites only become the thermodynamically preferred reaction-product in the presence of a template. However, as discussed in chapter one, it appears that a template molecule imposes its effective inverse shape on the framework by maximizing its interactions with the silica, thereby selecting a certain cage-type, but that this selectivity is not influenced by the specific nature and strength of the interactions alone. Although this chapter focuses on zeolites, the general methodology developed herein is most likely also applicable to other framework materials as diverse as metallophosphates, silicon clathrates, fullerenes and carbon nanotubes.

6.2 Computational details

Silsesquioxanes and related silica clusters have been widely used as both experimental²¹⁻²⁵ and theoretical²⁶⁻³³ model-systems for zeolites, due to their similarities with their periodic analogues in terms of structure and rigidity²⁶. For these studies, ranging from investigations into the effect of ring-size and metal substitution on zeolite energetics to those focussing on vibrational modes of zeolites or on zeolite-based catalysis, the cluster approach with hydrogen termination was shown not to influence

the outcome of these studies. From a theoretical point of view, hydrogen termination has been shown to be an efficient and accurate method for saturating the dangling bonds of the silica cluster^{34,35}, owing much of its utility to the electronegativity of hydrogen lying between that of silicon and oxygen. For the purpose of calculations, we did not consider all of the possible isomers of all cages, but restricted ourselves to a combination of clusters found in zeolites, known isomers of silsesquioxanes and selected enumerated clusters. We explicitly decided to include non-zeolite like clusters (for instance containing two membered silica rings not found in zeolites but present in other silica polymorphs³⁶) to prevent biasing our results to known frameworks. Furthermore, we limited ourselves to clusters with a maximum of 24 T-atoms since accurate calculations on larger clusters would have been prohibitively demanding in terms of both computer-time and memory requirements. This choice of isomers allows for an optimal and efficient study of the effect of different face-size distributions on the stability of polyhedra.

All electron calculations were performed for twenty-nine different silsesquioxanes employing Density Functional Theory. The DF calculations were performed using the three parameter B3LYP³⁷ functional and a 6-31G** basis set³⁸⁻⁴⁰, as implemented in the program Gaussian98⁴¹. The geometric parameters for all clusters were fully optimised using tight optimisation criteria (max force = 150^{-6} au, RMS force = 100^{-6} au, max displacement 60^{-6} au, RMS displacement 40^{-6} au). To ensure that true minima were found, all clusters were optimised without any symmetry constraints. Furthermore, for all clusters with less than 10 T-atoms the use of symmetry in the wavefunction and gradient evaluation was explicitly disabled. Finally, it was verified that the symmetry for the converged clusters was equal or lower than that found in previous work^{26,31}.

All energies reported for the silsesquioxanes are binding energies or binding energy differences normalised to the number of T-atoms in the polyhedron (kJ/mol/T-atom). Binding energies were calculated from the difference between the total energy of the silsesquioxane and the corresponding isolated doublet H and triplet O and Si atoms at the same level of theory. All silsesquioxanes are described as if they were 3-valent 3-connected polyhedra in which every Si-H group represents a vertex. Following Agaskar and Klemper⁴², we use the notation of X^n to represent n

X-membered faces. For example, the double four-ring is given by 4^6 , while a double six-ring will be represented as 4^66^2 (see fig. 6.1).

6.3 Results

The binding energies calculated for all polyhedra and associated geometrical data are given in table 6.1.

N_v	Face-size distribution	$\langle X \rangle$	σ_x	E_b (kJ/mol T-atom)	Point group	Remark
4	3^4	3.00	0.00	-1411.1	T_d	DFH-1
4	2^24^2	3.00	1.00	-1373.6	D_{2h}	
6	3^24^3	3.60	0.49	-1439.3	D_{3h}	DFH-2
6	$2^13^25^2$	3.60	1.20	-1417.2	C_{2v}	
6	2^36^2	3.60	1.96	-1382.2	D_{3h}	
8	4^6	4.00	0.00	-1448.8	O_h	DFH-3
8	$3^24^25^2$	4.00	0.82	-1444.4	C_{2v}	
8	3^46^2	4.00	1.41	-1434.5	D_{2h}	
8	2^48^2	4.00	2.83	-1383.6	C_s	
10	4^55^2	4.29	0.45	-1450.2	D_{5h}	
10	$3^14^35^3$	4.29	0.70	-1448.5	C_{3v}	
10	$2^14^46^2$	4.29	1.28	-1436.8	C_1	
12	4^45^4	4.50	0.50	-1450.7	D_{2d}	
12	4^66^2	4.50	0.87	-1449.7	D_{6h}	DFH-6
12	$3^14^45^16^2$	4.50	1.00	-1448.6	C_s	
12	3^25^6	4.50	0.87	-1448.1	D_{3d}	DFH-4
12	3^46^4	4.50	1.50	-1443.5	C_{3v}	DFH-5
14	4^35^6	4.67	0.47	-1450.0	D_{3h}	
14	$4^45^46^1$	4.67	0.67	-1450.7	C_{2v}	
14	4^66^3	4.67	0.94	-1450.1	D_{3h}	
14	4^77^2	4.67	1.25	-1449.1	D_{7h}	
14	$3^24^58^2$	4.67	1.83	-1445.1	C_{2v}	
16	4^25^8	4.80	0.40	-1451.2	C_2	DFH-12
16	$4^45^46^2$	4.80	0.75	-1450.8	C_{2h}	DFH-9
16	4^66^4	4.80	0.98	-1450.2	C_s	DFH-10
16	4^88^2	4.80	1.60	-1448.4	D_{8h}	DFH-8
18	4^66^5	4.91	1.00	-1450.1	C_{2v}	DFH-17
20	5^{12}	5.00	0.00	-1451.2	D_2	
24	4^66^8	5.14	0.99	-1449.7	O_h	DFH-27

Table 6.1 Face-size distribution, average face-size, standard deviation (square root of the variance), binding energy normalised to the number of Si atoms (E_b) and point group of the polyhedra. (DFH-N corresponds to polytope N, as defined by Delgado-Friedrichs and Huson¹⁸).

An intriguing initial observation is that those polyhedra of this set, that have actually been found in zeolites, lie in a 3 kJ/mol/T-atom envelope above the lowest energy cage (see figure 6.2). Secondly, it is noteworthy that within this region lie also two three-face containing polyhedra.

The average face size of a polyhedron can be calculated from the face size distribution of a polyhedron via:

$$\langle x \rangle = \frac{\sum_{i=1}^{N_F} x_i}{N_F} \quad (6.1)$$

In which N_f is the total number of faces and x_i the face size of the i th face of the polyhedron. Furthermore, one can define the number of vertices of a polyhedron, N_v , in terms of the constituent faces *via*:

$$N_V = \frac{1}{3} \sum_{i=1}^{N_F} x_i \quad (6.2)$$

While N_f can be expressed as a function of the number of vertices by applying Euler's equation and by realising that the stoichiometry of those polyhedra, that contain three connected vertices exclusively, fix the ratio between vertices and edges as 1:3

$$N_V + N_F - N_E = 2 \quad (6.3a)$$

$$N_F = 2 + \frac{1}{2} N_V \quad (6.3b)$$

Substitution of the latter two results in equation one gives the formula for the average face size of a polyhedron:

$$\langle x \rangle = \frac{3N_V}{2 + \frac{1}{2}N_V} \quad (6.4)$$

The average face size, thus, only depends on the number of vertices (T-atoms) of a polyhedron and is, therefore, equal for all isomers.

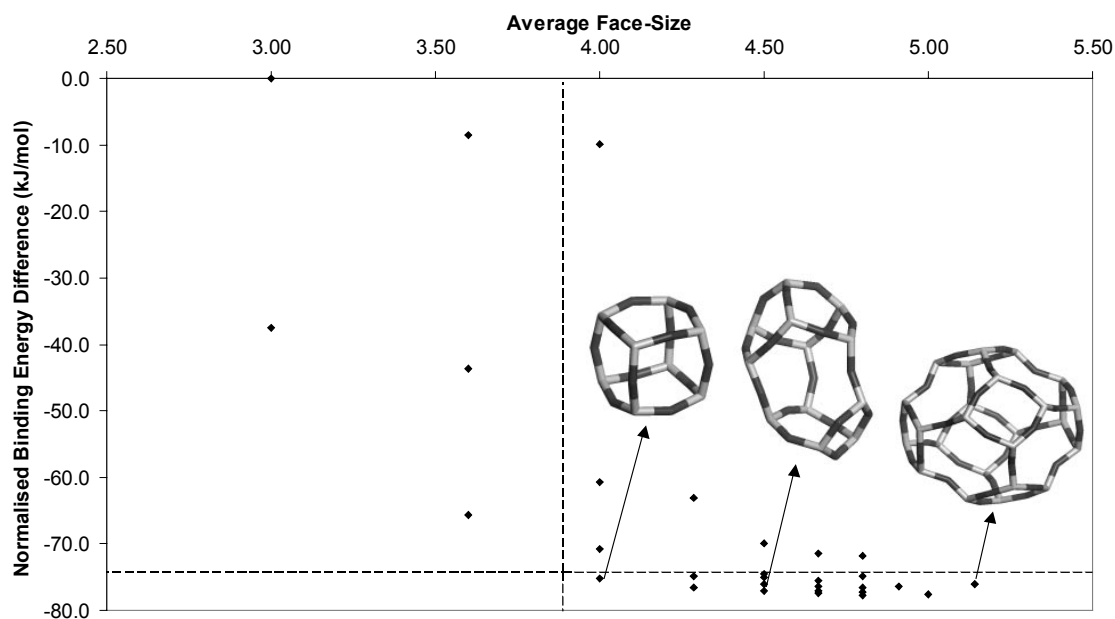


Figure 6.2 Calculated binding energies (normalised to the number of Si atoms) versus the average face-size of the polyhedra (box as discussed in text). The terminating hydrogen atoms are omitted for ease of visualisation.

Figure 6.2 shows how the binding energies of the polyhedra vary with the average face size. While it clearly shows the effect of isomers, i.e. multiple energy values for one average face size, it also shows a correlation between the lowest energy isomers and their corresponding average face sizes. Average face size thus, as to be expected from the fact that it is equal for isomers, only describes part of the energetics of the polyhedra. Furthermore, the graph shows an effective upper boundary to the binding energy of three connected polyhedra given by polyhedra of a $(2^{n/2}n^2)$ nature.

The second cumulant (variance) can be calculated from the face size distribution of a polyhedron via:

$$\sigma_X^2 = \frac{\sum_{j=1}^{N_F} (X_j - \langle X \rangle)^2}{N_F} \quad (6.5)$$

Figures 6.3a-b shows how the binding energy of isomeric polyhedra changes with their associated variance^B. For each set of isomers, one can observe a strong and closely similar correlation between binding energy and the variance of their face-size distribution. Furthermore, the slope of the correlation consistently decreases with increasing average face size. Both observations are consistent with the energetics of three-connected polyhedra being described by a surface defined in terms of the average and variance of the face-size distribution. One point of interest can be observed in figure 6.3b for an average face size of 4.5, where there are two cages ((3^25^6) and (4^66^2)) with the same variance but different binding energies. In such rare cases, when two polyhedra have equal average and variance but a different face-size distribution, our two-parameter description is inherently not sufficient to distinguish between their energies.

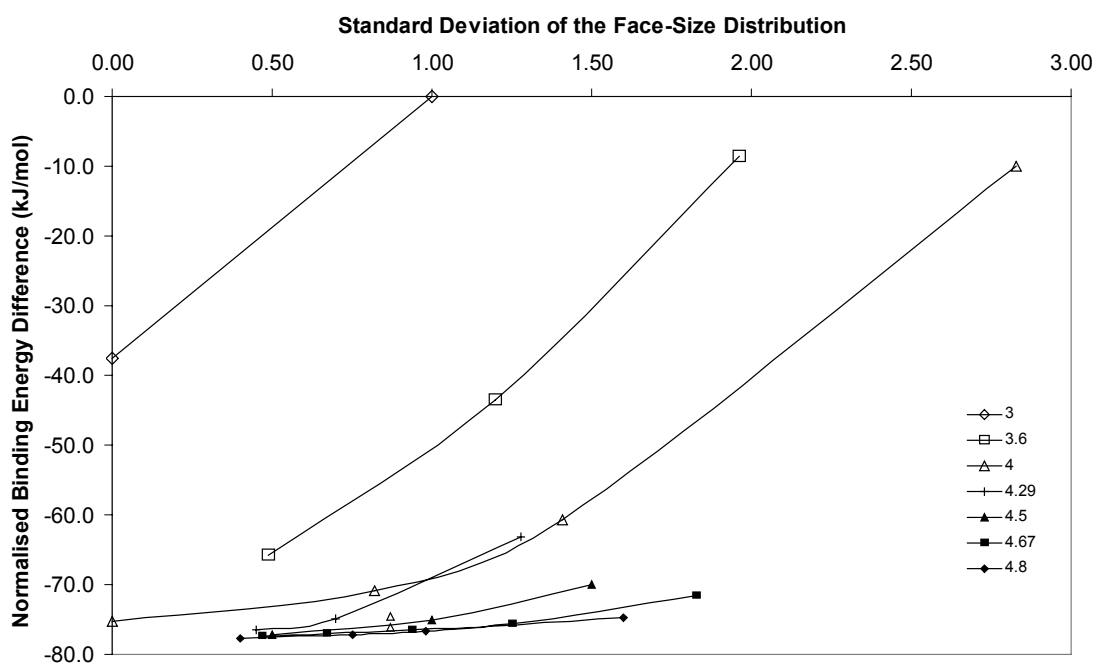


Figure 6.3a Calculated binding energies (normalised to the number of Si atoms) versus the standard deviation (square root of the variance) of the face-size distribution for the various sets of isomers. The lines are guides to the eyes.

^B For ease of visualisation, we plot the standard deviation rather than the variance. The standard deviation equals the square root of the variance.

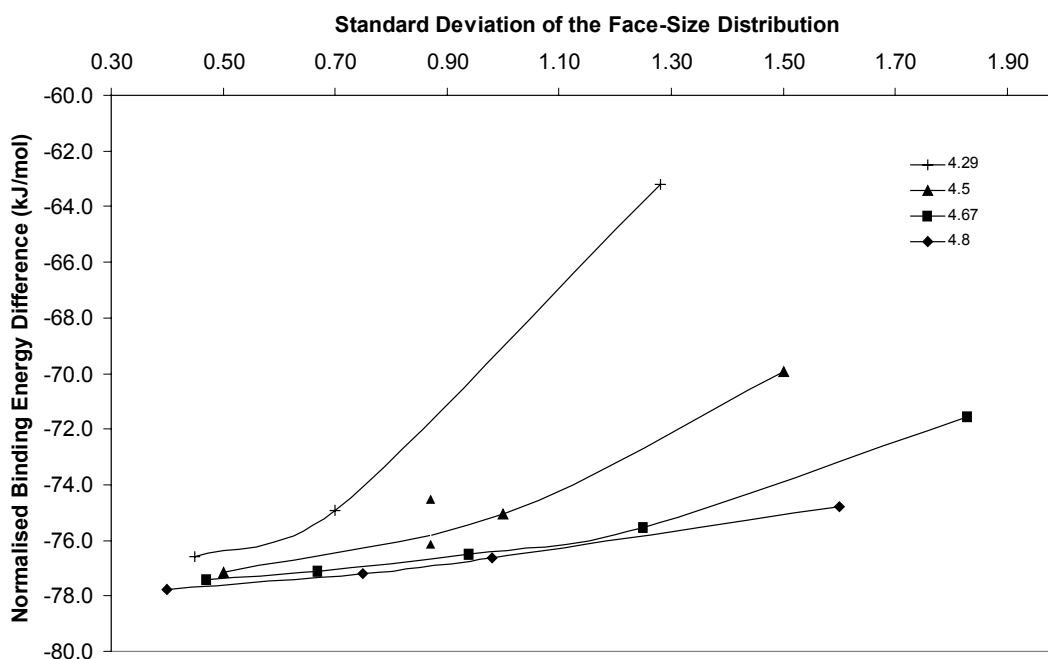


Figure 6.3b Calculated binding energies (normalised to the number of Si atoms) versus the standard deviation (square root of the variance) of the face-size distribution for the various sets of isomers (magnification of figure 6.3a). The lines are guides to the eyes.

6.4 Discussion

The energetics of the polyhedra can be described in terms of the average and the variance of their face-size distribution. However, for these descriptors to have any more value than merely statistical, one has to understand their physical significance. It is known from previous calculations that smaller rings are more strained than larger rings and that their binding energy is inversely proportional to a function of their ring size^{43,44}. It should, therefore, be expected that if the average face-size would be a complete description of the system, the energy would also vary with inverse proportionality to the average face-size. This trend is indeed clearly recovered for the cages when considering only the lowest energy cages for each average ring size (see figure 6.4). To these special cages we will refer to hereafter as ‘principal polyhedra’. It is interesting to note that the larger principle polyhedra ($\langle x \rangle \geq 4$) are all commonly found in clathrasils⁴⁵.

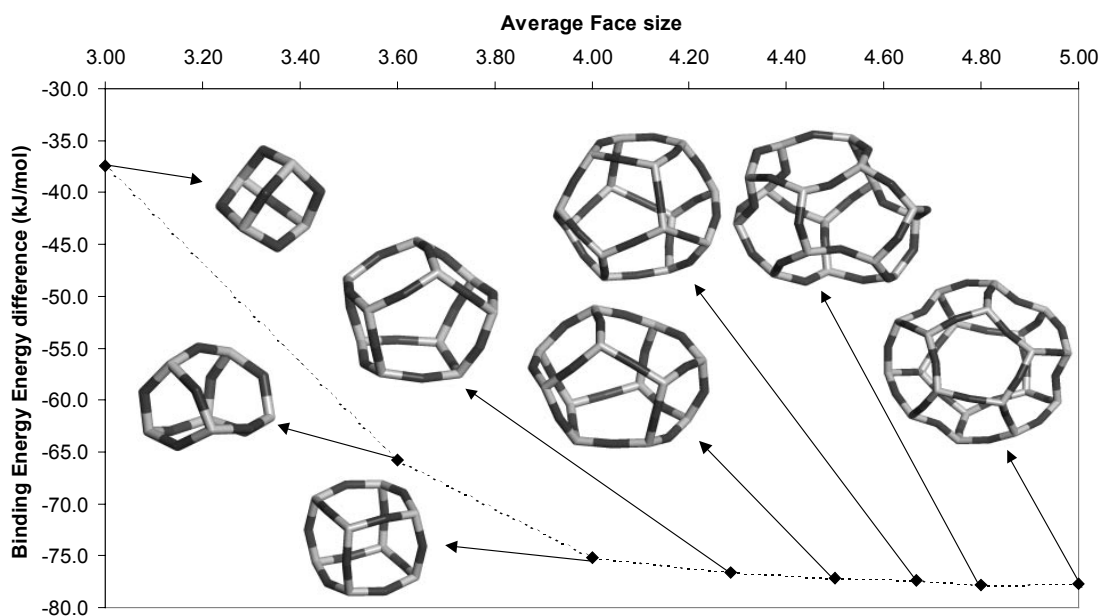


Figure 6.4 Calculated binding energies (normalised to the number of Si atoms) versus the average face-size of the principal polyhedra. The terminating hydrogen atoms are omitted for ease of visualisation.

Principal polyhedra are found to be those cages consisting of either only one face-size (if the average face size is integral) or of those solely consisting of the two types of faces closest to the average face size. Thus, by definition, principal polyhedra are the polyhedra with minimal variance for each set of isomers. To investigate this further, a model of how the energies of cages vary with the different faces possibly present has been developed. A first approximation, neglecting everything but the energies, E_i , of the individual faces (normalised to the number of T-atoms in the face, kJ/mol/T-atom), results in the following expression for the cage energy:

$$E_{cluster} = \frac{1}{3N_V} \sum_{i=1}^{N_F} x_i E_i \quad (6.6)$$

Assuming that E_i is a well-behaved function of the face-size, E_i can be expressed in terms of a power series in x_i :

$$E_i = \alpha_0 + \frac{\alpha_1}{x_i} + \frac{\alpha_2}{x_i^2} + \dots \quad (6.7)$$

Substitution of Eq. 6.7 in Eq. 6.6 results in:

$$E_{cluster} = \frac{1}{3N_V} \sum_{i=1}^{N_F} (\alpha_0 x_i + \alpha_1 + \frac{\alpha_2}{x_i} + \dots) \quad (6.8)$$

By applying Eq. 6.2 to the first term in the summation, this can be written, in turn, as:

$$E_{cluster} = \alpha_0 + \frac{\alpha_1}{\langle X \rangle} + \frac{1}{3N_V} \sum_{i=1}^{N_F} (\frac{\alpha_2}{x_i} + \dots) \quad (6.9)$$

While this expression is only an approximation and while we have no knowledge about the precise magnitude of the coefficients, it clearly shows that energy should vary with inverse proportionality to the size of the face and linearly with its occurrence as long as E_i decreases monotonically and has a horizontal asymptote. The principal polyhedra now should be the isomers, which minimize the cage energy (Eq. 6.9) within the boundary conditions imposed by equation 6.3b. While such a minimization is far from facile due to the general nature of the energy function, it is possible to study, by inspection, the correlation between binding energy and variance. Increasing the variance corresponds to replacing faces close to the average face-size with both smaller and larger faces, while keeping the total number of faces constant as required by Euler's equation (Eq. 6.3b). Therefore, upon increasing the variance of a polyhedron, the face-size distribution becomes broader and more asymmetric, resulting in more and more faces being smaller than the average face-size and less and less faces being larger than the average. The combination of the latter with the fact, that according to the form of Eq. 6.9, smaller faces raise the energy of a polyhedron considerably (while larger faces only slightly decrease the energy) provides an explanation for the observed positive correlation between the variance and binding energy of isomers. Minimisation of the cage energy for a certain polyhedron size, N_v , corresponds to a minimisation of the variance, while keeping the average face-size constant. The

principal polyhedra are, therefore, as observed, those polyhedra with minimal variance for each set of isomers.

In the same way as the principal polyhedra were shown to be the isomers with minimal variance, the effective upper boundary of binding energies can be defined by polyhedra which maximise the variance. Although again no formal proof will be given, one can easily see that for $N_v=n$ an isomer of ring-like nature ($2^{n/2}n^2$) will have the highest variance obtainable for that polyhedron. All the binding energies of three-connected polyhedra, thus, lie in an envelope (not shown), with the energies of the ($2^{n/2}n^2$) isomers as upper boundary and the energies of the principal polyhedra as lower boundary. Summarizing, the energy of polyhedra can be described as a surface defined by the average and variance of the face-size distribution, with the line connecting the principal polyhedra as limits for minimal variance and the line connecting the ($2^{n/2}n^2$) polyhedra as limit for the maximal variance.

The results discussed above for three-connected polyhedra, and thus silsesquioxanes, now can be expanded to understand zeolites. As discussed in the introduction, there exists a significant portion of zeolites, which can be fully decomposed into solely three-connected polyhedra. For such zeolites, the polyhedra would be expected to be more than only model systems and the correlations obtained for the polyhedra would be expected to also hold for these zeolites. When expressing the energetic stability of such zeolites as their transition enthalpy to quartz^{12,13}, we should therefore expect a decreasing transition enthalpy with the average face size and an increasing transition enthalpy with increasing variance of the face-size distribution. Moreover, due to the generality of the derivation (Eqs. 6.6-6.9), which make no reference to the specific chemical constitution of the polyhedra involved, we expect our predicted correlations to hold also for substituted zeolites, and metallophosphates.

Before investigating the problem of zeolite stability in general, it is worth focussing upon the energetics of polyhedra with three-faces as it has been suggested in the past that zeolites containing such cages are especially disadvantageous²⁶. This assumption is supported by the fact that no three-face-containing zeolite framework has, thus far, been crystallised in the all-silica form and that three-face containing zeolites mostly contain special T-atoms (Be, Li, Zn). Our results, in contrast, indicate that the presence of small faces is not, by definition, as detrimental to the energetic stability of zeolites as previously thought. The presence of three-faces, indeed, increases the energy

compared to larger faces, but the size of this destabilisation critically depends on the concentration of such faces. Two of our three-face-containing polyhedra lie within 3 kJ/mol/T-atom of the lowest energy polyhedron, just slightly above the cube (“double four ring D-4R”). These results are of special interest since one of these cages is the three-face containing cage found in ZSM-18 (MEI framework). The reason other authors²⁶ found that three-face-containing structures were significantly less stable than those only containing larger faces is that only very small silsesquioxanes (e.g. tetrahedron) were studied, all of which possess high three-face concentrations. Three-face-containing zeolites are, thus, very likely to be more stable than previously expected.

Generally, our conceptual approach can further explain some important characteristics of zeolites decomposable in solely three-connected polyhedra. Since the pores/channels in zeolites are an integral part of the crystal structure, the rings controlling the diffusion through the channels should equal the faces of the constituting polyhedra. A zeolite with 8 and 12-ring channels should therefore, for example, consist of polyhedra with faces of 8 and 12 Si-atoms (although these do not necessarily have to be in the same polyhedron^C). The average face size of a three-connected polyhedron, however, has a limit of six: as can be seen from rewriting equation 4 as a constant and a term that vanishes as N_v tends to infinity.

$$\langle x \rangle = 6 - \frac{6}{1 + \frac{N_V}{4}} \quad (6.10)$$

This is inline with the average ring (face) size of polyhedra decomposable four-connected nets, as derived by O’Keeffe *et al* (eq. 3.15 in ref 15).

A three-connected polyhedron with faces larger than five should, therefore, always have faces smaller than six to compensate. Starting from a “dense”^D structure, consisting of principal polyhedra, creating and subsequently increasing the size of channels corresponds to increasing the variance, and thus to decreasing the energetic

^C Rings smaller than 8 Si atoms are commonly not seen as part of channels because they are assumed to be too small for molecular diffusion (although diffusion of He, H₂ and H₂O occurs through 6-rings) and only part of the faces of a polygon will thus be part of a channel.

^D Principal polyhedra always have only faces of six or smaller and a principal polyhedra can therefore never be part of a channel in a structure (see footnote F).

stability of the constituent polyhedra. The extra energetic cost of larger pores can be compensated somewhat by increasing the size of polyhedra the zeolite consists of, thereby increasing the average face-size (the other energy-dependent parameter of our descriptor), provided the number of vertices is far from the limit. This effect can be observed when comparing the 8 Si-atom ($3^2 4^2 5^2$) and the 24 Si-atom ($4^6 6^8$) cages: whilst the larger cage has eight 6-faces, larger than any face in the smaller cage, and, furthermore, has a less energetically favourable variance than the smaller cage, it is 5.3 kJ/mol/T-atom lower in energy than the smaller cage due to its larger average face size. While this effect becomes negligible at average face-sizes larger than 4.8, where the energy difference between cages with similar variance is insignificant (< 0.1 kJ/mol – see for example the flattening of trend shown in figure 6.4), large cages are still an energetically favourable means to incorporate large pores. This is simply due to the fact that cages with an increased size, and therefore more vertices, allow for face sizes closer to the limiting value of 6 to be used for compensation for the introduction of large pores (e.g. many five-faces instead of few three-faces) thereby lowering the variance, and thus the energy. Normally, zeolites consist of a mixture of different polyhedra. The inclusion of low variance (principal) polyhedra lowers the energy of the framework^E by diluting the energetic disadvantage of the higher variance polyhedra. The resulting zeolite, however, will always be higher in energy than a zeolite solely consisting of low variance (principal) polyhedra.

Based on the above, one can now calculate the minimum cage-sizes (three-connected polyhedra) needed to accommodate certain types of catalytically interesting channel-systems, when assuming that they only contain the desired faces (corresponding to extra-large pores) and compensating three-, four- or five-faces. The results of these calculations for several (extra-) large channel systems (12***, 14***, 18***, 14**, 18**, 14*, 18*, where the number of asterisk's denotes the dimensionality of the pore system) can be found in table 6.2. The first thing to note is, since the energy of these large polyhedra is described by only the variance of their face-size distribution (see above) and their energetic stability is inversely proportional to a function of this variance, the ordering of the energetic stability of the channel-systems for the same pore-size is predicted to go as one-dimensional (2 extra-large faces) > two-dimensional (4 extra-large faces) > three-dimensional (6 extra-large faces). Furthermore, using the

^E Under the reasonable assumption that $E_{\text{zeolite}} \propto \sum E_{\text{polygon}}$

same argument the energetic ordering of channel-systems is predicted to be as $12 > 14 > 18$. From an energetic point of view, we would, therefore, expect that the probability of synthesizing extra-large-pore zeolites decreases with both the dimensionality of its channel-system and the size of the pores.

Channel system	Face-size distribution	N_v	$\langle X \rangle$	σ_x
12***	$5^{48}12^6$	104	5.78	2.20
14*	$5^{28}14^2$	56	5.6	2.24
14**	$5^{44}14^4$	92	5.75	2.49
14***	$5^{60}14^6$	128	5.82	2.59
18*	$5^{36}18^2$	72	5.68	2.90
18**	$5^{60}18^4$	124	5.81	2.18
12***	$4^{24}12^6$	56	5.60	3.20
18***	$5^{84}18^6$	176	5.87	3.24
14*	$4^{14}14^2$	28	5.25	3.31
14**	$4^{22}14^4$	48	5.54	3.61
14***	$4^{30}14^6$	68	5.67	3.73
12***	$3^{16}12^6$	40	5.45	4.01
18*	$4^{18}18^2$	36	5.40	4.20
18**	$4^{30}18^4$	64	5.65	4.51
18***	$4^{42}18^6$	92	5.75	4.63
14***	$3^{20}14^6$	48	5.54	4.63
18*	$3^{12}18^6$	24	5.14	7.07
18**	$3^{20}18^4$	44	5.50	5.59
18***	$3^{28}18^6$	64	5.65	5.72

Table 6.2 Face-size distribution, number of vertices, average face-size and standard deviation (square root of the variance) of the minimum cages needed to accommodate five catalytically interesting channel-systems in order of increasing variance. The number of asterisks indicates the dimensionality of the pore-system.

The data in table 6.2 also shows that, as explained above, for the same channel-system dimensionality and pore-size, the variance can be lowered by increasing the size of compensating faces. The lowest variance polyhedra from table 6.2 are all larger than 56 vertices, while the largest polyhedra currently known in synthetic zeolites have 48 vertices^F. A natural zeolite containing a 96 vertices cage is known (TSC, $4^{24}6^88^{18}$) but this cage contains a non-removable $\text{Cu}^{2+}_{48}(\text{OH})^{-}_{128}$ cluster⁴⁶. Synthesizing zeolites with such large cages poses a significant synthetic challenge. Furthermore,

upon increasing the size of the compensating faces clathrasil cages containing only 5- and 6-faces become quickly more stable than the higher-variance large-faced cages, further decreasing the chance of a successful synthesis of the large-faced cages.

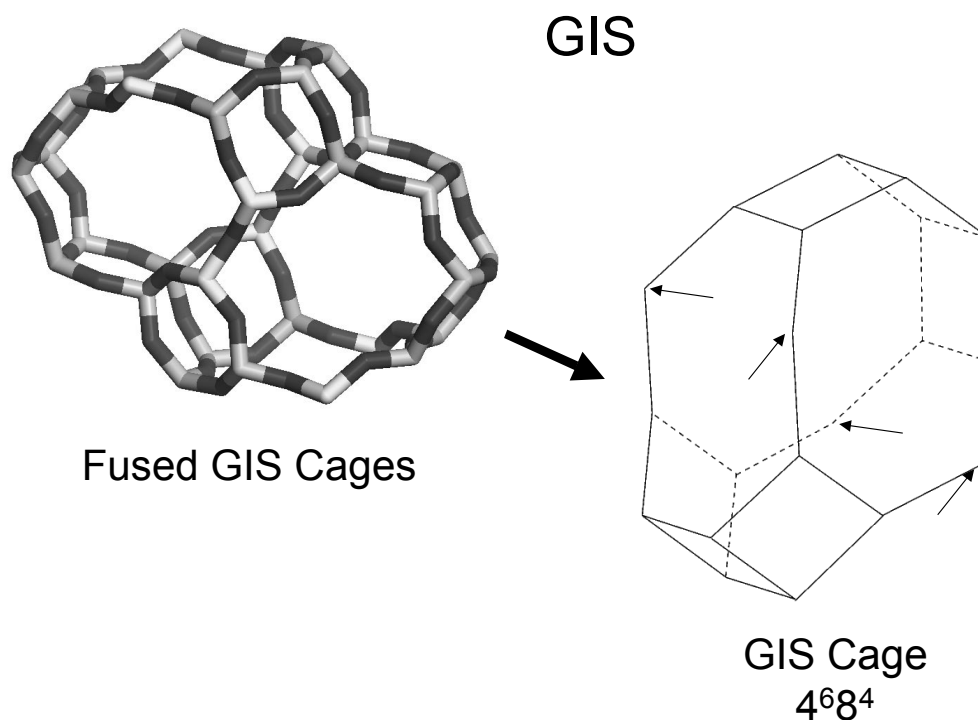


Figure 6.5 Decomposition of the GIS framework into a space filling set of polyhedra (2-connected vertices highlighted).

For zeolites that can be decomposed in polyhedra containing both two and three connected vertices (mixed-vertex polyhedra), the situation is somewhat more complicated. While upon adding two-connected vertices to a polyhedron the number of faces remains constant, the face-size of the faces in which the vertices are inserted increases. Taking λ to equal the ratio between two and three connected vertices (for example GIS: $N_{v2} = 4$, $N_{v3} = 16$, $\lambda = 4/16$, see figure 6.5) of a polyhedron, the average face size equals:

$$\langle x \rangle = \frac{(3+2\lambda)N_{v3}}{2+\frac{1}{2}N_{v3}} \quad (6.11)$$

^F LTA, RHO, KFI: 4¹²6⁸8⁶; FAU: 4¹⁸6⁴12⁴

This, in turn, can be written in a way analogous to Eq. 6.10:

$$\langle x \rangle = 6 + 4\lambda - \frac{(6+4\lambda)}{1 + \frac{N_{V3}}{4}} \quad (6.12)$$

The average face size of mixed-vertex polyhedra, thus, has a limit of $6+4\lambda$ as N_{V3} tends to infinity and only faces larger than $5+4\lambda$ need compensating by smaller faces. The fact that the average face size increases with increasing λ , suggests that increasing λ might be an alternative route to extra-large pores. Preliminary calculations suggest that polyhedra with $\lambda \neq 0$ are slightly more energetically stable than their $\lambda = 0$ analogues. An observation that is supported by experimental calorimetric measurements^{12,13} where all low-lying silica polymorphs are those (partly) decomposable into mixed-vertex polyhedra. The data in table 6.2 is calculated for three-connected polyhedra ($\lambda = 0$). To calculate the equivalent of table 6.2 for polyhedra with $\lambda \neq 0$ would be a formidable task because of the extra degree of freedom. It is evident, however, that when allowing λ to change freely, one can accommodate channel-systems in much smaller cages than when $\lambda = 0$ (even with a lower variance). This is clearly illustrated by the 12^6 ($\lambda = 3$) cage found in zeolite ITQ-21⁴⁷.

Applying our conceptual methodology to the prediction and rationalisation of actual experimental all-silica syntheses is complicated by many factors. However, from cage energetics alone, one would expect (at least for $\lambda = 0$ zeolites) the formation of frameworks containing many principal polyhedra, i.e. clathrasil-like structures. Clathrasils are, indeed, often found as product in $\text{SiO}_2/\text{template}/\text{H}_2\text{O}$ systems⁴⁵ e.g. AST, DOH, MEP, MTN, SOD (all $\lambda = 0$). However, besides such materials a range of larger-faced porous all-silica structures, for example the $\lambda = 0$ materials: Chabazite (CHA), Deca-dodecasil 3R (DDR), SSZ-23 (STT), RUB-3 (RTE), and the $\lambda \neq 0$ materials: Beta (BEA), ITQ-4 (IFR), SSZ-24 (AFI), CIT-5 (CFI), have also been synthesized successfully^{45,48,49}. The formation of these larger-faced structures, at first sight, appears to be in contradiction with the results of our calculations. However, on closer examination this issue can be resolved by considering further the role of the template. Molecules with a small aspect ratio, like small cyclic molecules, whilst

rotating effectively fill the lowest-energy cages (principal polyhedra). Template molecules with a large aspect ratio, such as linear or branched molecules, do not fill, or even fit into, these cages. Such large aspect ratio templates seem to force their structure upon the cages, resulting in cages other than principal polyhedra, but possibly with the desired larger faces. Such a model of the influence of template molecule is in line with the experimental observation of Gies and Marler that, while clathrasils are the exclusive product when the template is a small mono- bi- or tricyclic molecule. Upon changing the template to a linear or branched molecule, the products display tubular structures⁴⁵. A similar change of structural characteristics has also been observed by Nakagawa *et al*⁵⁰ upon increasing the size of their bridged bicyclic template molecule. We, thus, speculate that siliceous zeolite cages with the desired large or extra-large faces are necessarily non-spherical and can only be synthesized from template molecules having a high aspect ratio. An experimental illustration of this prediction is that the small aspect ratio tert-butyltrimethylammonium cation templates the $4^6 6^{12}$ cage in AST⁵¹, while the higher aspect ratio N, N, N-trimethyladamantammonium cation templates the $4^{12} 6^2 8^6$ cage of CHA⁵². Thus the fact that using the 18-Crown-6 complex of sodium as template in the synthesis of the non-all-silica zeolite MCM-61⁵³ (MSO framework) results in the formation of large clathrasil cages ($4^6 6^{20}$) rather than the desired large-faced cages, can, also most likely be explained by the small aspect ratio of the template employed. Whether this observation holds for zeolites generally, is a more complex question, since metal substitution may change the relation between a cage-type (face-size distribution) and its energetic stability, and thus perhaps preferably stabilise large-faced cages, in line with observations by Corma *et al* for Germanium substituted frameworks⁵⁴ (see chapter 8).

On the basis of the above one can conclude that synthesizing extra-large-pore zeolites corresponds, at least for zeolites decomposable in $\lambda = 0$ polyhedra, to steering the synthesis mixture towards a combination of small rings and large cages, probably *via* the use of large aspect ratio templates. The presence of sufficient small rings herein is critical since otherwise the more energetically stable polyhedra, with predominantly five- and six-faces, will be formed most probably, resulting in clathrasils rather than extra-large-pore zeolites. Therefore, additives that promote the formation of a certain number of 3-rings may point the way towards large-pore zeolites. For zeolites decomposable into $\lambda \neq 0$ polyhedra the situation is considerably less clear. However,

based on the results achieved so far, we feel confident that eventually for all zeolites the presence of extra-large-pores can be coupled to properties of their constituting polyhedra and that more general rules regarding the synthesis of extra-large-pore zeolites will be derived.

6.5 Conclusions

Synthesising extra-large-pore zeolites appears, thus, to be all about striking a fine balance between face- and cage-sizes with the energetic stability of large-faced cages depending predominantly on the variance of the face-size distribution. Our investigation has shown that decomposing zeolites into polyhedra combined with Euler's rule and DF calculations can give remarkable insights into the fundamental properties of zeolites. In particular, we have shown that the energetic destabilisation of zeolites by small rings depends on their concentration and can be as small as only 2.6 kJ/mol. We further demonstrate that the energetics of three-connected polyhedra, as modelled by silsesquioxanes, can be understood in terms of a two parameter descriptor utilising both the *average* and *variance* of their face-size distribution, and propose that the same correlations should hold for all zeolites which can be thought of as completely decomposable in to three-connected polyhedra. For the same class of zeolites we have formally established that large pores require compensation by small faces and that the more energetically stable, extra-large pore zeolites are the ones consisting of large polyhedra. Finally, we demonstrate that steering the synthesis mixture towards small rings and large cages most likely offers a route to extra-large-pore zeolites.

References

- ¹ Davis M.E. *Chem. Eur. J.* **1997**, 3, 1745.
- ² Davis M.E., Saldarriaga C., Garces J., Crowder C. *Nature* **1988**, 331, 698.
- ³ Estermann M., McCusker, L.B., Baerlocher C., Merrouche C.A., Kessler H. *Nature* **1991**, 352, 320.
- ⁴ Jones R.H., Thomas J.M., Chen J., Xu R., Huo Q., Li S., Ma Z., Chippindale A.M. *J. Solid State Chem.* **1993**, 102, 204.
- ⁵ Balkus, K.J., Gabrierlov A.G., Sandler N. *Mater. Res. Soc. Symp. Proc.* **1995**, 368, 369.
- ⁶ Balkus K.J., Khanmamedova A., Gabrierlov A.G., Zones S.I. *Stud. Surf. Sci. Catal.* **1996**, 101, 1341.
- ⁷ Lobo R.F., Tsapatsis M., Freyhardt C.C., Khodabandeh S., Wagner P., Chen C.Y., Balkus K.J., Zones S.I., Davis M.E. *J. Am. Chem. Soc.* **1997**, 119, 8474.
- ⁸ Strohmaier K.G., Vaughan D.E.W. *J. Am. Chem. Soc.* **2003**, 125, 16035.
- ⁹ Petrovic I., Navrotsky A. *Microporous Mat.* **1997**, 9, 1.
- ¹⁰ Piccione P.M., Yang S., Navrotsky A., Davis M.E. *J. Phys. Chem B.* **2002**, 106, 3629.
- ¹¹ Yang S., Navrotsky A. *Chem. Mater.* **2002**, 14, 2803.
- ¹² Piccione P.M., Laberty C., Yang S., Cambor M.A., Navrotsky A., Davis M.E. *J. Phys. Chem B.* **2000**, 104, 10001.
- ¹³ Piccione P.M., Woodfield B.F., Navrotsky A., Davis M.E. *J. Phys. Chem B.* **2000**, 104, 10001.
- ¹⁴ Wells A.F., Sharpe R.R. *Acta. Cryst.* **1963**, 16, 857.
- ¹⁵ O'Keeffe M., Hyde B.G., Crystal Structures I - Patterns and Symmetry: Mineralogical Society of America: Washington, DC, 1996.
- ¹⁶ O'Keeffe M. *Acta. Cryst.* **1998**, A54, 320.
- ¹⁷ Delgado Friedrichs O., Dress A.W.M., Huson D.H., Klinowski J., Mackay A.L. *Nature* **1999**, 400, 644.
- ¹⁸ Delgado Friedrichs O., Huson D.H. *Discrete. Comput. Geom.* **2000**, 24, 279.
- ¹⁹ Foster M.D., Delgado Friedrichs O., Bell R.G., Almeida Paz F.A., Klinowski J. *Angew. Chem. Int. Ed.* **2003**, 42, 3896.
- ²⁰ Simperler A., Foster M.D., Bell R.G., Klinowski J. *J. Phys. Chem. B* **2004**, 108, 869.
- ²¹ Bornhauser P., Calzaferri G. *J. Phys. Chem* **1996**, 100, 2035.
- ²² Marcolli C., Lainé P., Bühler R., Calzaferri G., Tomkinson J. *J. Phys. Chem. B* **1997**, 101, 1171.
- ²³ Krijnen S., Harmsen R.J., Abbenhuis C.L., Van Hooff J.H.C., Van Santen R.A. *Chem. Commun.* **1999**, 501.
- ²⁴ Duchateau R., Harmsen R.J., Abbenhuis H.C.L., Van Santen R.A., Meetsma A., Thiele S.K.H., Kranenburg M. *Chem. Eur. J.* **1999**, 5, 3130.
- ²⁵ Liu F., John K.D., Scott B.L., Baker R.T., Ott K.C., Tumas W. *Angew. Chem. Int. Ed.* **2000**, 39, 3127.
- ²⁶ Earley C.W. *J. Phys. Chem.* **1994**, 98, 8693.
- ²⁷ Hill J.R., Sauer J. *J. Phys. Chem.* **1994**, 98, 1238.
- ²⁸ Hill J.R., Sauer J. *J. Phys. Chem.* **1995**, 99, 9536.
- ²⁹ de Man A.J.M., Sauer J. *J. Phys. Chem* **1996**, 100, 5025.
- ³⁰ Tossell J.A. *J. Phys. Chem* **1996**, 100, 14828.
- ³¹ Xiang K.H., Pandey R., Pernisz U.C., Freeman C. *J. Phys. Chem. B* **1998**, 102, 8704.
- ³² Uzunova E.L., Nikolov G.S. *J. Phys. Chem. A* **2000**, 104, 5302.
- ³³ Kudo T., Gordon M.S. *J. Phys. Chem. A* **2001**, 105, 11276.
- ³⁴ Sauer J. *Chem. Rev.* **1989**, 89, 199.
- ³⁵ Kessi A., Delley B. *Int. J. Quantum Chem.* **1998**, 68, 135.
- ³⁶ Weiss A. *Z. Anorg. Allg. Chem.* **1954**, 276, 95.
- ³⁷ Becke A.D. *J. Chem. Phys.* **1993**, 98, 5648.
- ³⁸ Hehre W.J., Ditchfield R., Pople J.A. *J. Chem. Phys.* **1972**, 56, 2257.
- ³⁹ Francel M.M., Petro W.J., Hehre W.J., Binkley J.S., Gordon M.S., DeFrees D.J., Pople J.A. *J. Chem. Phys.* **1982**, 77, 3654.
- ⁴⁰ Hariharan P.C., Pople J.A., *Theor. Chimica Acta* **1973**, 28, 213.
- ⁴¹ Frisch M.J. *Gaussian 98*, Revision A.9, Gaussian, Inc.: Pittsburgh PA, 1998.
- ⁴² Agaskar P.A., Klemperer W.G. *Inorg. Chim. Acta.* **1995**, 229, 335.
- ⁴³ Kudo T., Nagase S. *J. Am. Chem. Soc.* **1985**, 107, 2589.
- ⁴⁴ Kramer G.J., de Man A.J.M., van Santen R.A. *J. Am. Chem. Soc.* **1991**, 113, 6435.
- ⁴⁵ Gies H., Marler B. *Zeolites* **1992**, 12, 42.
- ⁴⁶ Effenberger H., Giester G., Krause W., Bernhardt H.J. *Am. Mineral.* **1998**, 83, 607.
- ⁴⁷ Corma A., Diaz- Cabañas M.J., Martinez-Triguero J., Rey F., Rius J. *Nature* **2002**, 418, 514.
- ⁴⁸ Marler B., Grünwald-Lüke A., Gies H. *Zeolites* **1995**, 15, 388.

-
- ⁴⁹ Cambor M.A., Villaescusa L.A., Diaz-Cabañas M.J. *Topics in Catalysis* **1999**, 9, 59.
- ⁵⁰ Nakagawa Y., Zones S.I. in *Synthesis of Microporous Materials* vol. 1 (222); Ocelli M.L., Robson H.: Van Nostrand Reinhold: New York, 1992.
- ⁵¹ Villaescusa L.A., Barrett P.A., Cambor M.A. *Chem. Mater.* **1998**, 10, 3966.
- ⁵² Diaz-Cabañas M.J., Barrett P.A., Cambor M.A. *Chem. Commun.* **1998**, 1881.
- ⁵³ Shantz D.F., Burton A., Lobo R.F. *Microporous Mesoporous Mater.* **1999**, 31, 61.
- ⁵⁴ Blasco T., Corma A., Diaz-Cabañas M.J., Rey, F., Vidal-Moya J.A., Zicovich-Wilson C.M. *J. Phys. Chem. B* **2002**, 106, 2634.

7

Understanding the thermodynamic viability of zeolite frameworks using a simple topological model

Abstract

Building further upon the work discussed in chapter six, in this chapter, it is shown how the decomposition of extended zeolite frameworks into polyhedral tiles, and the analysis of the face-size distribution obtained (using topological descriptors and periodic atomistic calculations on both synthesized and hypothetical frameworks) can lead to definite predictions regarding the thermodynamic viability of their hydrothermal synthesis. Moreover, it is demonstrated that pore-size and framework density cannot be varied freely, but that they, at least for frameworks corresponding to simple tilings, are intimately connected to the thermodynamic viability of the framework's synthesis through its topology. These new insights allow one, not only to rationalize the thermodynamic viability of a range of desirable (but as yet unmade) frameworks, but also to begin to understand the physical and topological boundaries which inherently limit attempts to synthesize frameworks with ever-larger pores and lower framework densities.

The contents of this chapter have been accepted for publication in:

Zwijenburg M.A., Bromley S.T., Foster M.D., Bell R.G., Delgado-Friedrichs O., Jansen J.C., Maschmeyer T. *Chem. Mater.*.

7.1 Introduction

More than 140 different zeolite frameworks have been synthesized (or found in nature^A)¹, but as reviewed in the first chapter of this thesis many applications however still call for zeolites with larger pores, lower framework densities and/or higher specific absorption volumes, than found in the currently available frameworks²⁻⁴. While, in principle, once a possible framework structure has been postulated one can calculate any of its specific properties using a range of atomistic and electronic modelling methods, such calculations do not provide general insight in how the framework thermodynamic viability depends on its global structural characteristics nor the physical and topological constraints delimiting the range of viable zeolite structures. In order to rationalize synthetic progress and to understand structural trends, it would therefore be very advantageous if one could predict and understand the properties of zeolites, based only on their underlying topology. In chapter six, we described a general methodology to predict the energetics of polyhedral cages based only on their face-size distribution (i.e no reference is made to the precise chemical constitution or geometry of the cages), and successfully applied it to rationalize trends in polyhedral silica-cage energetics. Building on this result, we now for the first time demonstrate that decomposing zeolites into a space-filling set of face-sharing polyhedral cages (henceforth referred to as polyhedral tiles), and analyzing the face-size distribution^B obtained, leads to powerful insights into the dependence of the thermodynamic viability of zeolites synthesis upon changes in structural properties such as pore-size and framework density.

In this chapter we will concentrate ourselves on frameworks constituted of only silicon and oxygen atoms so as not to complicate thermodynamic comparisons between different phases (i.e. no disproportionation is allowed). Although focusing on a particular chemical framework representation, this does not limit our choice of framework topology, upon which our methodology is based. The structural diversity and abundance of framework topologies is considerable richer when we do not limit ourselves to synthesized frameworks only, hence, in this chapter we analyze a selection of both synthesized and hypothetical zeolite frameworks. Of this large set of

^A Throughout we use “synthesized” in a general sense to include also “naturally synthesized” zeolites.

^B The face-size distribution is defined as $x_3^{a^3} x_4^{a^4} \dots x_n^{a^n}$ (with x_n a face of n T-atoms and a^n its occurrence, e.g. 4^6 for a cube). The face-size distribution of a framework is the sum of the face-size distribution of its constituent space-filling polyhedra (i.e. polyhedral tiles).

frameworks we mainly focus on zeolites that can be decomposed solely into three-connected polyhedral tiles. As these frameworks can be derived from the Simple Tilings⁵, we will subsequently refer to them as ST-frameworks. Such frameworks constitute a significant fraction of all thus far synthesized zeolite frameworks, including: SOD, LTA, FAU, RHO, KFI, CHA, AST, MEI, TSC and DOH. Also discussed are zeolite frameworks that are decomposable solely into sets of polyhedral tiles in which some tiles have a number of two-connected vertices (so-called $\lambda \neq 0$ polyhedra tiles, see chapter six), such as MFI, VFI, GIS and MOR. Of the set of hypothetical frameworks (as enumerated by Delgado-Friedrichs *et al*^{5, 6}, containing all mathematically possible ST-frameworks with up to three symmetrically independent T-atoms) a large representative sample is considered, including all frameworks with pores circumscribed by 14 or more T-atoms.

7.2 Methodology

As reviewed in the first and previous chapter of this thesis, the thermodynamics of zeolite synthesis are still surrounded by uncertainties, especially due to the limited amount of data present for such complex systems. However, independent of whether the zeolites formed are metastable or stable under the hydrothermal synthesis conditions, one can assume that the probability of synthesizing zeolites in general decreases rapidly with increasing thermodynamic instability. The thermodynamic viability of synthesizing a framework in the form of a zeolite is, therefore, strongly related to its thermodynamic stability compared to the most thermodynamically stable phase for its chemical composition (i.e. α -Quartz for SiO_2), often approximated by the transition enthalpy^{7,8}. Ideally, one would like to use experimentally determined transition enthalpy values for the different zeolites. However, only limited thermodynamic data is available (i.e. for about 15 out of more than 140 synthesized zeolite frameworks⁸). Therefore, we rather employ the results of accurate atomistic calculations of the lattice enthalpy of zeolite frameworks.

In the atomistic calculations, the interaction between silicon and oxygen ions was described by the Sanders force field^{9,10}, consisting of a Coulomb, Buckingham and a harmonic three-body term. The oxygen ions are modelled using the shell model of Dick and Overhauser¹¹, allowing for the effective polarizability of each oxygen ion to

vary as a function of its environment. All initial structures of synthesized frameworks were taken from the Zeolite Atlas of the International Zeolite Association¹ and were made all-siliceous where needed, while, the structures of the hypothetical frameworks were taken from the library of structures enumerated through dualization of tetrahedral tilings by Delgado-Friedrichs *et al*^{5, 6}, and prepared for evaluation as described by Foster *et al*¹². The lattice enthalpy of 34 synthesized and 90 hypothetical frameworks was then minimized without symmetry constraints using a constant pressure optimization algorithm as implemented in the program GULP¹³ (i.e. both atom-positions and cell-volume were optimized). All energies quoted for zeolites are relative energies compared to quartz, normalized to the number of T-atoms per unit cell.

To verify the applicability of the Sanders force field for calculating accurate values of the lattice enthalpies, the calculated relative energies for eight silica polymorphs were compared with experimentally measured values by Piccione *et al*⁸. Like Henson *et al*¹⁴, who compared the Sanders potential to more limited measurements (i.e data available for less structures) by Petrovic *et al*⁷, we observe a good quantitative agreement between calculated relative energies and experimental transition enthalpies ($r^2 = 0.84$). However, due to the experimental error in the calorimetry (± 1 kJ/mol) and inherent small scattering, structures differing by less than 1 kJ/mol become difficult to distinguish and can even be misplaced relative to each other. Frameworks containing three-rings were excluded from our analysis as the accuracy of the lattice enthalpies for these materials could not be verified with experimental results.

The synthesized frameworks were decomposed into sets of three-connected polyhedral tiles (the smallest set of polyhedral tiles that fills space by translation only) by means of visual inspection, and verified where possible by the results of enumeration⁶. The decomposition of the hypothetical frameworks results inherently from the dualization of the tetrahedral tilings used in their enumeration. Structure comparison was performed by calculating the coordination sequence of a framework¹⁵ until the thirteenth shell by means of the ZeoTsites package¹⁶.

Following on from chapter six, we employ the first two cumulants of the face-size distribution obtained, i.e. the average and variance, as a descriptor of the framework topology. The use of such a topological descriptor as compared to more conventional geometric descriptors (framework density, non-bonded distances, mean T-O-T angle) has two distinct advantages. Firstly, one does not require accurate crystal

data but merely the framework topology to predict properties of frameworks. Secondly, topologically independent concepts, such as framework density, are often not very intuitive when comparing and/or characterizing (novel) frameworks. For instance, LOV and MTN frameworks have comparable FD's (LOV FD = 18.3, MTN FD = 18.7) but completely different structures¹. Furthermore, although we do not explicitly incorporate specific geometric details into our model, by considering the framework connectivity (i.e. topology) together with how the constituent atoms bond together (e.g. bond strength and direction), we implicitly define and take into account the geometry of the framework.

7.3 Results

The decomposition results and the associated face-size distribution for the synthesized zeolite frameworks studied are given in table 7.1. An intriguing first observation is that a major fraction of the synthesized frameworks (18 out of 32) has an average face-size of 5.14, while twelve frameworks have a lower and two a higher average face-size. Secondly, it is noteworthy that several sets of face-isomers (i.e. frameworks with identical face-size distribution) and one set of tile-isomers (i.e. frameworks that can be constructed from identical sets of tiles) AFS/BPH is present.

Zeolite Framework	Polyhedral decomposition	Face-Size distribution	$\langle x \rangle$	Var(x)
AFG	$(4^6 6^5)^3 (4^6 6^{17})^1$	$4^3 6^4$	5.14	0.980
AFS	$(4^6 6^3)^2 (4^{12} 6^6 12^2)^1 (4^{18} 8^6 12^2)^1$	$4^{21} 6^6 8^3 12^2$	5.25	4.688
AFX	$(4^6 6^2)^2 (4^9 6^2 8^3)^1 (4^{15} 6^2 8^9)^1$	$4^9 6^2 8^3$	5.14	2.694
AFY	$(4^6)^2 (4^{18} 8^6 12^2)^1$	$4^{15} 8^3 12^1$	5.05	4.787
AST	$(4^6)^1 (4^6 6^{12})^1$	$4^1 6^1$	5.00	1.000
AWW	$(4^6 6^4)^1 (4^8 6^8 8^2)^1$	$4^7 6^6 8^1$	5.14	1.551
BPH	$(4^6 6^3)^2 (4^{12} 6^6 12^2)^1 (4^{18} 8^6 12^2)^1$	$4^{21} 6^6 8^3 12^2$	5.25	4.688
CHA	$(4^{12} 6^2 8^6)^1 (4^6 6^2)^1$	$4^9 6^2 8^3$	5.14	2.694
DOH	$(5^{12} 6^8)^1 (4^3 5^6 6^3)^2 (5^{12})^3$	$4^3 5^{30} 6^7$	5.10	0.240
EAB	$(4^6 6^2)^1 (4^9 6^2 8^3)^1 (4^9 6^8 8^3)^1$	$4^4 6^2 8^1$	5.14	2.122
EMT	$(4^{21} 6^5 12^5)^1 (4^{15} 6^2 12^3)^1 (4^6 6^8)^2 (4^6 6^2)^4$	$4^9 6^4 12^1$	5.14	4.408
ERI	$(4^6 6^2)^1 (4^6 6^5)^1 (4^{12} 6^5 8^6)^1$	$4^4 6^2 8^1$	5.14	2.122
FAU	$(4^{18} 6^4 12^4)^1 (4^6 6^8)^1 (4^6 6^2)^2$	$4^9 6^4 12^1$	5.14	4.408
FRA	$(4^6 6^{11})^1 (4^6 6^5)^1 (4^6 6^8)^3$	$4^{15} 6^{20}$	5.14	0.980
KFI	$(4^{12} 6^8 8^6)^1 (4^{12} 8^6)^3 (4^6 6^2)^4$	$4^9 6^2 8^3$	5.14	2.694
LEV	$(4^6 6^2)^1 (4^9 6^5 8^3)^2$	$4^4 6^2 8^1$	5.14	2.122
LIO	$(4^6 6^{11})^1 (4^6 6^{17})^1 (4^6 6^5)^4$	$4^9 6^{12}$	5.14	0.980
LOS	$(4^6 6^5)^1 (4^6 6^{11})^1$	$4^3 6^4$	5.14	0.980
LTA	$(4^{12} 6^8 8^6)^1 (4^6 6^8)^1 (4^6)^3$	$4^{18} 6^8 8^3$	4.97	1.826
MEI	$(4^{12} 5^6 7^6 12^2)^1 (3^1 4^3 5^3)^3$	$3^1 4^9 5^6 7^3 12^1$	5.10	3.690
MEP	$(5^{12})^1 (5^{12} 6^2)^3$	$5^8 6^1$	5.11	0.099
MTN	$(5^{12})^2 (5^{12} 6^4)^1$	$5^9 6^1$	5.10	0.090
RHO	$(4^{12} 6^8 8^6)^1 (4^8 8^2)^3$	$4^9 6^2 8^3$	5.14	2.694
RTE	$(4^6 5^4 6^6 8^2)^1 (4^4 5^4 6^2)^1$	$4^5 5^4 6^4 8^1$	5.14	1.265
RTH	$(4^8 5^4 6^4 8^4)^1 (4^4 5^4)^2$	$4^4 5^{13} 6^1 8^1$	5.00	1.750
RUT	$(4^4 5^4 6^2)^1 (4^4 5^6 6^5 8^1)^2$	$4^6 5^8 6^6 8^1$	5.14	0.980
SAS	$(4^6 6^2)^2 (4^8 6^{12} 8^2)^1$	$4^{10} 6^8 8^1$	5.05	1.418
SAT	$(4^6 6^2)^1 (4^6 6^5)^2 (4^{12} 6^8 8^6)^1$	$4^{15} 6^{10} 8^3$	5.14	1.837
SGT	$(5^{12} 6^8)^1 (4^3 5^6)^2$	$4^3 5^{12} 6^4$	5.05	0.366
SOD	$(4^6 6^8)^1$	$4^3 6^4$	5.14	0.980
TSC	$(4^6 6^2)^8 (4^6 6^8)^2 (4^8 8^2)^6 (4^{12} 6^8 8^6)^1 (4^{24} 6^8 8^{18})^1$	$4^{12} 6^4 8^3$	5.05	2.260
UFI	$(4^4 5^4)^2 (4^5 5^4 6^4 8^1)^2 (4^6)^1 (4^{12} 6^8 8^6)^1$	$4^9 5^4 6^4 8^2$	5.05	1.629

Table 7.1 Polyhedral decomposition result, face-size distribution, average face-size and the variance of the face-size distribution of the various synthesized ST-frameworks.

In the previous chapter it was demonstrated, by using Eulers equation, that the average face-size of a 3-connected polyhedral cage is a simple function of its number of vertices. For a space-filling packing of polyhedral tiles a similar analysis¹⁷ shows that its average face-size can be calculated from the total number of faces in a repeat set of tiles (the smallest set of polyhedral tiles that fills space by only applying translations), via (Eq. A3.15 in O’Keeffe and Hyde¹⁷):

$$\langle X \rangle = 6 - \frac{6N_{P,p}}{N_{F,p}} \quad (7.1)$$

Here, $N_{P,p}$ and $N_{F,p}$ are respectively the number of polyhedra and the total number of faces present in the repeat set. In a 4-connected framework every face is shared by 2 polyhedral tiles and $N_{F,p}$ can be written as the sum:

$$N_{F,p} = \frac{1}{2} \sum_{j=1}^{N_{P,p}} N_{F,j} \quad (7.2)$$

Here, $N_{F,j}$ is the number of faces of polyhedral tile j . Assuming that the polyhedral tile is three-connected, $N_{F,j}$ can be expressed in terms of the number of vertices (T-atoms) of the polyhedral tile ($N_{V,j}$), via (Eq. 6.3b):

$$N_{F,j} = 2 + \frac{1}{2} N_{V,j} \quad (7.3)$$

Using the latter two results, the average face-size of a space-filling packing of three-connected polyhedral tiles can be expressed as:

$$\langle X \rangle = 6 - \frac{6N_{P,p}}{N_{P,p} + \frac{1}{4} \sum_{j=1}^{N_{P,p}} N_{V,j}} \quad (7.4)$$

Which can finally be simplified into:

$$\langle X \rangle = 6 - \frac{6}{1 + \frac{1}{4N_{P,p}} \sum_{j=1}^{N_{P,p}} N_{V,j}} \quad (7.5)$$

The average face-size of a space-filling packing of three-connected polyhedral tiles, thus, only depends on the average polyhedron size (in vertices) and is, hence, equal for all frameworks with the same ratio between number of vertices (sum $N_{V,j}$) and polyhedra ($N_{P,p}$) in the repeat set. This important result demonstrates, just as established in chapter six for isolated polyhedral cages, that the average face-size of a ST-framework has a limit of six T-atoms. Any ST-framework with faces larger than five T-atoms should, therefore, always have faces smaller than six T-atoms to compensate. The pore-size of a ST-framework can consequently not be freely varied, as any pore (by definition larger than a six T-atoms) requires small faces for compensation.

Figure 7.1 shows how the relative energies of both the synthesized and the hypothetical zeolite frameworks vary with the average face-size. Just as previously observed for individual polyhedra tiles, the graph clearly shows that for each average face-size there are a multitude of frameworks with differing energetics, while, on the other hand it also displays a correlation between the lowest energy framework for each average face-size and the average face-size. The frameworks differ in their limiting behavior to the individual polyhedral cages (see chapter six). For the lowest energy polyhedral tiles the binding energy seems to decrease monotonically and to have a horizontal asymptote, while in contrast the relative energy for the lowest energy frameworks appears to increase again for average face-sizes larger than 5.14.

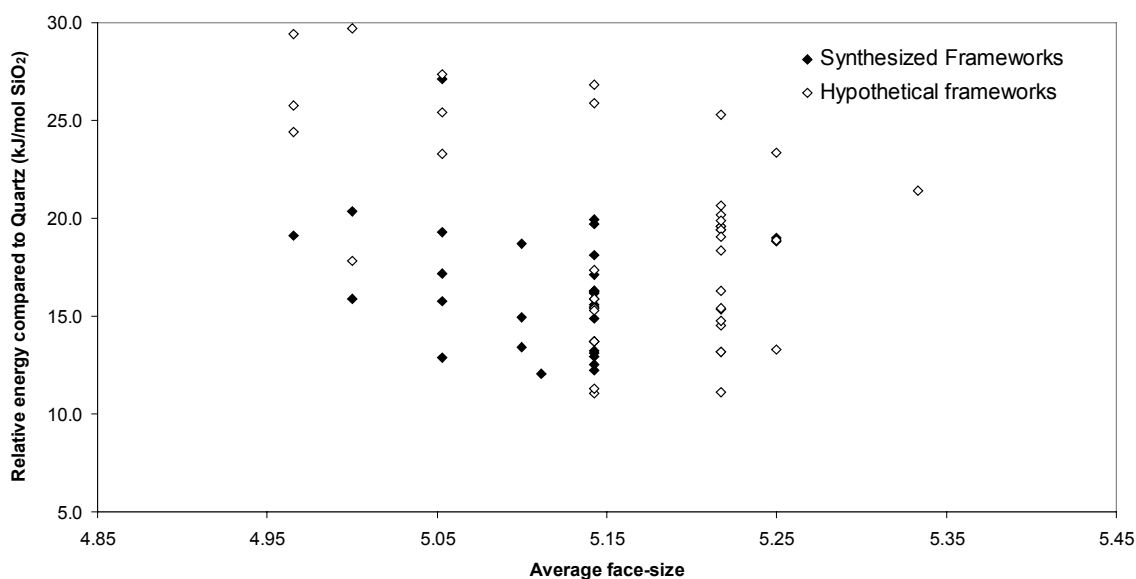


Figure 7.1 Calculated relative energies (normalized to numbers of T-atoms) versus the average face-size (view delimited to 30 kJ/mol SiO₂).

The other parameter of our descriptor, the second cumulant (variance) cannot be calculated from the face-size distribution of the constituting polyhedral tiles, but can be calculated from the face-size distribution of the framework via:

$$\sigma_X^2 = \frac{\sum_{i=1}^{N_f} (X_i - \langle X \rangle)^2}{N_f} \quad (7.6)$$

Figure 7.2 shows how the relative energy of the synthesized frameworks with an average face-size of 5.14 changes with their associated variance. One observes a strong correlation ($r^2 = 0.92$) between relative energy and variance of the face-size distribution, demonstrating that the energetics of these synthesized all-silica zeolites can be predicted based on only their topology (i.e. no specific geometric information is required). Furthermore, one can clearly see the face-isomers (which by definition have equal variance), forming narrow bands of points of maximum 2 kJ/mol width, comparable in magnitude to the uncertainty in the relative energy. It thus appears that the energetics of these frameworks with equal average face-size is well described by the variance.

Finally, it is interesting to note that the tile-isomers (by definition also face-isomers) have near identical energies (18.83 and 18.98 kJ/mol SiO₂ for AFS/BPH).

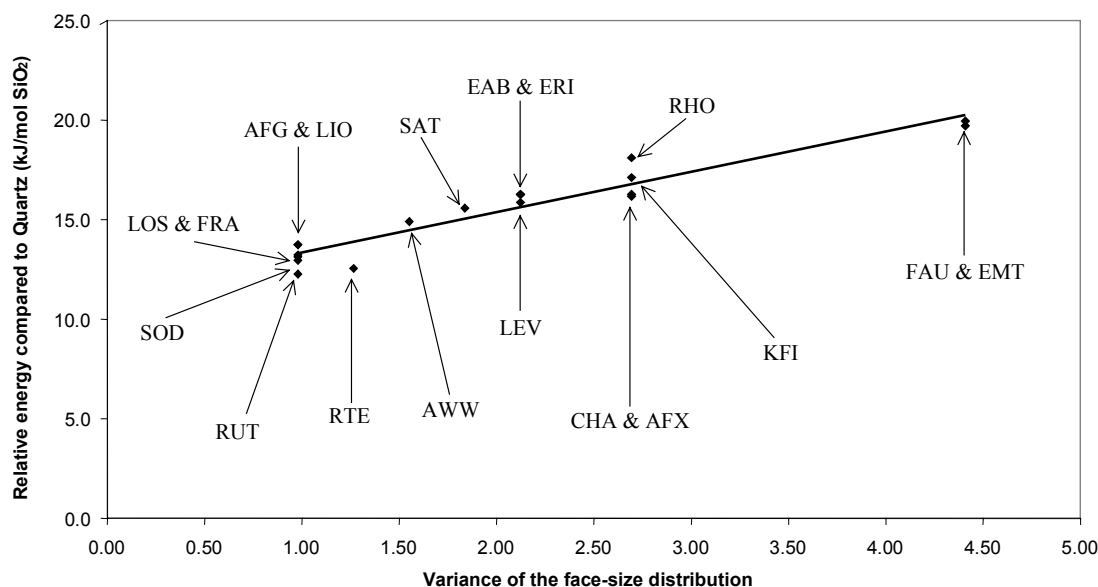


Figure 7.2 Calculated relative energies of the synthesized ST-frameworks with an average face-size of 5.14 versus the variance of their face-size distribution. The line shown is the best linear least squares fit to the data points.

Figure (7.3a-c) shows how the relative energy changes with the variance for three sets of frameworks (both synthesized and hypothetical) with different average face-sizes, respectively 5.00, 5.05 and 5.14. We again observe a strong correlation ($r^2 > 0.9$) between the relative energy and variance of the face-size distribution for all synthesized, and for a large part of the hypothetical, frameworks. However, a significant number of the hypothetical frameworks lie considerably higher in relative energy than simply expected from their variance alone. Visual inspection of the topology of these higher energy frameworks reveals that many contain certain combinations of polyhedral tiles known to be energetically disadvantageous (e.g. chains of 2 or 3 double six-rings, see figure 7.4, or large 2D rosettes, see figure 4A and D in⁵). Furthermore, hypothetical frameworks can be found that are tile-isomers of known synthesized frameworks, but lie significantly higher in relative energy. An example of such a set of tile-isomers are the four frameworks: dt3_717 (50.63 kJ/mol), dt3_718 (50.67 kJ/mol), AFS (18.83 kJ/mol) and BPH (18.98 kJ/mol), the former two higher energy frameworks being hypothetical

and the latter two lower energy frameworks being synthesized. These four tile-isomers can all be decomposed into the same set of polyhedral tiles, but correspond to different packings, as can be verified by the fact that all four frameworks have different coordination sequences.

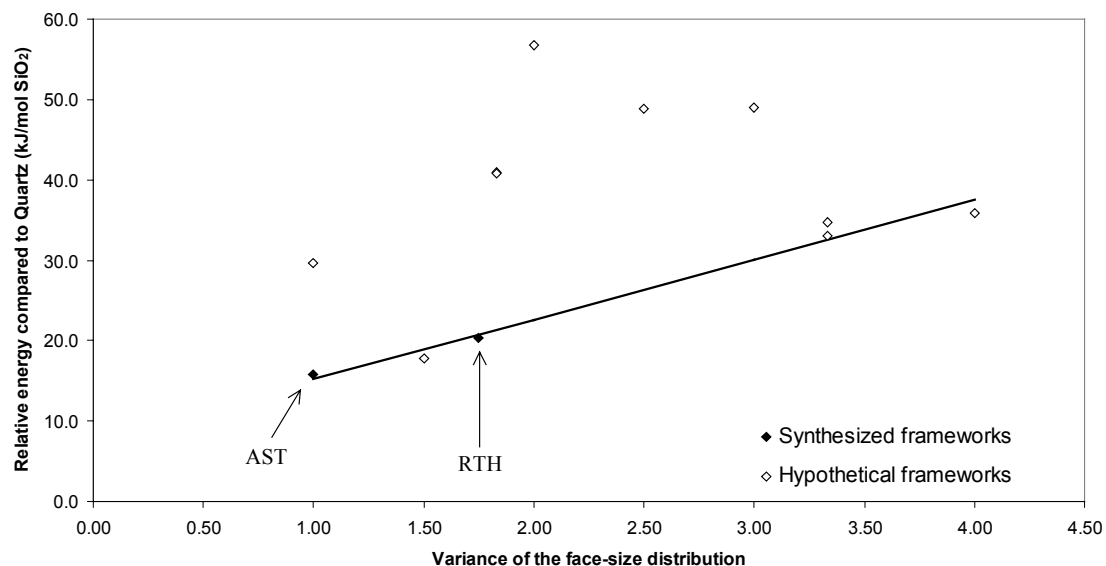


Figure 7.3a Calculated relative energy versus the variance of the face-size distribution for frameworks with an average face-size of 5.00. The line shown corresponds to the best linear least squares fit to the synthesized framework data points.

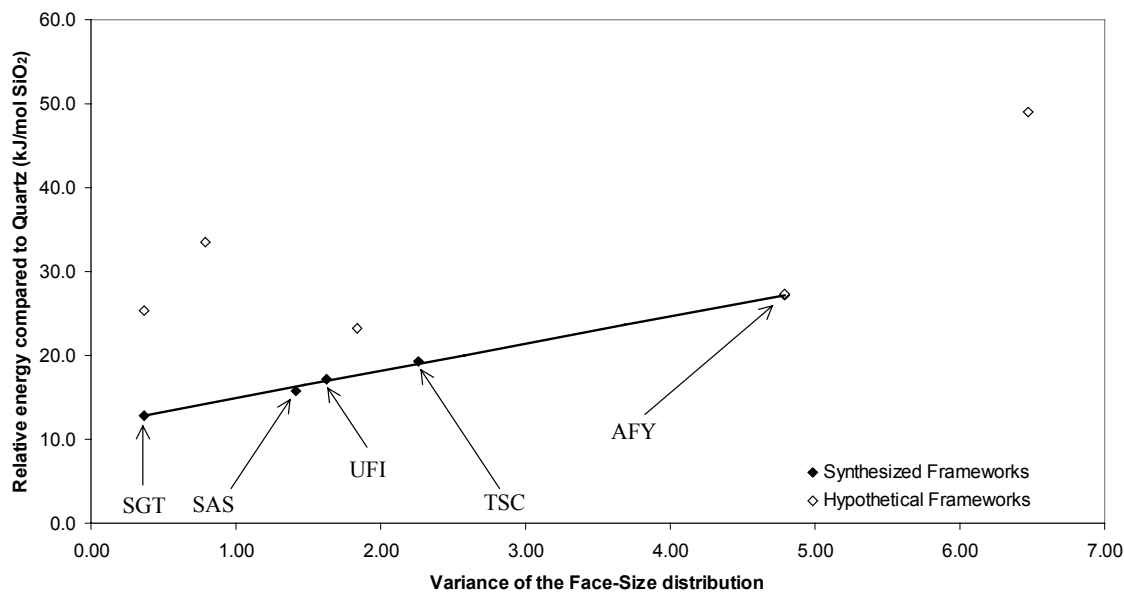


Figure 7.3b Calculated relative energy versus the variance of the face-size distribution for frameworks with an average face-size of 5.05. The line shown corresponds to the best linear least squares fit to the synthesized framework data points.

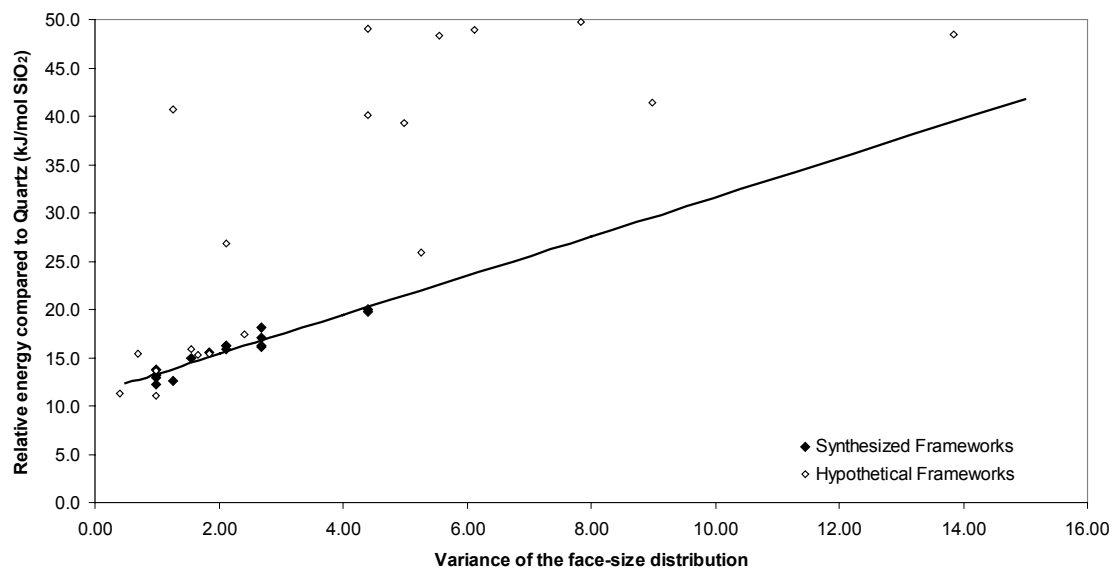


Figure 7.3c Calculated relative energy versus the variance of the face-size distribution for frameworks with an average face-size of 5.14. The line shown corresponds to the best linear least squares fit to the synthesized framework data points. Please note that the synthesized frameworks points correspond to the points in figure 7.2.

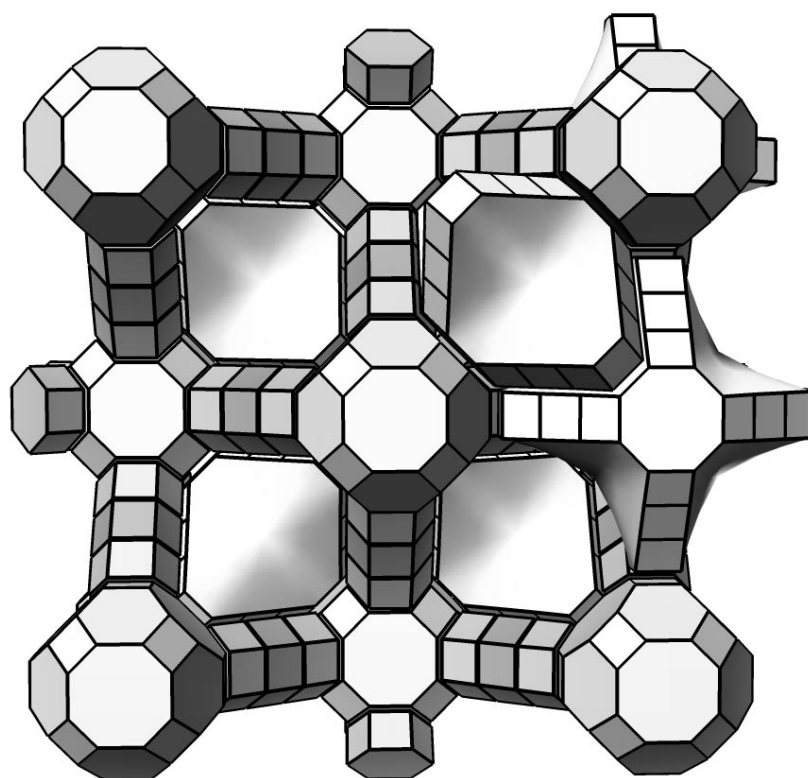


Figure 7.4 Part of the hypothetical extra-large pore ST-framework dt2_32, showing the 16 T-atom pore-windows and the D6R chains.

It thus appears that, just as for polyhedral silica cages, the energetics of zeolite frameworks can be described as a function of the average and variance of the face-size distribution, while, for some of the hypothetical frameworks an additional positive energy contribution due to packing is present. The relative energy (derived from the average and variance of the face-size distribution) predicts the minimum framework energy, which is expected to increase with variance and be minimal around an average face-size of 5.14. Although, the framework energy, as has been noted, can be increased above this lower limit via energetically unfavorable tile packing, it is important to note that for all synthesized frameworks our method predicts the correct relative energy ordering indicating that for such frameworks the effect of tile packing is negligible.

7.4 Discussion

7.4.1 Understanding the framework energetics

To rationalize the observed trends between average and variance of the face-size distribution of a framework and the energy of the corresponding all-silica zeolite, one requires a theoretical model linking framework topology and energetics. In the previous chapter, we successfully demonstrated that a simple physical model based around the energies attributed to faces explains the observed correlations for isolated polyhedral tiles. Such a model predicts correctly that the polyhedral tiles become more stable with increasing average face-size and with decreasing variance. As we do not expect any changes in the basic physical rationale underlying this model, we would expect the model to hold for (zeolite) frameworks also. While indeed the overall observed trends for the reported frameworks fit with the predictions of the physical model developed for isolated tiles, we also observe two minor additional effects: (i) an energetic packing penalty for a significant portion of the hypothetical frameworks and (ii) the relative energy minimum around an average face-size of 5.14.

The first effect, the packing penalty, is due to the fact that we approximate the topology of the framework by a set of distinct polyhedral tiles, and make no reference to the way these tiles are packed together, although this can lead to strain and an associated energetic destabilization. In the previous chapter, it is shown that for freely relaxed polyhedral silica cages (i.e. geometry optimized without any constraints) the energetics are well-described by our model, thus, we expect that for frameworks which can be constructed with minimal geometrical distortion of the constituting polyhedral tiles, the energetics would be equally well-predicted. This hypothesis is verified by fact that all synthesized, and a large fraction of the hypothetical, frameworks show no obvious extra energetic destabilization, while many of the frameworks with a notable energetic destabilization contain packing motifs known to be particularly energetically disadvantageous (e.g. double 4- and double 6-ring chains). Further evidence for packing as origin of the extra destabilization is given by those tile-isomers that consist of the same polyhedral tiles but differ in packing and relative energy (differences of the order 10-40 kJ/mol are observed, comparable in magnitude to the energetic destabilization attributed to packing effects). To fully take into account this energetic packing penalty

on the relative energy, a more elaborate descriptor would be required that additionally does take into account the tile arrangement (e.g. the Delaney symbol^{5,18,19}). However, as such descriptors are inherently more complex, insight is traded for precision. Finally, the lack of an obvious extra energetic destabilization for most frameworks implies that the face-size distribution is the principal factor determining their energetics (see figures 7.2 and 7.3a-c).

The second effect, the apparent relative energy minimum around average face-size 5.14, is not so much a deviation from the model but, rather, seems to result from topological limitations inherent to four-connected frameworks. For distinct polyhedral cages the lowest energy isomers are easily shown to be the “principal” polyhedra, i.e. those consisting of only one size of face (if the average face size is integral) or those solely consisting of the two types of faces closest to the average face size (see chapter six). More importantly, for almost all even numbers of vertices there seems to exist such a principal polyhedron. However, the same is not necessarily true for ST-frameworks (including the full collection of hypothetical frameworks) for which we only find “principal” frameworks (defined in a similar way as for “principal” polyhedra above) with average face-sizes 5.10 (MTN, 5^96^1) and 5.11 (MEP, 5^86^1). Furthermore, figure 7.5 shows that principal frameworks are not only rare, but also that the minimal variance of a framework increases dramatically while lowering or increasing the average face-size away from 5.10-5.11. The lowest energy frameworks are thus, with the two exceptions noted above, not the principal frameworks, but, rather, the frameworks with the lowest topologically realisable variance. It should be noted that although our collection of frameworks used for figure 7.5 is not complete, over 1000 different frameworks and all classes of enumerated ST-frameworks (uninodal, binodal, trinodal) contained therein show the same behaviour. The shape of the line connecting the lowest points of figure 7.1 is, thus, not determined by the average-face size, as for polyhedra, but rather, by the apparent topological restrictions of the four-connected framework. Furthermore, it appears that if we assume that the quality of packing can be judged by the variance of its associated face-size distribution, then the best possible space-filling packing of three-connected polyhedral tiles has an average face-size around 5.10-5.11; the latter region lying very close to the ‘centre of gravity’ (the average average-face-size) for all synthesized ST-frameworks (5.12).

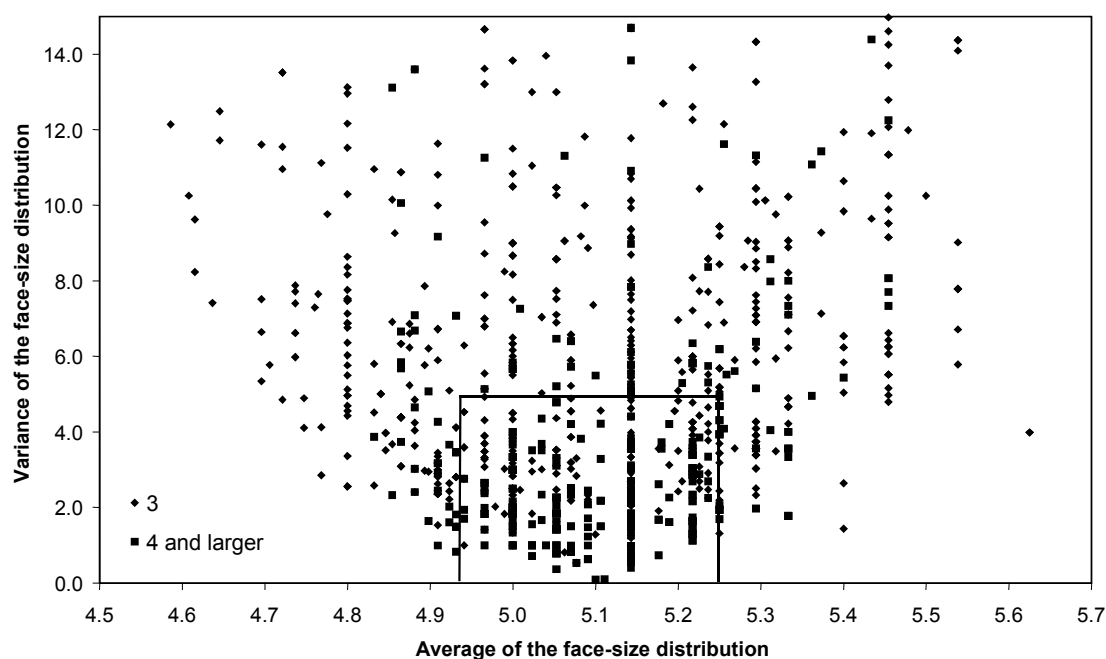


Figure 7.5 Variance of the face-size distribution for all the hypothetical ST-frameworks versus their corresponding average face-size. View delimited to a variance of 15, style of the symbol signifies size of smallest face present and box shows ranges for synthesized frameworks.

Based on the above, it is clear that the embedding of the polyhedral tiles in a space-filling packing results in additional topological constraints not present for isolated tiles. More specifically, these constraints appear to lead to a minimum in the energy difference compared to quartz (around average face-size of 5.14) instead of the inverse proportional behavior found for isolated tiles, and an additional positive packing contribution to the energy. As the latter energetic packing penalty is negligible for all 34 considered synthesized ST-frameworks (irrespective from the fact, whether they were ever synthesized in an all-siliceous form), we propose that a minimal packing penalty is critical in order for a framework to be synthesized.

7.4.2 Understanding structural trends

On the basis of our results and the discussion above, one can now link structural properties of zeolite frameworks (e.g. pore-size, framework density) with the thermodynamic viability of their synthesis.

7.4.2.1 Pore-size

In chapter six we have successfully demonstrated that topological considerations (i.e. Euler's formula) dictate that large pores in ST-frameworks require small faces as compensation. Furthermore, we showed that this compensation by small faces leads to a rise in variance and a decrease in the energetic stability of a polyhedral tile with an increasing number and size of the large faces associated with pores. On basis of these findings we predicted that the energetic stability of a zeolite framework would decrease with increasing pore-size and pore-system dimensionality (i.e. through how many pores the cage can be entered and left). All these predictions were, however, based on energy calculations for isolated polyhedral tiles. As we have demonstrated above that a similar compensation mechanism holds for frameworks corresponding to space-filling packings of polyhedral tiles, these predictions are now tested against our data for the synthesized ST-frameworks.

Pore-system	Variance window	Relative energy window	Frameworks
Clathrasils	0.980	12.3-13.7	AFG, FRA, LIO, LOS, RUT, SOD
8*	1.265-1.551	12.6-14.9	AWW, RTE
8**	2.122	15.9-16.3	EAB, LEV
8***	1.837-2.694	15.6-18.1	AFX, CHA, ERI, KFI, RHO, SAT
12**	4.408	19.7-20.0	FAU, EMT

Table 7.2 Pore-systems present among the synthesized ST-frameworks with an average face-size of 5.14 and the associated variance and relative energy (values in kJ/mol SiO₂) windows.

Table 7.2 shows which pore-systems can be found among the synthesized frameworks with an average face-size of 5.14, and the associated relative energy and variance windows. It is clear, despite of some overlap, that both the relative energy and the variance increase with, both, pore-size and pore-system dimensionality as clathrasils > 8* > 8** > 8*** > 12** (asterisks indicating pore-system dimensionality), verifying our earlier prediction. Based on the relative energy we would, therefore, expect that the

thermodynamic viability of synthesizing ST-frameworks decreases with both increasing pore-size and pore-system dimensionality.

For all the extra-large pore zeolite frameworks (zeolites with pores circumscribed by 14 or more T-atoms) in the collection of hypothetical ST-frameworks a considerable packing penalty (10-40 kJ/mol) is observed that is induced by the associated packing motifs (e.g. chains of double 6-rings, chains of double 4-rings, rosettes of small tiles etc.). The origin of this packing penalty is the fact that extra-large pores require large polyhedral tiles ($N_v > 48$) to be accommodated (see table 6.2), and that such tiles need to be compensated for by smaller tiles in order to reach an average face-size close to the best possible packing. Note, furthermore, that even for $\langle X \rangle = 5.45$, the largest $\langle X \rangle$ in the collection of hypothetical ST-frameworks used, N_v equals 40 and is thus still smaller than 48. Taking, for example, a framework that is decomposable into three different polyhedral tiles (large tiles, tiles equal to the average face-size and small tiles), one can calculate the ratio between small tiles and large tiles needed to obtain an average face-size $\langle X \rangle$ via:

$$R = \frac{N_{vl} - N_{va}}{N_{va} - N_{vs}} \quad (7.7)$$

Where N_{vl} is the number of vertices of the large tile, N_{vs} the number of vertices of the small tile and N_{va} the analogous number for a tile corresponding to the average face-size $\langle X \rangle$. A large polyhedral tile of size N_{vl} , thus, requires R small polyhedral tiles of size N_{vs} for compensation, where R rises rapidly with increasing N_{vs} , irrespective of the actually feasibility of the space-filling packing. For a large polyhedral tile of 96 vertices one needs, for instance, either 18 tiles of 20 vertices or 6 tiles of 12 vertices to reach an average face-size of 5.14. Extra large-pore ST-frameworks, thus, have either very large repeat units (e.g. 456 T-atoms for $N_{vs}=20$ in the example above) or relatively large number of small tiles. In which case the relatively large number of small tiles, in the latter option, significantly increases the chance of energetically unfavorable packing motifs such as double 6-ring chains. Table 7.3 gives data for three extra-large pore zeolite frameworks with an average face-size of 5.14, and clearly shows that without the packing penalty two out of the three frameworks would have quite reasonable relative

energies (judged from the relative energies extrapolated along the correlation found for synthesized frameworks). Based on the above, it seems unlikely that one could synthesize extra-large pore ST zeolites.

Framework	Polyhedral decomposition	Pore system	Variance	Relative Energy	Extrapolated relative energy
dt2_31	$(4^6 6^2)^6 (4^6 6^8)^1 (4^{42} 6^4 24^4)^1$	24**	13.837	48.5	39
dt2_32	$(4^6 6^2)^{12} (4^{12} 6^8 8^6)^1 (4^{28} 8^2 16^2)^3$	16*	7.837	49.8	27
dt2_33	$(4^6 6^2)^3 (4^{24} 6^2 12^6)^1$	12***	6.122	48.9	24

Table 7.3 Three extra-large pore ST-frameworks with an average face-size of 5.14 and their pore-system, variance, relative energy (in kJ/mol SiO₂), extrapolated relative energy without packing (kJ/mol SiO₂) and with the actual packing motif of chains of three double six-rings.

7.4.2.2 Framework density

The framework density of ST-frameworks is strongly related to the volume of the tiles. The volume of a tile should (under the reasonable assumption that the external surface area of a polyhedron is some increasing function of N_v and that its volume scales as its surface area to the power 2/3) scale as:

$$V \propto N_v^{\frac{2}{3}} \quad (7.8)$$

Suggesting that the framework density should scale approximately as:

$$FD \propto \frac{\sum_{j=1}^{N_p} N_{v,j}}{\sum_{j=1}^{N_p} N_{v,j}^{\frac{2}{3}}} \quad (7.9)$$

From the form of equation 7.9 it is apparent that the framework density of a framework is expected to decrease with the number of large polyhedral tiles present. Moreover, as the number of large polyhedral tiles present tends to increase with the variance, one can propose a simple relationship between variance of the face-size distribution of a framework and its framework density. Figure 7.6, shows this relationship for frameworks with an average face-size of 5.14. It clearly shows the expected negative linear relationship between variance and framework density ($r^2 > 0.95$) for all synthesized, and a large fraction of the hypothetical, frameworks. Some of the hypothetical frameworks lie considerably above the correlation found, and it turns out that these are the same frameworks that show a packing effect in their energetics. The effect of packing on the framework density is most likely geometric of origin (i.e. through deformation of the tiles) as those tile-isomers that differ in energetics also differ in framework density. The two hypothetical frameworks: dt3_718 and dt3_717 have, for instance, a considerably higher framework density than their tile-isomers: AFS and BPH ($17.50 \text{ T}/1000\text{\AA}^3$ instead of $14.84 \text{ T}/1000\text{\AA}^3$).

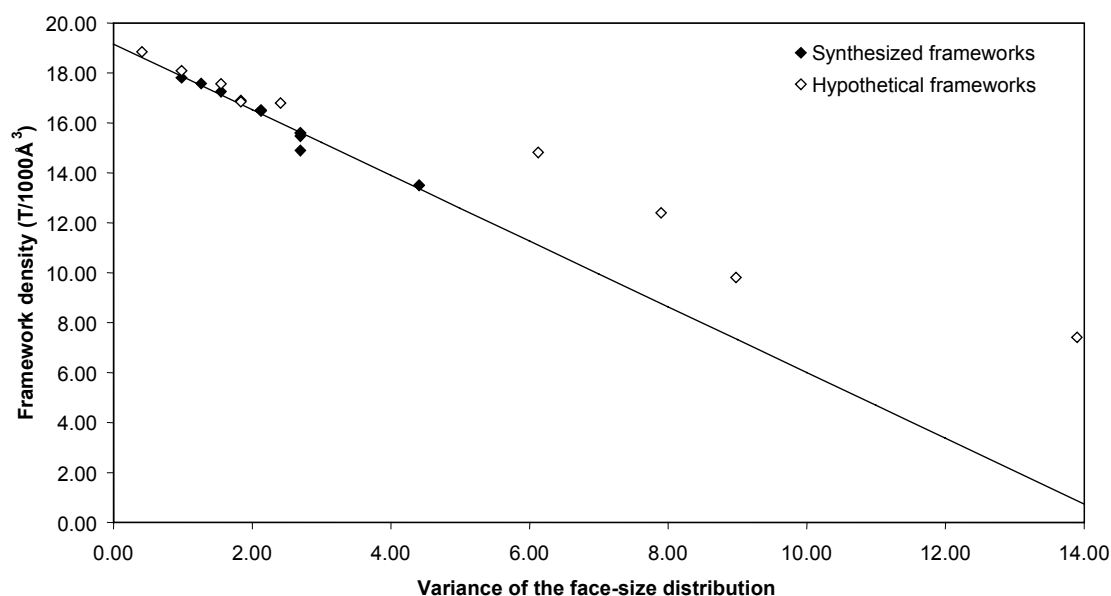


Figure 7.6 Framework density of ST-frameworks with an average face-size of 5.14 versus the variance of their face-size distribution.

For other average face-sizes similar graphs are found. As the variance increases with decreasing framework density and the relative energy increases with increasing

variance, the correlation found agrees with the negative trend between framework density and relative energy found by other authors^{7,8,12,14}. Based on the relative energy, we would expect that the thermodynamic viability of synthesizing ST-frameworks decreases with decreasing framework density. Furthermore, as a low framework density requires large polyhedral tiles, as also needed for extra-large pores, packing effects most probably will limit the lowest attainable framework density for ST-frameworks.

7.4.3 Beyond ST-frameworks

As discussed in the introduction, besides the cage-like ST-frameworks also channel-like frameworks exist that are decomposable into a mixture of $\lambda = 0$ and $\lambda \neq 0$ polyhedral tiles (λ equals the ratio between two- and three-connected vertices in the polyhedral tile, see chapter six). These channel-like frameworks are derivable from Non-Simple Tilings, and are subsequently referred to as NST-frameworks. Polyhedral analysis of these NST-frameworks is more complicated than for ST-frameworks, as there can be multiple equally valid decompositions into $\lambda \neq 0$ polyhedral tiles, hindering rapid decomposition. Furthermore, the average face-size is not solely a simple function of the polyhedra sizes anymore but, rather, depends also on the number of the three-connected vertices and λ 's of the polyhedra. The maximum face-size that does not need compensation by smaller faces (5 for ST-frameworks) is now no longer independent of the actual polyhedra it is shared between, as it depends on λ (i.e. $5+4\lambda$, see chapter six). This extra degree of freedom allows tiles of any face-size distribution (e.g. the $\lambda = 3, 12^6$ cage of ITQ-21²⁰), however, there might not necessarily be a realizable four-connected framework containing it. For example, while polyhedral tiles with $\lambda \neq 0$ might have any average face-size, the average face-size of the uninodal hypothetical NST-frameworks appears to be limited to values between 5.42 and 9.43 (as calculated from the polyhedral decomposition of the uninodal hypothetical frameworks). As the nature of the framework (ST or NST) does not influence the energetics of the faces present, in spite of the complications discussed above, one would still assume that the relative energy of the NST-frameworks could be described in terms of the average and variance of their face-size distribution. Figure 7.7 shows how the relative energy changes with the variance of the face-size distribution for unital (i.e.

decomposable into one tile only) NST-frameworks with an average face-size of 5.6 (including the synthesized frameworks ABW (see figure 7.8) and GIS (see figure 6.5)). We observe again a strong correlation between the variance and relative energy of the lowest energy frameworks and also again a number of tile-isomers with considerable packing penalties (high energy points in figure 7.7). The NST-frameworks, thus, appear to show behavior similar to the ST-frameworks. Table 7.4 gives the face-size distribution and relative energies for the lowest energy frameworks in figure 7.7 (for which the correlation is observed), dt1_219, ABW and GIS.

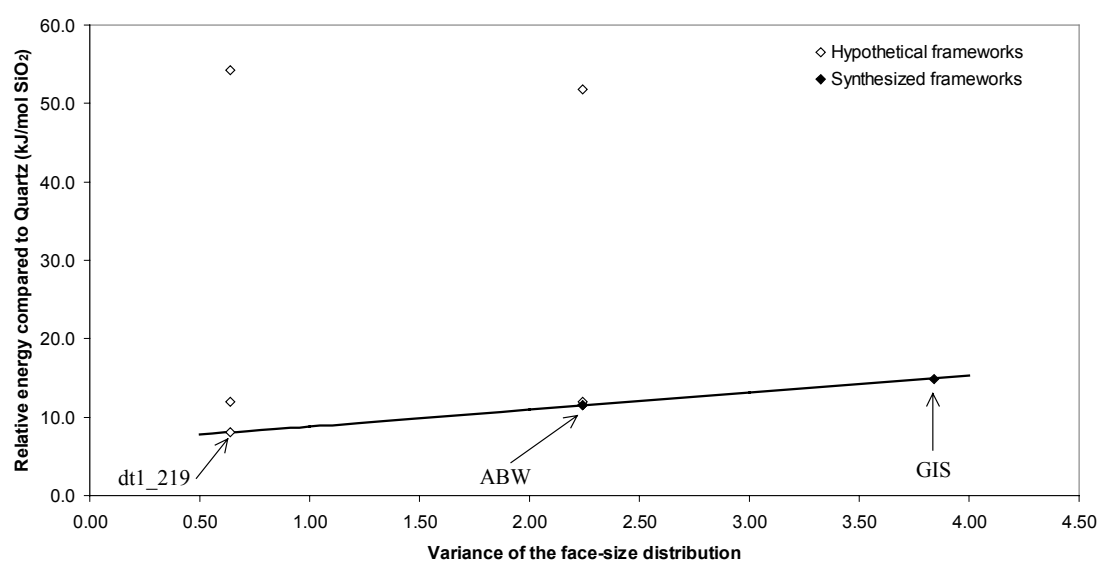


Figure 7.7 Calculated relative energies of unitilal frameworks with an average face-size of 5.6 versus the variance of their face-size distribution. The line shown is the best linear fit to the three lowest energy frameworks (dt1_219, ABW, GIS).

Framework	Polyhedral decomposition	3-connected polyhedron	λ	Pore system	Variance	Relative energy
dt1_219	$(4^26^8)^1$	(4^25^8)	0.25	clathrasil	0.640	8.01
ABW	$(4^46^48^2)^1$	$(4^45^46^2)$	0.25	8*	2.240	11.60
GIS	$(4^68^4)^1$	(4^66^4)	0.25	8**	3.840	14.87

Table 7.4 Polyhedral decomposition, 3-connected polyhedron (from which the $\lambda \neq 0$ polyhedron is obtained), λ , pore system, variance and relative energies (in kJ/mol) for three NST-frameworks with an average face-size of 5.6.

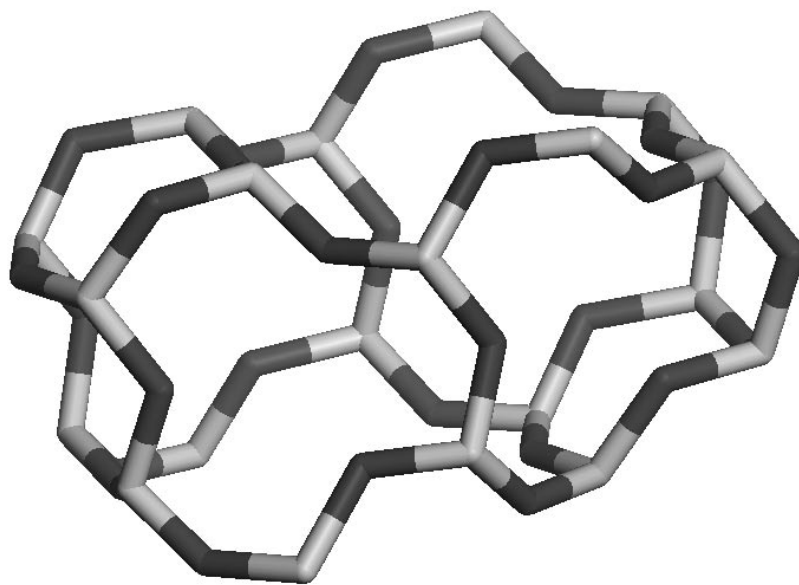


Figure 7.8 The $4^46^48^2$ ABW polyhedral tile (dark grey represents oxygen atoms; light grey represents silicon atoms).

Regarding the structural properties of NST-frameworks, it is interesting to note that all three frameworks of table 7.4 have lower relative energies than their ST counterparts with similar pore-systems (see table 7.2). Furthermore, while the extra-large pore ST-frameworks of table 7.3 seem to have inevitably energetically disadvantageous packing motifs, their $\lambda \neq 0$ analogues CFI and VFI ($6^{18}18^2$ polyhedral tile with $\lambda = 0.5$, see figure 7.9) have much more reasonable relative energies (12.30, 19.11 kJ/mol respectively). Moreover, all currently synthesized extra-large pore frameworks (AET, CFI, DON, OSO, SFH, SFN and VFI), including the recently reported “18-ring” framework ECR-34²¹ (ETR), have $\lambda \neq 0$ tiles. It, thus, appears that the increased structural versatility of NST-frameworks compared to their ST counterparts, allows for much more synthetically viable candidates for extra-large, and by analogy extra-low framework density, frameworks. Even for these frameworks, however, there appear to be limits, the largest average face-size in the collection of uninodal frameworks equals 9.43 (and the largest face-size in the same set with a variance below 15 is only 7.76).

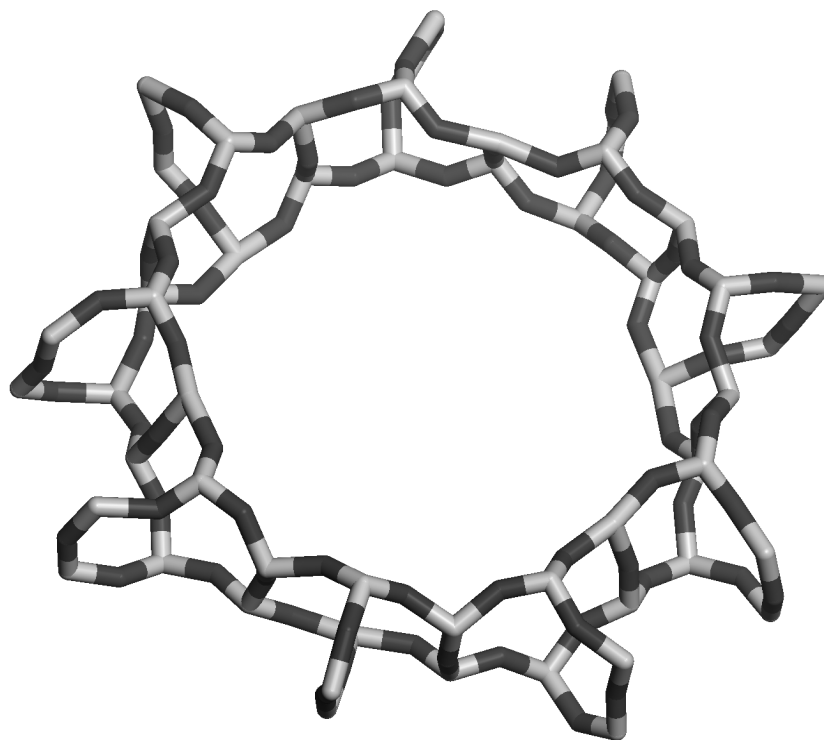


Figure 7.9 The extra-large pore $6^{18}18^2$ polyhedral tile of VFI (dark grey represents oxygen atoms; light grey represents silicon atoms).

7.4.4 Beyond all-silica zeolites

The realm of framework materials is broader than the all-silica zeolites on which the bulk of this chapter focuses (e.g. AlPOs, germantates, metal organic frameworks²²⁻²⁸ and chalcogenides²⁹⁻³²). For tetrahedral frameworks in general the basic results discussed above should hold without limitations, as the origin of the observed constraints is topological rather than chemical in nature. We thus expect these frameworks to follow the same general trends between framework energetics and the average and variance of its face-size distribution as found for their all-silica equivalents. The specific energy values (energy differences between lowest topological realizable variance frameworks, slope of the correlation between energy and variance) however are expected to change as their values are intimately linked to the strength of the inverse proportionality between face-size and face energy (i.e “ring-strain”), which is known to be dependent on the chemical nature of the T-atoms. This hypothesis is strongly supported by the preliminary results for ST-frameworks with average face-size 5.14 in their GeO_2 and AlPO_4 form, as shown in figure 7.10.

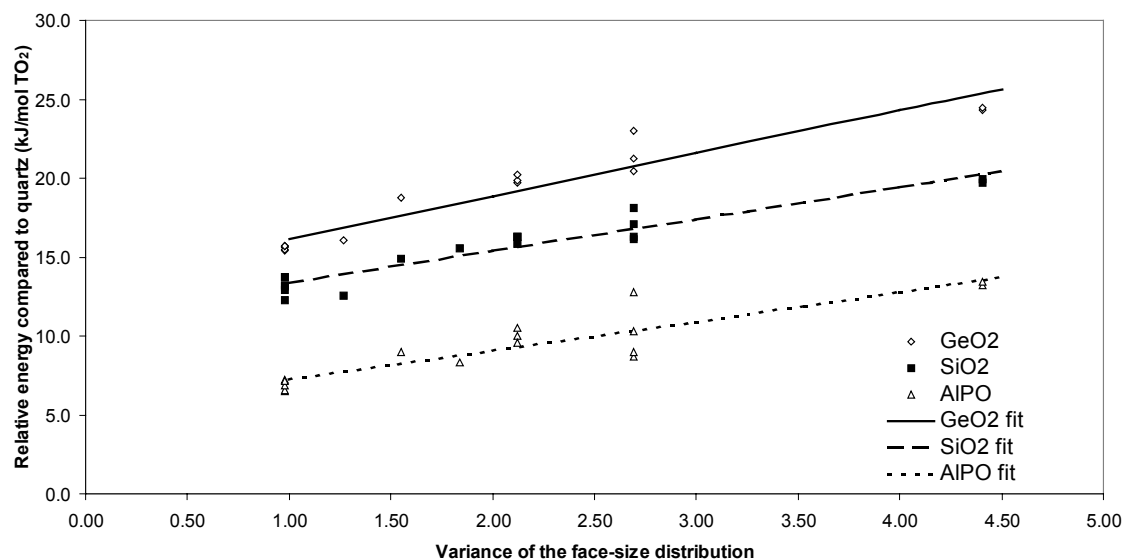


Figure 7.10 Calculated relative energies of the synthesized ST-frameworks with an average face-size of 5.14 (in their GeO₂, SiO₂ and AlPO₄ form) versus the variance of their face-size distribution. The GeO₂ data was calculated using the George force field³³, while the data for the AlPO₄ frameworks was obtained from Dr. A. Simperler³⁴ (who employed a force field developed by Gale and Henson³⁵). All energies are given relative to Quartz in the respective chemical composition.

It is known experimentally that partial substitution of the Si atoms by other metal atoms (Zn, Be)³⁶⁻³⁹ can induce the formation of frameworks with smaller faces (e.g. synthesis of zeolites containing faces of 3 T-atoms, see also chapter six). Although in our model such faces would increase the variance of the face-size distribution and thus decrease the relative thermodynamic viability of a framework, this effect would be offset by the decrease in the slope of the correlation between energetics and variance induced by the strain-accommodating change in chemical composition of the framework. For non-tetrahedral (pentahedral, octahedral) or mixed coordination frameworks (e.g. the microporous sodium niobates SOMS^{40,41} and the ETS-4⁴² and ETS-10⁴³ titanosilicates), a similar topological analysis to the one presented in this paper, should result in comparably rich insights into the topological and physical constraints imposed upon these frameworks.

7.5 Conclusions

A topological analysis method, consisting of decomposing the zeolite framework into sets of polyhedral tiles and analyzing the obtained face-size distribution, is shown for the first time to yield powerful insights into the energetics of zeolites and the feasibility of their synthesis. In particular, we have demonstrated that the relative energies of synthesized frameworks that correspond to Simple-Tilings (ST-frameworks) can be understood in terms of the average and the variance of the face-size distribution (as for isolated polyhedral tiles). Furthermore, we show that to properly describe a part of the studied hypothetical frameworks an additional packing penalty term is required, which, is negligible for all synthesized frameworks. We further verify our previous prediction that for these ST-frameworks the relative energy increases (and the thermodynamic viability of their synthesis, thus, decrease) with increasing pore-size and pore-system dimensionality. For the same class of frameworks, we show that all extra-large pore frameworks considered have energetically disadvantageous packing motifs and a considerable associated packing penalty, and we provide an explanatory model linking this to pore-size. For frameworks corresponding to Non-Simple Tilings (NST-frameworks) similar trends as for ST-frameworks are found, although NST-frameworks appear to have lower relative energies for comparable pore-systems. Furthermore, we show that the structural versatility (λ) of NST-frameworks opens the possibility of extra-large pore frameworks without energetically disadvantageous packing motifs, and thus to yield many more synthetically viable candidates than ST-frameworks for extra-large pore, and extra low framework density, frameworks. Preliminary calculations on non-siliceous frameworks further confirm our confidence that the proposed methodology is applicable to framework materials in general.

References

- ¹Baerlocher C., Meier W.M., Olson D.H. Atlas of Zeolite Framework Types: Elsevier, Amsterdam, The Netherlands, 2001 (updates on <http://www.iza-structure.org/>).
- ²Martinez-Triguero, J.; Diaz-Cabañas, M.J.; Cambor, M.A.; Fornés, V.; Maesen, Th.L.M.; Corma, A. *J. Catal.* **1999**, 182, 463.
- ³Jones C.W., Zones Z.I., Davis M.E. *Appl. Catal.A-Gen.* **1999**, 181, 289.
- ⁴Corma A., González-Alfaro V., Orchillés A.V. *J. Catal.* **2001**, 200, 34.
- ⁵Delgado Friedrichs O., Dress A.W.M., Huson D.H., Klinowski J., Mackay A.L. *Nature* **1999**, 400, 644.
- ⁶Delgado Friedrichs O., Huson D.H. *Discrete. Comput. Geom.* **2000**, 24, 279.
- ⁷Petrovic I., Navrotsky A., Davis M.E. Zones S.I. *Chem. Mater.* **1993**, 5, 1805.
- ⁸Piccione P.M., Laberty C., Yanf S., Cambor M.A., Navrotsky A., Davis M.E. *J. Phys. Chem. B* **2000**, 104, 10001.
- ⁹Sanders M.J., Leslie M., Catlow C.R.A. *J. Chem. Soc. Chem. Commun.* **1984**, 1271.
- ¹⁰Schröder K.P., Sauer J., Leslie M., Catlow C.R.A., Thomas J.M. *Chem. Phys. Lett.* **1992**, 188, 320.
- ¹¹Dick B.G., Overhauser A.W. *Phys. Rev.* **1958**, 112, 90.
- ¹²Foster M.D., Delgado Friedrichs O., Bell R.G., Almeida Paz F.A., Klinowski J. *Angew. Chem. Int. Ed.* **2003**, 42, 3896.
- ¹³Gale J.D. *J. Chem. Soc. Faraday Trans.* **1997**, 93, 629.
- ¹⁴Henson N.J., Cheetham A.K., Gale J.D. *Chem. Mater.* **1994**, 6, 1647.
- ¹⁵Meier W.M., Moeck H.J. *J. Solid State Chem.* **1979**, 27, 349.
- ¹⁶Sastre G., Gale J.D. *Microporous Mesoporous Mater.* **2001**, 43, 27.
- ¹⁷O'Keeffe M., Hyde B.G., Crystal Structures I - Patterns and Symmetry: Mineralogical Society of America: Washington, DC, 1996.
- ¹⁸Dress A.W.M. *Lecture Notes in Mathematics* **1985**, 1172, 56.
- ¹⁹Dress A.W.M. *Adv. Math.* **1987**, 196.
- ²⁰Corma A., Diaz-Cabañas M.J., Martinez-Triguero J., Rey F., Rius J. *Nature* **2002**, 418, 514.
- ²¹Strohmaier K.G., Vaughan D.E.W. *J. Am. Chem. Soc.* **2003**, 125, 16035.
- ²²James S.L. *Chem. Soc. Rev.* **2003**, 32, 276.
- ²³Shiu K.B., Lee H.C., Lee G.H., Ko, B.T., Wang Y., Lin C.C. *Angew. Chem. Int. Ed.* **2003**, 42, 2999.
- ²⁴Chae H.K., Siberio-Pérez D., Kim J., Go J., Eddaoudi M., Matzger A.J., O'Keeffe M., Yaghi O.M. *Nature* **2004**, 427, 523
- ²⁵Rosi N.L., Eckert J., Eddaoudi M., Vodak D.T., Kim J. O'Keeffe M., Yaghi O.M. *Science* **2003**, 300, 1127.
- ²⁶Pan L., Sander M.B., Huang X., Li J., Smith M., Bittner E., Bockrath B., Johnson K. *J. Am. Chem. Soc.* **2004**, 126, 1308.
- ²⁷Guillou N., Livage C., Drillon M., Ferey G. *Angew. Chem. Int. Ed.* **2003**, 42, 5314.
- ²⁸Maspoch D., Ruiz-Molina D., Wurst K., Domingo N., Cavallini M., Biscarini F., Tejada J., Rovira C., Veciana J. *Nature* **2003**, 2, 190.
- ²⁹Li H., Eddaoudi M., Laine A., O'Keeffe M., Yaghi O.M. *J. Am. Chem. Soc.* **1999**, 121, 6096.
- ³⁰Li H., Laine A., O'Keeffe M., Yaghi O.M. *Science* **1999**, 283, 1145.
- ³¹Zheng N., Bu X., Wang B., Feng P. *Science* **2002**, 298, 2366.
- ³²Zheng N., Bu X., Feng P. *Nature* **2003**, 426, 428.
- ³³George A.R., Catlow C.R.A., Thomas J.M. *J. Solid State Chem.* **1993**, 104, 6.
- ³⁴Simperler A., Foster M.D., Bell R.G., Klinowski J. *J. Phys. Chem. B* **2004**, 108, 869.
- ³⁵Gale, J.D., Henson N.J. *J. Chem. Soc. Faraday Trans.* **1994**, 90, 3175.
- ³⁶Annen M.J., Davis M.E., Higgins J.B., Schlenker J.L. *Chem. Commun.* **1991**, 1175.
- ³⁷McCusker L.B., Grosse-Kunstleve R.W., Baerlocher Ch., Yoshikawa M., Davis M.E. *Microporous Mater.* **1996**, 6, 295.
- ³⁸Merlino S. *Eur. J. Mineral.* **1990**, 2, 809.
- ³⁹Petersen O.V., Giester G., Brandstätter F., Niedermayr G. *Can. Mineral.* **2002**, 40, 173.
- ⁴⁰Nymann M., Tripathi A., Parise J.B., Maxwell R.S., Harrison W.T.A., Nenoff T.M. *J. Am. Chem. Soc.* **2001**, 123, 1529.
- ⁴¹Nymann M., Tripathi A., Parise J.B., Maxwell R.S., Nenoff T.M. *J. Am. Chem. Soc.* **2002**, 124, 1704.
- ⁴²Kuznicki S.M., Bell V.A., Nair S., Hillhouse N.W., Jacubinas R.M., Braunbarth C.M., Toby B.H., Tsapatsis M. *Nature* **2001**, 412, 720.
- ⁴³Anderson M.W., Terasaki O., Oshuna T., Philippou A., MacKay S.P., Ferreira A., Rocha J., Lidin S. *Nature* **1994**, 367, 347.

8

Computational insights into the role of Ge in stabilizing double-four ring containing zeolites

Abstract

The partial substitution of silicon by germanium in zeolite synthesis mixtures is well-known to direct zeolite synthesis towards double-four ring (D4R) containing frameworks. Whereas the structure-directing effect of Ge is well described, the chemistry behind the effect is less well understood. In this study, we show that the structure-directing effect is strongly linked to the lowering of the energetic destabilisation of D4Rs compared to large, large-faced, cages, and more in particular that low Ge-substitution increases the probability of synthesizing frameworks containing D4Rs with respect to all other cage types on thermodynamic grounds. Furthermore, we demonstrate that the symmetry lowering of D4Rs with Ge-substitution, predicted on geometric grounds by O’Keeffe *et al*, can be rationalised in terms of the energy released by symmetry lowering.

The contents of this chapter have been published in:

Zwijenburg M.A., Bromley S.T., Jansen J.C., Maschmeyer T. *Microporous Mesoporous Mater.* **2004**, 73, 171.

8.1 Introduction

In recent years a series of novel double-four ring (D4R) containing zeolite frameworks, with catalytically interesting pore-systems, have been synthesized¹⁻⁷. The synthesis of these frameworks e.g. ITQ-17^{2,3}; ITQ-21^{4,6} and ITQ-22⁵, depends strongly on the presence of Ge in the synthesis mixture, as otherwise often different, non-D4R-containing, frameworks are formed. Furthermore, for ITQ-7 and ITQ-13 (which can be synthesized in the all-silica form) the rate of nucleation is increased strongly when Ge atoms are introduced into the synthesis mixture^{1,7}. Moreover, analysis of ¹⁹F and ²⁹Si MAS NMR data for ITQ-7^{8,9} and ITQ-13¹⁰ suggests that the Ge is selectively incorporated at D4R positions. Whereas the structure-directing effect of Ge towards D4R-containing zeolite frameworks is thus well described, the chemistry behind the effect is less well understood. Blasco *et al*⁹ propose it to be thermodynamic in origin and showed that increasing the Ge/(Si+Ge) ratio of D4R cages drives their formation enthalpy to more and more negative values, increasing their stability relative to all-silica D4R cages. While these calculations do demonstrate that Ge-substitution in D4R cages is thermodynamically favoured, they do not give any insight on the thermodynamic preference for D4R formation relative to other possible cages with equal Ge/(Ge+Si) ratio. In this communication we will demonstrate that differences in the heat of formation between D4Rs and larger cages give insight into the role of Ge in directing zeolite synthesis towards D4R-containing frameworks.

In chapter six, we reported density functional calculations on hydrogen-terminated polyhedral silica cages (H_nSi_nO_{1.5n}) in which we studied the influence of ring(face)-size on the energetics of all-silica zeolite frameworks. The use of hydrogen-terminated polyhedral silica cages (i.e. silsesquioxanes, which due to their similarities with their periodic analogues in terms of structure and rigidity¹¹, are known to be good theoretical and experimental model-systems for zeolites¹¹⁻²³) allowed us to extensively sample a wide range of possible structures. Based on these DF calculations, we showed that the energetics of polyhedral silica cages could be described in terms of the average and variance of their face-size distribution, and furthermore, demonstrated that this knowledge can be exploited to understand how zeolite energetics depends on the structure of the polyhedral cages. For all-silica polyhedral cages we found that their energetic stability increases with increasing average face-size, eventually reaching a

limit for an average face-size larger than 4.8. Polyhedral cages with small faces, like the D4R (average face-size: 4), were found to be destabilised considerably compared to their higher average face-size equivalents (D4R lying 2.45 kJ/mol SiO₂ above the 5¹² cage, see chapter six). As frameworks synthesised in the all-silica form typically do not contain D4Rs and other small faced-cages (with the AST framework as the only exception), one could propose that this energetic destabilisation might be the origin of their absence. The observed D4R-promoting effect of Ge should then be related to a lowering of this energetic destabilisation. To investigate if the effect of Ge is indeed energetic, we repeated our calculations for Ge-substituted polyhedral cages (H_nGe_(n-p)Si_pO_{1.5n}), as model-systems for Ge-substituted zeolites.

8.2 Computational details

Five different polyhedral cages (cage-A: H₄T₄O₆ (3⁴); cage-B: H₆T₆O₉ (3²4³); cage-C: H₈T₈O₁₂ (4⁶); cage-D: H₁₂T₁₂O₁₈ (4⁴5⁴); cage-E H₂₀T₂₀O₃₀ (5¹²); T = Si, Ge), with varying degree of Ge substitution, were geometry optimised by density functional calculations, employing the B3LYP²⁴ functional and a 6-31G** basis-set²⁵⁻²⁷ as implemented in the program Gaussian98²⁸. To ensure that true minima were found, all cages were optimised without any symmetry constraints, and the eigenvalues of the Hessian matrix verified to be all-positive. Furthermore, for all clusters with 10 or less T-atoms, the use of symmetry in the wave function was explicitly disabled.

For all polyhedral cages binding energies were calculated from the difference between the total energy of the cage and the corresponding isolated doublet H and triplet Si, Ge and O atoms at the same level of theory, normalised to the number of T-atoms. The binding energies obtained were subsequently normalised with respect to a set of 120 T-atoms with a fixed Ge/(Si+Ge) ratio (i.e 30*(cage-A) = 20*(cage-B) = 15*(cage-C) = 10*(cage-D) = 6*(cage-E)) to allow for facile comparison^A.

^A e.g. for Ge/(Si+Ge) equal to 0.04, the reference composition corresponds to H₁₂₀Si₁₁₅Ge₅O₁₈₀ and the normalised binding energy of cage A (E_{A0.04}) can thus be calculated from (1/120)(5E_{binding}(H₄Si₃Ge₁O₆) + 25E_{binding}(H₄Si₄O₆)), and in a similar manner the normalised binding energies of cages B-E can be obtained (e.g. for cage E: E_{E0.04}=(1/120) (5E_{binding}(H₂₀Si₁₉Ge₁O₃₀) + 1E_{binding}(H₂₀Si₂₀O₃₀)). As we are only interested in energy differences, the normalised binding energies for each Ge/(Si+Ge) ratio are subsequently shifted such that they are equal in the high average face-size limit (E_E).

8.3 Results and Discussion

Figure 8.1 shows the variation in normalised binding energies of the cages against their average face-size for three Ge substitution levels (Ge/(Si+Ge) ratio: 0, 0.04 and 0.09).

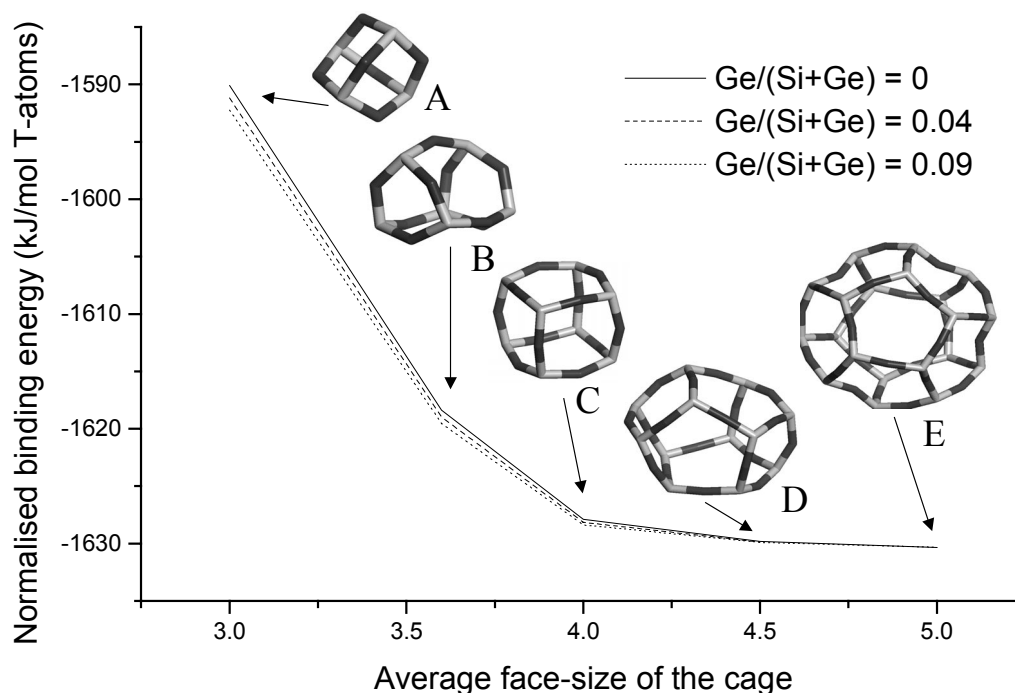


Figure 8.1 Variation of the normalized binding energy with the average face-size of the cages for three different Ge/(Si+Ge) ratios.

The trend observed for all-silica cages is recovered, but more importantly a shift is observed towards lower average-face size. It appears that with increasing Ge/(Si+Ge) ratio the energetic destabilisation of the small-faced cages compared to the high average face-size limit (cage E) decreases. The energetic destabilisation of D4Rs, calculated from the difference in normalised binding energies between cages C and the large-face limit cage E, is given in table 8.1. This demonstrates that incorporation of small numbers of germanium atoms in D4Rs results in a significant reduction (up to 20%) of its energetic disadvantage (E_{ds}) with respect to larger, larger-faced, cages. Low Ge-substitution, hence, appears to increase the relative probability of synthesizing frameworks containing D4Rs with respect to all cage types on thermodynamic grounds. Table 8.1 also shows some influence of the distribution of a fixed number of Ge atoms

over and in the cages, but it is small compared to the effect of changing the Ge/(Si+Ge) ratio. Figure 8.2 shows how E_{ds} changes with the Ge/(Si+Ge) ratio, and demonstrates that, even when considering different Ge distributions, E_{ds} decreases linearly with increasing Ge/(Si+Ge) ratio.

Ge distribution over C cages	Ge/(Si+Ge)	E_{ds} (kJ/mol T-atoms)
0 Ge (all-siliceous)	0	2.5
5 Ge, one per cage	0.04	2.2 (-10.9 %)
10 Ge, one per cage	0.09	2.0 (-20.4 %)
10 Ge, two per cage (both on the same edge)	0.09	1.9 (-23.7 %)
10 Ge, two per cage (both on a face diagonal)	0.09	2.0 (-18.3 %)

Table 8.1 Calculated energetic destabilisation of D4Rs (kJ/mol T-atoms) compared to the high average face-size limit for different Ge/(Si+Ge) ratios and Ge-distributions.

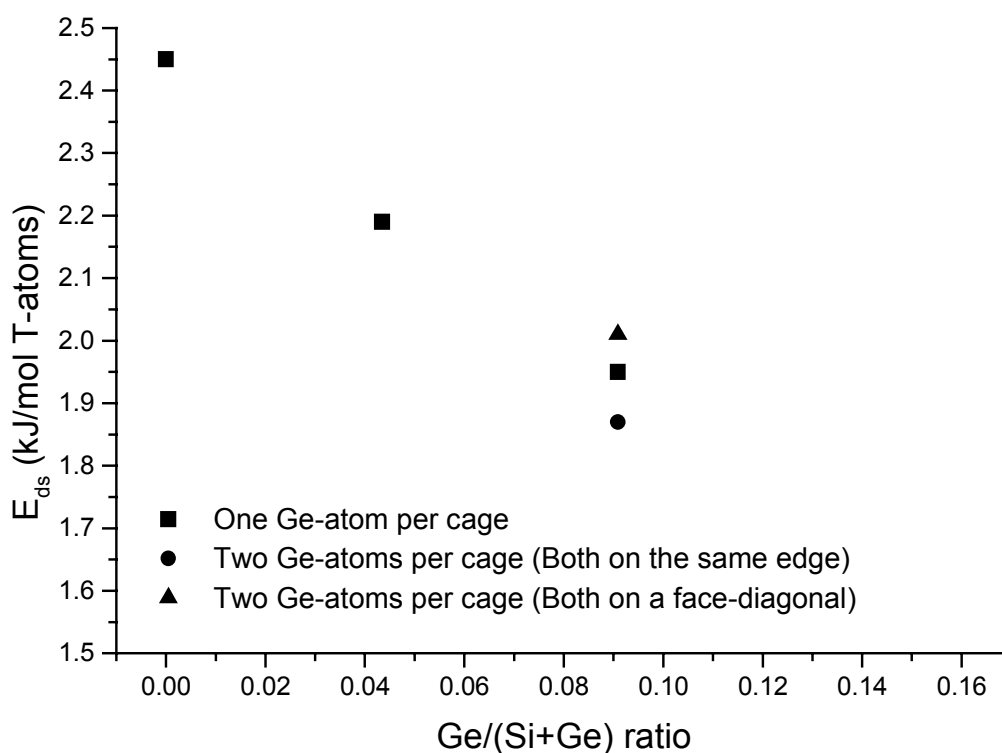


Figure 8.2 Variation of the D4R energetic destabilisation with the Ge/(Si+Ge) ratio of the cages.

The observed significant reduction of the energetic disadvantage of the D4R and other small-faced cages with increasing levels of Ge-substitution most probably originates from slight changes in the geometry. Table 8.2 gives the O-T-O angles for the smallest face in the cages with one Si atom substituted by Ge and for their all-siliceous counterparts. Clearly, the O-T-O angles in the small-faced Ge-substituted cages (A, B and C) are much closer to the tetrahedral angle (109.5°) than the O-T-O angles in their all-siliceous equivalents, even for faces opposite to the face in which the Ge-atom is substituted, while for the larger-faced cages (D and E) the reverse holds. This geometric observation is in line with the fact that small cages appear to be more energetically stabilised by Ge-substitution than their larger, large-faced, analogues.

Cage	Ge/Si+Ge ratio	O-T-O	O-T-O
		1 Ge	All-siliceous
A	0.250	105.1 (105.9)	101.6
B	0.167	107.1 (106.7)	100.1
C	0.125	109.8 (109.7)	110.2
D	0.083	110.6	110.0
E	0.050	108.8	109.9

Table 8.2 O-T-O angles for the smallest face in cages, substituted with 1 Ge-atom and for their all-siliceous counterparts. Values in parenthesis correspond to the face opposite to the face containing the Ge-atom.

Calculating the energetic destabilisation for D4Rs with higher Ge/(Si+Ge) ratios was not possible, as the additionally introduced Ge increased the flexibility of the cages resulting in the appearance of many more local minima (most notably for cage E), making it difficult to find the true minima. An example of this effect of Ge can be observed for the structure of the D4R as function of the Ge/(Si+Ge) ratio. On geometric grounds O’Keeffe *et al*²⁹ predicted that a GeO₂ D4R should have the symmetry lowered from O_h (symmetry of the cube) to T_d (symmetry of the tetrahedron), a fact recently observed for the isolated D4Rs in [Ge₈O₁₂(OH)₈F](C₁₁NH₂₄) crystals³⁰. Figure 8.3

shows the energy difference between the D4R with T_d and O_h symmetry as function of the Ge/(Si+Ge) ratio. At low Ge/(Si+Ge) ratios the T_d form of the D4R cannot be stabilised and spontaneously converts into the O_h form, while at higher Ge/(Si+Ge) ratios the T_d form becomes increasingly more stable than its O_h equivalent, rationalising O’Keeffe’s prediction on energetic grounds for isolated D4Rs.

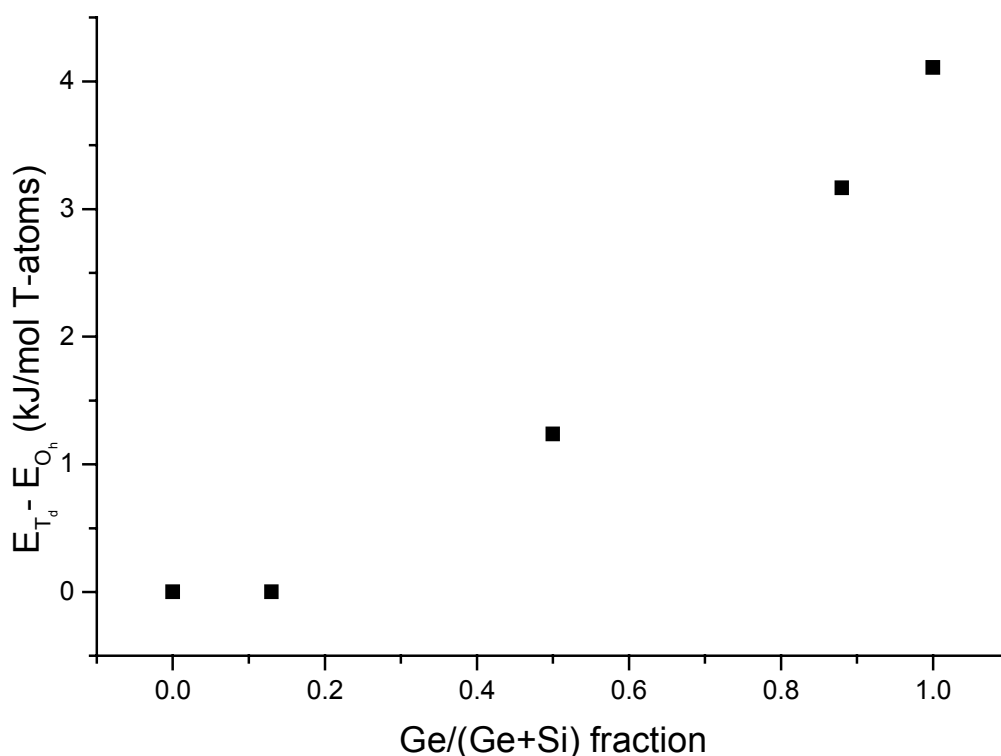


Figure 8.3 Variation of the energy difference between the T_d and O_h form of a D4R as function of the fraction Ge substituted.

Effects of Ge in directing zeolite synthesis towards D4R containing frameworks have been observed for synthesis mixtures resulting in structures with Ge/(Si+Ge) ratios between approximately 0.12 and 0.5¹⁻⁷. The performed calculations thus only describe the bottom of this range. However, extrapolating the linear trend of figure 8.2 leads to an E_{ds} of roughly 1.6-1.9 kJ/mol for Ge/(Si+Ge) 0.12^B, which, is comparable to the E_{ds} calculated in chapter six for the two most energetically destabilised polyhedral cages actually found in synthesized all-silica zeolites: the double-six ring and the sodalite cage

(see table 6.1 and figure 6.2). The onset of the effect of Ge in directing zeolite synthesis towards D4R-containing frameworks, therefore, appears to be strongly linked to the decrease in E_{ds} of D4Rs with increasing Ge/(Si+Ge) ratio. The effect of higher Ge/(Si+Ge) ratios remains unclear, however, from the calculations on the symmetry lowering in D4Rs one can expect that it will be associated with considerable changes in the symmetry of the structure.

8.4 Conclusions

The experimentally observed effect of Ge in directing zeolite synthesis towards double-four ring (D4R) containing frameworks is shown to be strongly linked to the lowering of the energetic destabilisation of D4Rs compared to large, large-faced, cages. In particular, we have shown that low Ge-substitution increases the relative probability of synthesizing frameworks containing D4Rs with respect to larger larger-faced cage types on thermodynamic grounds. Furthermore, the symmetry lowering of D4R with Ge-substitution (from O_h to T_d), predicted on geometric grounds by O’Keeffe *et al*, is rationalised in terms of the energy released by symmetry lowering.

^B Depending on which of the three points, differing in Ge-distribution, is used for the Ge/(Si+Ge) 0.09 D4R (2 Ge atoms, one in each of two cages/ 2 Ge atoms, both on the same edge in one cage/ 2 Ge atoms, both on a face diagonal in one cage).

References

- ¹ Corma A., Díaz-Cabañas M.J., Fornés V. *Angew. Chem. Int. Ed.* **2000**, 39, 2346.
- ² Corma A., Navarro M.T., Rey F., Valencia S. *Chem. Commun.* **2001**, 1486.
- ³ Corma A., Navarro M.T., Rey F., Rius J., Valencia S. *Angew. Chem. Int. Ed.* **2001**, 40, 2277.
- ⁴ Corma A., Díaz-Cabañas M.J., Triguero J.M., Rey F., Rius J. *Nature* **2002**, 418, 514.
- ⁵ Corma A., Rey F., Valencia S., Jorda J.L., Rius J. *Nature Materials* **2003**, 2, 493.
- ⁶ Corma A., Díaz-Cabañas M.J., Rey F. *Chem. Commun.* **2003**, 1050.
- ⁷ Corma A., Puche M., Rey F., Sankar G., Teat S.J. *Angew. Chem. Int. Ed.* **2003**, 42, 1156.
- ⁸ Sastre G., Vidal-Moya J.A., Blasco T., Rius J., Jordá J.L., Navarro M.T., Rey F., Corma A. *Angew. Chem. Int. Ed.* **2002**, 41, 4722.
- ⁹ Blasco T., Corma A., Díaz-Cabañas M.J., Rey F., Vidal-Moya J.A., Zicovich-Wilson C.M. *J. Phys. Chem. B* **2002**, 106, 2634.
- ¹⁰ Vidal-Moya J.A., Blasco T., Rey F., Corma A., Puche M. *Chem. Mater.* **2003**, 15, 3961.
- ¹¹ Earley C.W. *J. Phys. Chem.* **1994**, 98, 8693.
- ¹² Bornhauser P., Calzaferri G. *J. Phys. Chem* **1996**, 100, 2035.
- ¹³ Marcolli C., Lainé P., Bühler R., Calzaferri G., Tomkinson J. *J. Phys. Chem. B* **1997**, 101, 1171.
- ¹⁴ Krijnen S., Harmsen R.J., Abbenhuis C.L., Van Hooff J.H.C., Van Santen R.A. *Chem. Commun.* **1999**, 501.
- ¹⁵ Duchateau R., Harmsen R.J., Abbenhuis H.C.L., Van Santen R.A., Meetsma A., Thiele S.K.H., Kranenburg M. *Chem. Eur. J.* **1999**, 5, 3130.
- ¹⁶ Liu F., John K.D., Scott B.L., Baker R.T., Ott K.C., Tumas W. *Angew. Chem. Int. Ed.* **2000**, 39, 3127.
- ¹⁷ Hill J.R., Sauer J. *J. Phys. Chem.* **1994**, 98, 1238.
- ¹⁸ Hill J.R., Sauer J. *J. Phys. Chem.* **1995**, 99, 9536.
- ¹⁹ de Man A.J.M., Sauer J. *J. Phys. Chem* **1996**, 100, 5025.
- ²⁰ Tossell J.A. *J. Phys. Chem* **1996**, 100, 14828.
- ²¹ Xiang K.H., Pandey R., Pernisz U.C., Freeman C. *J. Phys. Chem. B* **1998**, 102, 8704.
- ²² Uzunova E.L., Nikolov G.S. *J. Phys. Chem. A* **2000**, 104, 5302.
- ²³ Kudo T., Gordon M.S. *J. Phys. Chem. A* **2001**, 105, 11276.
- ²⁴ Becke A.D. *J. Chem. Phys.* **1993**, 98, 5648.
- ²⁵ Hehre W.J., Ditchfield R., Pople J.A. *J. Chem. Phys.* **1972**, 56, 2257.
- ²⁶ Francel M.M., Petro W.J., Hehre W.J., Binkley J.S., Gordon M.S., DeFrees D.J., Pople J.A. *J. Chem. Phys.* **1982**, 77, 3654.
- ²⁷ Hariharan P.C., Pople J.A., *Theor. Chimica Acta* **1973**, 28, 213.
- ²⁸ Frisch M.J. *Gaussian 98*, Revision A.9, Gaussian, Inc.: Pittsburgh PA, 1998.
- ²⁹ O'Keeffe M., Yaghi O.M. *Chem. Eur. J.* **1999**, 5, 2796.
- ³⁰ Villaescusa L.A., Lightfoot P., Morris R.E. *Chem. Commun.* **2002**, 2220.

Martinus Antonius Zwijnenburg: “Understanding Ordered Silica: Linking Topology and Energetics”.

Summary

Silica is an enormously versatile material, exhibiting a large and diverse spectrum of natural and synthetic polymorphs. Together with the related silicate minerals, silica is the most abundant material on earth, comprising more than 90% by weight and volume of the earth’s mantle and crust. Furthermore, silica-based materials have found widespread application in the chemical industry (adsorbent, catalyst support), the rubber and plastic industry (filler) and in optical and microelectronic devices. This thesis describes research into two specific classes of silica materials, the all-silica zeolites and the silica nanoclusters, for which is attempted to predict which hypothetical structures can be experimentally realised.

The first chapter of this thesis gives a short introduction to Silica, all-silica zeolites and silica nanoclusters. Discussed are typical structures and synthesis routes, as well as possible and realised applications. Furthermore, this chapter contains a concise introduction to the theoretical chemistry methods applied in the remainder of the thesis.

In the second chapter of this thesis the nature of the chemical bond between the Si and O atoms in Silica is studied. Charges for the Si and O atoms and the related ionicities of the bonds between them, are calculated for structural fragments from seven all-silica zeolites and two silica minerals, using three different charge analysis schemes (the Mulliken, Hirshfeld and Bader methods). The results of the calculations show that the ionicity of the Si-O bond is correlated with its respective bond-length, and suggest a possible link between the energetic stability of a bulk silica polymorph and the ionicities of its Si-O bonds.

The third chapter of this thesis describes a novel class of silica nanocluster, the $(\text{SiO}_2)_N$ molecular rings. These clusters, composed of edge-sharing Si_2O_4 units, have as special property that they are fully coordinated, i.e. that all Si and O atoms are linked by the same number of bonds as in the bulk. These rings are shown to display frequency modes in remarkable agreement with infrared (IR) bands measured on dehydrated silica surfaces, suggesting their potential use as models of strained extended silica systems.

Chapter four of this thesis describes more extensive calculations of infrared spectra of fully coordinated silica nanoclusters, and their application as model systems

for dehydrated silica surfaces. The calculated spectra for the clusters display many peaks in the experimental window, with some in excellent frequency and intensity agreement with measured bands. The results are discussed with respect to the structural nature of the clusters and the possibility of collective two-ring surface modes.

In chapter five of this thesis a novel synthetic route towards well-defined stoichiometric silica nanoclusters is proposed, based upon computational considerations. Density functional calculations demonstrate the viability of a route based on siloxane cage thermolysis, while molecular dynamics calculations were performed to test the stability of the cages formed. Based on the calculations, it is predicted that for small siloxane cages defect-rich structures are the main product, while for larger siloxane cages fully-coordinated silica nanoclusters are formed. Overall, thermolysis of siloxane cages is demonstrated to present a potential route towards specific types of metastable yet, well-defined silica nanoclusters, not obtainable by less targeted cluster generation methods.

The sixth chapter of this thesis describes the basis of a novel methodology to predict the energetics of zeolites based on only the topology of the underlying framework. This analysis, based around the face-size distribution of a framework, formally demonstrates why smaller rings in such structures naturally compensate and help to stabilise large pores.

Chapter seven of this thesis describes an extension of the work discussed in chapter six. It shows how the decomposition of extended zeolite frameworks into polyhedral tiles, and the analysis of the face-size distribution obtained, can lead to definite predictions regarding the thermodynamic viability of their hydrothermal synthesis. Moreover, it is demonstrated that pore-size and framework density cannot be varied freely, but that they, at least for frameworks corresponding to simple tilings, are intimately connected to the thermodynamic viability of the framework's synthesis through its topology. These new insights allow one, not only to rationalize the thermodynamic viability of a range of desirable (but as yet unmade) frameworks, but also to begin to understand the physical and topological boundaries, which inherently limit attempts to synthesize frameworks with ever-larger pores and lower framework densities.

In chapter eight finally the effect of partial substitution of Si by Ge on the formation of double-four ring containing framework is discussed. Calculations based on

the methodology developed in chapter six, show that this structure-directing effect is strongly linked to the lowering of the energetic destabilisation of D4Rs compared to large, large-faced, cages, and more in particular that low Ge-substitution increases the probability of synthesizing frameworks containing D4Rs with respect to all other cage types on thermodynamic grounds. Furthermore, it is demonstrated that the symmetry lowering of D4Rs with Ge-substitution, predicted on geometric grounds by O’Keeffe *et al*, can be rationalised in terms of the energy released by symmetry lowering.

Martinus Antonius Zwijnenburg: “Inzicht in Geordend Silica: het Verband tussen Topologie en Energetica”.

Samenvatting

Silica (SiO_2) is een veelzijdig materiaal. Het kan in vele verschillende polymorfen (kristalstructuren) gesynthetiseerd worden en heeft een groot aantal belangrijke toepassingen in de chemische industrie, de rubber- en kunstofindustrie en in elektronische en optische schakelingen. Naast deze technologische applicaties is silica ook een geologisch belangrijk materiaal, daar het samen met de verwante silicaten verantwoordelijk is voor zowel 90% van de massa als 90% van het volume van de aardmantel en –korst. Dit proefschrift richt zich op twee specifieke klassen van silica materialen, de “all-silica” zeolieten en de silica nanoclusters, voor welke getracht is theoretisch te voorspellen welke hypothetische structuren ook daadwerkelijk experimenteel gerealiseerd kunnen worden.

Hoofdstuk één van dit proefschrift is een korte inleiding op het gebied van silica in het algemeen en “all-silica” zeolieten en silica nanoclusters in het bijzonder. Behandeld worden de typische structuren en synthese routes, alsmede mogelijke en gerealiseerde toepassingen. Verder bevat dit hoofdstuk een korte inleiding tot de verder in het proefschrift toegepaste chemisch theoretische methoden.

In hoofdstuk twee van dit proefschrift wordt de aard van de chemische binding tussen Si en O atomen in silica bestudeerd. Voor structuurfragmenten van zeven “all-silica” zeolieten en twee silica mineralen, worden de ladingen van de Si en O atomen en het ionische gehalte van de onderlinge bindingen (de “ionicity”) bepaald met drie verschillende “charge partitioning” methoden (die van Mulliken, Hirshfeld en Bader). De verrichte berekeningen laten zien dat het ionische gehalte van de Si-O binding correlatie vertoont met de lengte van de betreffende binding en suggereren verder een mogelijk verband tussen de ionische gehalten van de Si-O binding en de energetische stabiliteit van de betreffende silica polymorf.

In hoofdstuk drie van dit proefschrift wordt een nieuwe klasse van silica nanoclusters beschreven: de silica nanoringen. Deze clusters, bestaande uit zogenaamde “edge-sharing” Si_2O_4 eenheden, hebben als bijzondere eigenschap dat ze volledig gecoördineerd zijn, d.w.z. alle Si en O atomen zijn met hetzelfde aantal bindingen

verbonden als in bulk silica. Theoretische berekeningen laten zien dat dit soort silica nanoclusters infrarood spectra hebben, welke erg lijken op die van gedehydrateerde silica oppervlakken, en suggereren dat silica nanoclusters mogelijk interessante modelsystemen zijn voor dit soort oppervlakken.

Hoofdstuk vier van dit proefschrift beschrijft meer uitgebreide theoretische berekeningen van de infrarood spectra van volledige gecoördineerde silica nanoclusters en hun toepassing als modelsystemen voor gedehydrateerde silica oppervlakken. De berekende spectra tonen vele pieken in het experimenteel bestudeerde frequentievenster, waarvan sommige met een uitstekende overeenkomst in zowel frequentie als intensiteit met experimenteel gemeten banden. De verkregen resultaten suggereren dat de experimenteel waargenomen spectra wellicht het resultaat zijn van collectieve bewegingen van meerdere Si_2O_4 -tweeringen.

In hoofdstuk vijf van dit proefschrift wordt een op de resultaten van theoretische berekeningen geïnspireerde syntheseroute naar goed gedefinieerde en stoichiometrische silica nanoclusters beschreven. Voor deze route, welke uitgaat van siloxaan kooien, voorspellen onze berekeningen wanordelijke en defectrijke structuren voor kleine kooien terwijl volledige gecoördineerde clusters het verwachte product zijn bij het gebruik van grote kooien als reactant. Alles welbeschouwd voorspellen de resultaten van onze berekeningen dat de dehydratatie van siloxaan kooien naar alle verwachting een aantrekkelijke route is naar metastabiele doch goed gedefinieerde silica nanoclusters, welke niet met bekende grovere bereidingsmethoden gemaakt kunnen worden.

Hoofdstuk zes van dit proefschrift beschrijft de basis voor een methode om de energetica van zeolieten en de waarschijnlijkheid van hun synthese te voorspellen op basis van de topologie van het onderliggende “framework”. Deze analyse, gebaseerd op de vlakgrootteverdeling van het “framework”, toont formeel aan waarom voor een belangrijke groep zeolietstructuren de aanwezigheid van kleine ringen (drie- en vierringen) onontbeerlijk is voor de stabilisatie van “frameworks” met grote kanalen.

Hoofdstuk zeven van dit proefschrift beschrijft een uitbreiding van het werk beschreven in hoofdstuk zes. Het toont aan dat de decompositie van zeoliet “frameworks” in polyeders en analyse van de zo verkregen vlakgrootteverdeling gebruikt kan worden om de energetica van zeolieten succesvol te voorspellen. De onderliggende analyse toont verder aan dat de kanaalgrootte en “framework density”

van zeoliet “frameworks”, tenminste voor de “frameworks” gebaseerd op zogenaamde “simple tilings”, niet vrij gevarieerd kunnen worden en direct verbonden zijn met de topologie van het onderliggende “framework”.

In hoofdstuk acht van dit proefschrift tenslotte wordt het effect van het gedeeltelijk vervangen van Si door Ge op de vorming van zeoliet “frameworks” met dubbele vierringen (D4Rs) onderzocht. Berekeningen, gebaseerd op de methode beschreven in hoofdstuk zes, tonen aan dat de experimenteel waargenomen vergemakkelijking van de synthese van D4R bevattende “frameworks” verklaard zou kunnen worden door de relatieve energetische stabilisatie van D4Rs ten opzichte van grotere kooien. Verder wordt aangetoond dat de door O’Keeffe op geometrische gronden voorspelde symmetrieverlaging van dubbele vierringen, gerationaliseerd kan worden in termen van de energie die vrijkomt bij deze symmetrieverlaging.

Dankwoord

Vele mensen hebben op een of andere manier bijgedragen aan de inhoud van dit proefschrift. Nu de laatste letters op het papier staan, is het moment gekomen om eenieder te bedanken.

Ik wil beginnen met mijn (dagelijkse) begeleiders. Koos, bedankt dat je me nu al weer vier en een half jaar geleden hebt gevraagd om binnen jouw groep een promotieonderzoek te gaan doen; het is een erg interessante tijd geworden. Hoewel de inhoud van dit proefschrift waarschijnlijk heel anders is dan je vooraf had gedacht, heb je mij altijd alle ruimte gegeven om zelf mijn pad te trekken. Hiervoor mijn hartelijke dank. Je aanstekelijke enthousiasme en stortvloed aan ideeën zijn al zovaak aangehaald, dat ik me hier louter bij zal aansluiten; werken binnen jouw groep was nooit saai. Stef, thanks for introducing me to the wonderful and fruitful world of computational chemistry, I couldn't have wished for a better teacher. Also I would like thank you for the nice (scientific) discussions on the oddest times and locations, and overall for the good time we had together in our computer room in the far far corner of the building. I wish you (and Marta) all the luck in Barcelona. Thomas it's a shame you can't be here for my promotion, but herewith, I would like to thank you for all the advice you gave me and discussions we had when you were still in Delft. I hope to run into you again on a conference on the other side of the world soon. Geert-Jan van harte bedankt voor het op zo'n laat moment overnemen van het promotor stokje. Zonder jouw enthousiasme had dit laatste lootje wel eens een stuk zwaarder kunnen wegen.

Het werk beschreven in en het schrijven van dit proefschrift zou ook niet mogelijk geweest zijn zonder de (administratieve) ondersteuning van de beide Mieke's. Van harte bedankt voor het vele regelwerk dat jullie in de laatste vier en een half jaar voor mij verricht hebben. Zonder jullie zouden vele dingen hier in het honderd lopen.

Vele leden van de "zeoliet" en "computational" groep zijn onmisbaar geweest voor het in dit proefschrift beschreven onderzoek; hiervoor mijn hartelijke dank Zhiping, thanks for introducing me to the dark art of synthesizing mesoporous materials and the culinary delights of proper Chinese food. Leszek, your enthusiasm to discuss any aspect of zeolite chemistry and your knowledge in this field is highly appreciated. Guido, bedankt voor het nalaten van je bureau en bijbehorende stoel, lange tijd de beste plaats in de "Koos" labs (al weet ik nog steeds niet wat het doel van die schemerlamp

was). Leon, ons germanium verhaal staat helaas niet in dit proefschrift maar onze samenwerking heeft wel min of meer tot hoofdstuk acht geleid. Annemieke, dankje voor het vele proeflezen. Onze “vakanties” waren trouwens memorabel, Beijing volgende keer? Edwin, het was altijd fijn om terug te vallen op je wiskundige kennis. Jacek, met jou kreeg onze groep eindelijk de computergoeroe die we al zo lang misten en zonder jouw advies had dit proefschrift er dan ook ongetwijfeld minder fraai uitgezien.

Het onderhouden van een cluster is een dagtaak die ons gelukkig uit handen is genomen door de IT-groep. Peter en Arno, ik wil jullie hierbij bedanken voor alle hulp met computerproblemen en de moeite die jullie je getroost hebben om de beowulf draaiend te krijgen en te houden.

I would like to acknowledge the English (and increasingly American) connection. Rob, Martin, Alex, without our discussions and your input the final chapters of this thesis wouldn't have been possible, many thanks and I hope our cooperation will last into the far future. Naz, thanks for your friendship and hospitality. I wish you all the luck in Santa Barbara. I would also like to thank all the people from the RI and UCL whom I had the pleasure of meeting either, in London, or one of the many conferences I attended (Mount Holyoke, Nottingham, Cape Town), for the good times I had.

From the English connection it's only a small leap to the German connection. Olaf without your input chapter seven would have been impossible, thank you for your assistance. I hope we will continue to have such a fruitful cooperation in the future.

Naast werk was er gelukkig altijd nog ruimte voor gezelligheid: taart, Bierhuis, Delftse Hout, barbecue, feestjes. Daarom wil ik alle TOCK'ers en BOC'ers (en aanhang) bedanken voor de goede tijd die ik op het lab gehad heb. Paolo, for seldom agreeing but still liking to discuss, for introducing me to the beauty of Cinema and for allowing me to borrow most of the look and feel of this thesis. Angel, for the good times (both in Delft and Alicante) and for throwing the probably best party ever in Delft. Cesar, for the interesting discussions and your “reliability” in visiting the Bierhuis. Silvia, for your kindness and for showing me round Portugal. Adrie, Allard, Andrea, Andrzej, Aleksandra, Anne, Anne, Aniel, Antonio, Arné, Bert, Bowden, Bruno, Carla, Carlos, Chrétien, Cindy, Dean, Delia, Dirk, Donny, Elisa, Elna, Emrin, Erik, Ester, Eva, Ewald, Filip, Filipa, Frank, Fred, Fernando, Gema, Gerd-Jan, Giovannia, Govert, Göran, Greet, Guillaume, Hans, Heidi, Hilda, Isabel, Isabel Jacqueline, Jan, Jan,

Jan-Kees, Jeroen, Joop, José Miguel, Kristina, Lars, Lizete, Luca, Luka, Luuk, Maikel, Margreth, Marina, Marta, Mathias, Maurice, Menno, Mette, Michel, Michel, Michiel, Michiel, Mike, Moira, Nazely, Nina, Oki, Paloma, Patricia, Pedro, Peter, Petra, Pramatesh, Ulf, Raffaella, Remco, Rob, Robert, Roel, Rute, Sameh, Sander, Sandrine, Silvia, Ton, Valentina, Xavier, Yuxin, Zbigniew, en alle mensen die ik vergeten ben, van harte bedankt.

Dan zijn er ook nog mensen van buiten de scheikunde die ik wil bedanken. Allereerst, de mannen van de J.C. Resoluut (Bart, Bart, Erik, Hans, Hoi-Yip, Jeroen, Joost, Maarten, Maarten, Patrick, Robbert-Jan) voor de leuke tijd binnen en buiten Virgiel de laatste zeven jaar. Niets is namelijk zo ontspannend na een dag scheikunde als een zinloze discussie over politiek, voetbal etc. onder het genot van een lauw biertje. Ook wil ik het “welpen-team” (Marinieves, Rik, Saskia) bedanken voor hun vriendschap en de leuke tijd de laatste jaren.

Tenslotte wil ik mijn ouders en mijn zusjes bedanken voor alle steun en interesse tijdens mijn studie en promotie. Zonder jullie allen was ik nooit zover gekomen, bedankt!

Martijn

Publications and oral presentations

Publications

1. Zwijnenburg M.A., Bromley S.T., Van Alsenoy C., Maschmeyer T. "Factors affecting the ionicity in all-silica materials: a density functional cluster study" *J. Phys. Chem. A* **2002**, 106, 12376.
2. Bromley S.T., Zwijnenburg M.A., Maschmeyer T. "Fully coordinated silica nanoclusters: $(\text{SiO}_2)_N$ molecular rings" *Phys. Rev. Lett.* **2003**, 90, 035502.
3. Bromley S.T., Zwijnenburg M.A., Maschmeyer T. "Two-ring vibrational modes on silica surfaces investigated via fully coordinated nanoclusters" *Surf. Sci.* **2003**, 539, L544.
4. Zwijnenburg M.A., Bromley S.T., Jansen J.C., Maschmeyer T. "Towards understanding Zeolite Energetics and Topology: a Polyhedral Approach" *Chem. Mater.* **2004**, 16, 12.
5. Bromley S.T., Zwijnenburg M.A., Flikkema E., Maschmeyer T. "Reply: Fully coordinated SiO_2 nanoclusters as materials building blocks: the importance of stability and reactivity" *Phys. Rev. Lett.* **2004**, 92, 039602.
6. Zwijnenburg M.A., Bromley S.T., Flikkema E., Maschmeyer T. "Prospects for a synthetic route towards well-defined silica nanoclusters: from siloxane to silica" *Chem. Phys. Lett.* **2004**, 385, 389.
7. Zwijnenburg M.A., Bromley S.T., Jansen J.C., Maschmeyer T. "Computational insights into the role of Ge in stabilising double-four ring containing zeolites" *Microporous Mesoporous Mater.*, **2004**, 73, 171.
8. van de Water L.G.A., Zwijnenburg M.A., van der Waal J.C., Sloof W.G., Jansen J.C., Maschmeyer T. "The effect of Ge incorporation on the framework acidity of ZSM-5" *Chem. Phys. Chem.*, accepted for publication.
9. Zwijnenburg M.A., Bromley S.T., Foster M.D., Bell R.G., Delgado-Friedrichs O., Jansen J.C., Maschmeyer T. "Towards understanding the thermodynamic viability of Zeolites and related frameworks through a simple topological model" *Chem. Mater.*, accepted for publication.

10. Zwijnenburg M.A., Bromley S.T., Jansen J.C., Maschmeyer T. "Towards understanding the energetics and topology of zeolites, a polyhedral approach" *Stud. Surf. Sci. Catal.*, in press.
11. Zwijnenburg M.A., Bromley S.T., Jansen J.C., Maschmeyer T. "Towards understanding the energetics of zeolitic materials" *Advances in Science and Technology*, in press.
12. Bromley S.T., Flikkema E., Zwijnenburg M.A. "Fully coordinated silica nanoclusters: building blocks for novel materials" *Advances in Science and Technology*, in press.

Oral presentations and posters

1. Zwijnenburg M.A., Bromley S.T., Van Alsenoy C., Maschmeyer T. "Correlations between structure and ionicity in all-silica zeolites: a density functional cluster study" 3rd Netherlands Catalysis and Chemistry Conference, Noordwijkerhout, The Netherlands, **2002**: poster.
2. Zwijnenburg M.A., Bromley S.T., Jansen J.C., Maschmeyer T. "Silsesquioxanes as model systems for zeolites in computational chemistry" Gordon Research Conference on Zeolitic & Layered Materials, South Hadley MA, United States of America, **2002**: poster.
3. Zwijnenburg M.A., Bromley S.T., Jansen J.C., Maschmeyer T. "Towards low framework density and large pore zeolites: A computational & topological study" 4th Netherlands Catalysis and Chemistry Conference, Noordwijkerhout, The Netherlands, **2003**: oral presentation.
4. Zwijnenburg M.A., Bromley S.T., Jansen J.C., Maschmeyer T. "Towards understanding the energetics and topology of extra-large pore zeolites, a polyhedral approach" 26th annual meeting of the British Zeolite Association, Nottingham, United Kingdom, **2003**: oral presentation.
5. Zwijnenburg M.A., Bromley S.T., Jansen J.C., Maschmeyer T. "Understanding the viability of zeolite synthesis: a polyhedral approach" 5th Netherlands Catalysis and Chemistry Conference, Noordwijkerhout, The Netherlands, **2004**: poster.

6. Zwijnenburg M.A., Bromley S.T., Jansen J.C. “Molecular modelling as applied to the design of (extra-large) pore zeolites” Applied Molecular Modelling and Simulation workshop 2004, Parys, Republic of South Africa, **2004**: invited oral presentation.
7. Zwijnenburg M.A., Bromley S.T., Jansen J.C., Maschmeyer T. “Towards understanding the energetics and topology of extra-large pore zeolites, a polyhedral approach” 14th International Zeolite Conference, Cape Town, Republic of South Africa, **2004**: oral presentation.
8. Zwijnenburg M.A., Bromley S.T., Jansen J.C., Maschmeyer T. “Towards understanding the energetics of zeolitic materials” 3rd International Conference on Computational modelling and simulation of materials, Acireale, Italy, **2004**: oral presentation.

Curriculum vitae

Martijn Zwijnenburg werd op 8 juli 1976 te Den Haag geboren. In 1993 werd het HAVO diploma behaald aan het Interconfessioneel Makeblijde College te Rijswijk. In hetzelfde jaar begon hij aan een studie petroleum- en gastechnologie aan de Hogeschool van Amsterdam te Den Helder. De HTS studie werd afgerond met een afstudeeronderzoek bij Shell Research in Amsterdam op het gebied van gasreiniging, en het HTS diploma met de onderscheiding “met lof” werd in juni 1997 behaald. In September 1997 startte hij met een studie scheikundige technologie aan de Technische Universiteit Delft. Deze studie werd afgerond met een onderzoek naar de synthese en karakterisering van zirconia mesoporeuze materialen onder begeleiding van Dr. Z. Shan, Prof. Dr. J.C. Jansen en Prof. Dr. T. Maschmeyer. Het ingenieursexamen werd in februari 2000 afgelegd.

Per 1 februari 2000 begon hij aan zijn promotieonderzoek bij het laboratorium voor Toegepaste en Organische Chemie van de Technische Universiteit Delft. De resultaten van dit onderzoek zijn beschreven in dit proefschrift. De auteur continueert thans zijn loopbaan bij de Technische Universiteit Delft als postdoc verbonden aan het Ceramic Membrane Centre “the Pore”.